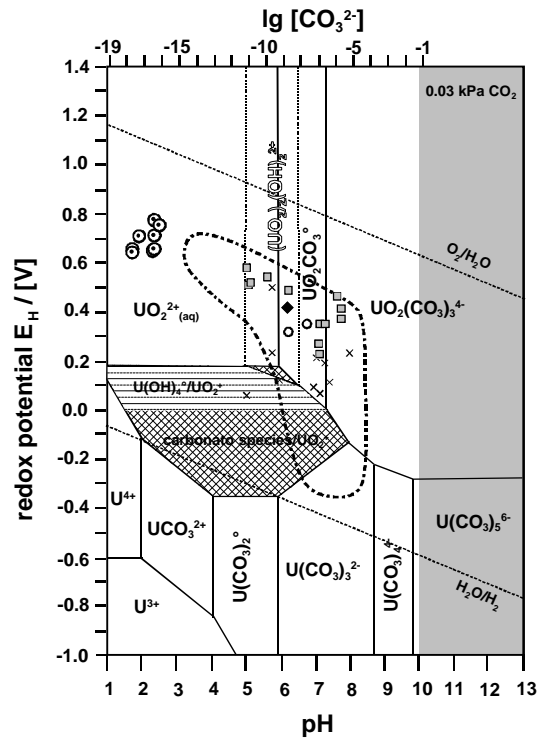




Freiberg On-line
Geoscience Vol. 1

FOG is an electronic journal
registered under ISSN 1434-7512.



Aquatic Chemistry of Uranium

A Review Focusing on Aspects of Environmental Chemistry

Günther Meinrath

Institute of Inorganic Chemistry, TU Bergakademie Freiberg
Institute of Geology, TU Bergakademie Freiberg
RER Consultants, Passau

for Andrea

This report summarizes work done during a DFG-funded research fellowship at Technical University Mining Academy Freiberg and University of Passau from January to September 1997. The Institute of Political Science, University of Dresden has assisted in validating the partly complicated computer programs created by the author for factor analytical data treatment.

The author is deeply indebted to U. Dirscherl and Prof. Dr. W.J. Patzelt at Dresden University, Prof. Dr. W. Voigt at Institute of Inorganic Chemistry, Prof. Dr. B.J. Merkel at Institute of Geology, Department of Hydrogeology, both Technical University Mining Academy Freiberg.

Dr. T. Kimura, Y. Kato and Dr. Z. Yoshida at Advanced Science Research Center/Japan Atomic Energy Research Institute in Tokai-mura/Japan deserve credit for their continued and cordial collaboration. Part of this report could be written during a stay in Tokai-mura in the framework of JAERI's Foreign Researcher Invitation program between October/November 1997.

The author would further like to express his appreciation to the following individuals: P. Volke (Freiberg), C. Helling (Freiberg), S. Fischer (Freiberg), Prof. K. Donner (Passau), K. Czielsa (Freiberg), Dr. P. Raabe (Passau), M. Schweinberger (Bad Tegelensee) und Prof. Dr. B. Kanellakopoulos (Karlsruhe).

Contents

Preface.....	4
1. Fundamental Properties of Hexavalent Uranium.....	6
1.1. Nuclear Properties	7
1.2. Electron Configuration	7
1.3. Redox Properties	7
1.4. Hydration Number of Uranyl(VI)	7
1.5. Properties of Uranyl Entity UO_2^{2+}	8
1.6. Coordinative Properties	8
2. Electronic Structure of UO_2^{2+}.....	9
2.1. Chronological Survey of Contributions Dealing with UO_2^{2+} Electronic Structure	10
2.2. Summary	16
3. Spectroscopic Properties.....	17
3.1. UV-Vis Absorption Spectroscopy	17
3.2. Emission Spectroscopy	19
3.2.1. Emission spectrum	20
3.2.2. Life Time	20
3.2.3. Photochemistry: Quench by Water and Carbonate	22
3.2.3.1. Quench by Water	22
3.2.3.2. Quench by Carbonate	23
3.2.4. Summary	24
4. Hydrolytic Behaviour of Uranium(VI).....	25
4.1. UV-Vis Absorption Spectroscopy of Hydrolyzed Solutions	28
4.2. Factor Analysis	29
4.3. Abstract Factor Analysis	32
4.4. Identification of Single Component Spectra	36
4.4.1. Identification of the Second Factor	37
4.4.2. Identification of the Third Factor	41
4.5. Statistical Treatment	43
4.6. Estimation of Uncertainties in pH Value	47
4.7. Evaluation of Formation Constants	48
5. Deconvoluted Spectra.....	50
6. Comparison with Fluorescence Spectra.....	57
7. Application in Characterization of Solid-Aqueous Phase Equilibria	64

8. Assessment of Uncertainties in Evaluation of pH.....	71
8.1. Methodology	73
8.2. Evaluation Procedure	74
8.2.1. Ordinary Linear Least Squares Regression	74
8.1.2. Maximum Likelihood Approach	80
8.3. Application Example	80
8.4 Statistical Calibration - A Comment	83
9. Uranium(VI) Spectroscopic Speciation.....	84
9.1 Speciation by UV-Vis Spectroscopy	85
9.2 Fluorescence Spectroscopy of Uranium(VI)	86
9.2.1. Application of TRLFS to Spectroscopic Speciation	86
9.2.2. Quenching	88
9.3 Speciation Needs in Natural Samples	89
10. References.....	92

Preface

The chemistry of hexavalent uranium has attracted a lasting interest since its discovery in Saxonian pitchblend from Johanngeorgenstadt near Freiberg/Germany by the analytical chemist M.H. Klaproth in 1789. Among those elements occurring naturally in weighable amounts, uranium displays some unique properties especially in its hexavalent state. Its linear molecular structure in turn gives hexavalent uranium an attractive potential to provide insight into a wide range of fundamental and applied scientific research areas.

During the past fifty years mainly nuclear application research of uranium was focused on. Uranium chemistry is seen nearly exclusively under the aspects of exploration, exploitation, nuclear fuel production, burn up, reprocessing and disposal of nuclear waste. The promising potential of uranium with respect to other aspects of science stood back.

Due to politically motivated, strategic interest in uranium physicochemical and nuclear properties a huge amount of literature is available. A present-day chemist is faced with the task to get a survey on this literature before contributing to this field. Research work described in the present report is based on careful study of about 1500 references on uranium chemistry from open and grey literature, collected during the past decade. All literature is available in copy at hand.

Nevertheless, researchers interested in uranium face the problem of often contradictory and even mutually exclusive interpretations of one and the same experimental observation. Attempts to resolve these contradictions and to design experiments that are able to give decisive evidence are scarce. Often, valuable data is forwarded, but apparently never applied to actual problems. To give an illustrating example, Rush & Johnson (1963) have evaluated single component spectra of hydrolysis species $(\text{UO}_2)_2(\text{OH})_2^{2+}$ and $(\text{UO}_2)_3(\text{OH})_5^+$ by early application of digital data treatment techniques in an still today admirable approach. The present report validates these spectra by a completely independent approach. Surprisingly however, after publication of Rush & Johnson's work, application of these spectra is not to the knowledge of the author. As a matter of fact, these valuable data have never been played the role they deserve.

The unique spectroscopic properties of 5f elements have contributed heavily to our current understanding of fundamental metal ion behaviour in nature. Speciation is a central topic. Even though the ability to obtain validated absorption and emission spectra of well-defined uranium species opens a wide field of new research and understanding, this report limits itself to speciation. Speciation of uranium is of considerable interest e.g. in remediation of former uranium mining areas in eastern part of Germany as well as many other countries in the world. It must be emphasized that the borderline between fundamental research, applied research and practical application is virtually non-existent here.

To uncover the speciation potential of uranium has been a major motivation of the author's scientific efforts during the past seven years. With support by Deutsche Forschungs-

gemeinschaft, Technische Universität Bergakademie Freiberg and Universität Passau as well as cordial collaboration with Advanced Science Research Center at Japan Atomic Energy Research Institute Tokai Establishment more than a dozen communications have been published that opened access to an application especially of the spectroscopic properties of hexavalent uranium. Among other results, previously enigmatic luminescence behaviour of U(VI) in aqueous solution could be explained unambiguously, single component UV-Vis absorption spectra of $[\text{UO}_2\text{CO}_3(\text{H}_2\text{O})_3]$, $[\text{UO}_2(\text{CO}_3)_2(\text{H}_2\text{O})_2]^{2-}$, $[(\text{UO}_2)_2(\text{OH})_2]^{2+}$ and $[(\text{UO}_2)_3\text{O}(\text{OH})_3]^+$ could be evaluated and applied successfully to quantitative resolution of multicomponent uranium(VI) spectra. Fundamental thermodynamic data e.g. for description of solubility behaviour of $\text{UO}_3 \cdot 2 \text{H}_2\text{O}(\text{s})$ could be obtained.

Prior to these studies, methods to determine composition of hydrolyzed and carbonate containing U(VI) solutions in a reliable and quantitative manner have not been available. Due to the high tendency of U(VI) to form hydrolysis and carbonate species both under natural and laboratory conditions, the inability to obtain reliable information on solution composition imposed a major obstacle in understanding aqueous behaviour of uranium.

These points will be discussed in detail in the following report. Discussion of experimental findings and interpretations will successively forward new results, that will be validated further by relations and correlations within results from separate experiments. Based on consistencies and inconsistencies obtained from this analysis, the resulting perception of U(VI) aqueous chemistry will be presented in a way that has not been possible on basis of previous data.

Application of computer-based multivariate chemometric and statistical techniques, e.g. Monte Carlo methods and non-parametric statistics, has been instrumental to achieve this goal. Subsequent analysis has forwarded a wealth of new insight and prospects that open the application of spectroscopic speciation techniques to an understanding of uranium(VI) aqueous solution chemistry.

At the end of the preface it is to point out that the findings reported in the sequel are not only of scientific interest offering further interesting insight in aqueous chemistry of metal ions. The results are also of fundamental importance to contemporary topics of utmost actuality like disposal of nuclear wastes and remediation of former mining area, especially of uranium mining areas. In addition, present work opens new access towards application of uranium e.g. in the investigation of still poorly understood processes of pyrite oxidation or description of concentrated electrolyte solution like evaporating sea water.

Freiberg and Passau/Germany in september 1997

1. Fundamental Properties of Hexavalent Uranium

The chemistry of uranium in aqueous solution is governed by the dioxo cation UO_2^{2+} (Langmuir 1978, Zachariassen 1948). Structural analogs are known from the actinides NpO_2^{2+} , PuO_2^{2+} and AmO_2^{2+} only, because the formal analogous transition group dioxo cations e.g. WO_2^{2+} , MoO_2^{2+} and CrO_2^{2+} are not linear, thermodynamically and kinetically more labile compared to UO_2^{2+} and show fundamental differences in the physicochemical properties (Tatsumi & Hoffmann 1980, Denning 1992, Schröder 1975). The actinide analogs are α -emitters with partly high specific activities, whose behaviour can be studied only under considerable security measures. Especially PuO_2^{2+} exhibits a considerable stability under conditions of natural aquatic systems. Its portion in the toxicity inventory of a nuclear disposal site is by far higher than that of uranium. In case of direct disposal plutonium even determines the toxicity inventory (Levi et al. 1990). Reliable thermodynamic data therefore are of crucial importance to ensure required predictive power of long term safety analysis of nuclear waste disposal sites in deep geological formations. As can be visualized by comparing proposed E_{H} -pH diagrams of Pu (e.g. (Brookins 1984, Lemire & Tremaine 1980, Krauskopf 1986, Brookins 1990)), the required reliable knowledge is not yet available. Uranium is the only analogue to be handled outside a controlled area with reasonable costs.

In aqueous solution, uranium forms oligomeric hydrolysis species. Beside the unambiguously characterized $(\text{UO}_2)_2(\text{OH})_2^{2+}$ species, the following additional oligomeric and monomeric hydrolysis species are discussed : $(\text{UO}_2)_3(\text{OH})_5^+$, $(\text{UO}_2)_3(\text{OH})_4^{2+}$, $(\text{UO}_2)_2\text{OH}^{3+}$, $(\text{UO}_2)_3(\text{OH})_7^-$, $(\text{UO}_2)_4(\text{OH})_7^+$, UO_2OH^+ , $\text{UO}_2(\text{OH})_2^\circ$, $\text{UO}_2(\text{OH})_3^-$ and $\text{UO}_2(\text{OH})_4^{2-}$ (Baran 1992, IAEA 1992, NEA 1992). In addition to the well-known monomeric carbonato species $\text{UO}_2\text{CO}_3^\circ$, $\text{UO}_2(\text{CO}_3)_2^{2-}$ and $\text{UO}_2(\text{CO}_3)_3^{4-}$ an oligomeric carbonato compound is reported: $(\text{UO}_2)_3(\text{CO}_3)_6^{6-}$ (Ciavatta et al. 1981). This variety especially in hydrolysis species has been proposed mainly by evaluation of potentiometric titrations (Sillén 54a, Sillén 1954b, Dunsmore et al. 1963). Formation of these species is inferred mainly from numerical modelling of titration curves using the criterion of best fit. With a few exceptions like $(\text{UO}_2)_2(\text{OH})_2^{2+}$, $(\text{UO}_2)_3(\text{OH})_5^+$ and $\text{UO}_2(\text{CO}_3)_3^{4-}$, where UV-Vis spectra (Rush & Johnson 1963, Baran 1965, O'Conneide et al. 1975, Meinrath 1997b), structures from solution X-ray studies (Åberg 1969, Åberg 1970) or EXAFS radial distribution studies (Allen et al. 1995) are discussed, no independent evidence is available for these species.

1.1 Nuclear properties

Atomic number of uranium is 92. All isotopes are radioactive. Six isotopes show half lives in the order of years: ^{232}U (72 a), ^{233}U (1.585×10^5 a), ^{234}U (2.44×10^5 a), ^{235}U (7.038×10^8 a), ^{236}U (2.3416×10^7 a) and ^{238}U (4.47×10^9 a). Naturally occurring nuclides of uranium (abundance) are ^{234}U (0.005 %), ^{235}U (0.72 %) and ^{238}U (99.276 %). ^{235}U and ^{238}U are primordial nuclides, while ^{234}U is a ^{238}U daughter.

1.2 Electron configuration

The electron configuration of atomic uranium is $[\text{Rn}] 7s^2 6d^1 5f^3$. The sixfold charged ion U^{6+} has configuration $[\text{Rn}] 7s^0 6d^0 5f^0$ (Cordfunke 1969). Uranyl(VI)-compounds exhibit correspondingly a weak temperature independent paramagnetism in solids (Belova et al. 1961) and solutions (Baran & Tympl 1962, Day & Venanzi 1966).

1.3 Redox Properties

The known redox states of uranium are U(II) (Mikeev 1989), U(III), U(IV), U(V) and U(VI). The reduction potentials are given in Fig. 1.1.

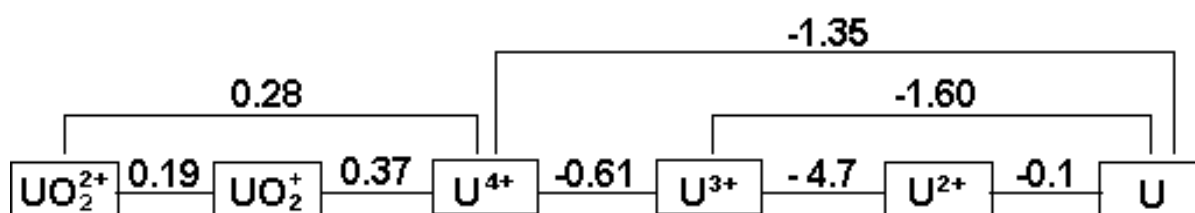


Fig. 1.1 : Standard reduction potentials E_0 of uranium (calculated from Fuger & Oetting (1976)). U^{2+} reduction potentials are calculated according to David et al. (1995). For formation of $\text{U}^{2+}_{(\text{aq})}$, see (Mikeev & Kamenskaya 1991, Morss 1995).

Under conditions of natural aquatic systems the states U(VI) and U(IV) only are stable. U(IV) is extremely insoluble. Hence the solution behaviour under those conditions is dominated by U(VI). The extreme contrast in the solubilities of the states U(VI) and U(IV) determines whether uranium is mobilized, precipitated, sorbed or immobilized in a given aqueous system.

1.4 Hydration Number of Uranyl(VI)

The chemistry of U(VI) is nearly exclusively dominated by the linear dioxo cation UO_2^{2+} . Only few exceptions are known, with negligible importance in the present context, e.g. UF_6 (Ruff & Heinzelmann 1909), UCl_6 (Zachariasen 1948) or $\delta\text{-UO}_3(\text{s})$ (Wait 1955, Weller et al. 1988). From direct determinations of the hydration number of $\text{UO}_2^{2+}(\text{aq})$, discrepant conclusions are reported. From studies of $^1\text{H-NMR}$ in $\text{H}_2\text{O}/\text{acetone}$ mixtures between $-85\text{ }^\circ\text{C}$ and $-100\text{ }^\circ\text{C}$ (Fратиello et al. 1969, Fratiello et al. 1970) and $-70\text{ }^\circ\text{C}$ (Ikeda et al. 1979), resp. a hydration number of 4 is evaluated (Tomiyasu & Fukutomi 1982). $^1\text{H-NMR}$ studies at $-90\text{ }^\circ\text{C}$ resulted in a hydration number of 6 (Sherbakov & Sherbakova 1976). From analysis of IR-spectra of perchlorate hydrates and aqueous perchlorate solutions, a species $[\text{UO}_2(\text{H}_2\text{O})_5]^{2+}$ was reported (Vdovenko et al. 1964). MCD spectra (Görrler-Walrand et al. 1982, Görrler-

Walrand & Colen 1982), X-ray diffraction of 1 M $\text{UO}_2(\text{ClO}_4)_2$ solutions, $^1\text{H-NMR}$ spectroscopy in $\text{H}_2\text{O}/\text{acetone-d}_6$ mixtures at $-80\text{ }^\circ\text{C}$ (Åberg et al. 1983) as well as potentiometry and Raman spectroscopy (Azenha et al. 1988) resulted in a hydration number of 5. Possible sources of errors in $^1\text{H-NMR}$ investigations are outlined (Åberg et al. 1983).

No convincing evidence for coordination of U(VI) by perchlorate ions in aqueous solutions is available (Vdovenko et al. 1964, Johansson 1974). In the following chapters, a species $[\text{UO}_2(\text{H}_2\text{O})_5]^{2+}$ is assumed as hydrated UO_2^{2+} . This species will be referred to as „free uranyl ion“ $\text{UO}_2^{2+}_{(\text{aq})}$.

1.5 Properties of Uranyl Entity UO_2^{2+}

The linear entity O-U-O was observed as characteristic unit in more than 180 single crystal structure determinations (Denning 1983, Leciejewicz et al. 1995). Deviations from 180° linearity caused by crystal symmetry were larger than 5° only in a small amount of compounds. The maximum deviation reported was 19° (O-U-O = 161°) in $\text{UO}_2(\text{ClO}_4)_2 \cdot 7 \text{H}_2\text{O}$ (Alcock & Esperàs 1977). The linear entity is both thermodynamically (Denning 1992) and kinetically (Gordon & Taube 1961) extraordinarily stable. Isotopic $^{16}\text{O}/^{18}\text{O}$ exchange experiments in 0.94 M and 0.094 M HClO_4 at $25\text{ }^\circ\text{C}$ and $\mu = 3.79$ indicate exchange rates for axial uranyl oxygens of $k = 5 \times 10^{-9} \text{ mol}^{-1} \text{ l s}^{-1}$. This rate corresponds to half lifes in the order of $4 \times 10^3 \text{ hr}$ (0.094 M HClO_4) and $4 \times 10^4 \text{ hr}$ (0.94 M HClO_4), resp. Exchange of axial oxygens is catalyzed by traces of UO_2^+ (Gordon & Taube 1961, Rabideau 1967).

Affinity of hexavalent uranium towards oxygen under formation of a linear uranyl(VI) entity is highly specific. The insertion reaction of atomic uranium into O_2 is strongly exothermic with -9.7 eV . In contrast, uranyl-analogous compounds with other ligands than oxygen in axial position are rare and unusual. An isosteric analog of UO_2^{2+} , linear UN_2 , has been recently reported to form in gas phase reaction $\text{U} + \text{N}_2 \rightarrow \text{N-U-N}$. It could be characterized by IR spectroscopy in matrix isolation technique in argon at $27 - 32 \text{ K}$ (Hunt et al. 1993). This reaction is endothermic. A further UO_2^{2+} analogs with linear O-U-N entity has been reported recently in the crystal structure of $\text{PPh}_4^-[\text{UOCl}_4\{\text{NP}(\text{m-Tol})_3\}]^+$ (Ph = phenyl, m-Tol = $\text{C}_6\text{H}_4\text{m-CH}_3$) (Brown et al. 1994). This substance is stable in contact with the air. The bond angle O-U-N is 179° .

1.6 Coordinative Properties

The ion UO_2^{2+} was reported only very recently uncoordinated „bare“ in the gas phase (Cornehl et al. 1996). Otherwise, UO_2^{2+} is only found coordinated in the plane equatorial to the axial oxygens. Coordination occurs exclusively equatorial to the axial uranyl oxygens by four, five or six coordinating ligands. The preferred equatorial coordination is pentagonal (Evans 1963, Denning 1983). Coordination number 4 is found mainly in presence of sterically demanding ligands, e.g. bromide in $\text{Cs}_2\text{UO}_2\text{Br}_4$ (Mikhailov & Kuznetsov 1971) or triphenyl-

phosphineoxide in $\text{UO}_2\text{Cl}_2(\text{OP}(\text{C}_6\text{H}_5)_3)_2$ (Bombieri et al. 1978). Coordination number 6 is observed in presence of multidentate ligands where coordination angle between the „bite“ of the ligand and coordinated uranium is smaller than 60° .

Tendency for pentagonal coordination of U(VI) is quite high. A series of compounds, where U(VI) was assumed to be equatorially coordinated hexagonally on basis of powder diffraction data before 1970 have been found as pentagonally coordinated from single crystal studies later. Examples are $\text{UO}_2(\text{HCOO})_2 \cdot \text{H}_2\text{O}$ (Dieke & Duncan 1949, Görrler-Walrand & de Jagere 1972) where single crystal diffraction revealed pentagonal coordination (Mentzen et al. 1977), and $\text{CsUO}_2(\text{HCOO})_3$ (Barclay et al. 1965) whose presumed hexagonal coordination (Görrler-Walrand & de Jagere 1972) was characterized to be pentagonal (Mentzen 1977).

Bond lengths of axial oxygens in uranyl(VI) compounds vary from 150 pm in $\text{UO}_2(\text{C}_9\text{H}_6\text{NO})_2 \cdot \text{C}_9\text{H}_7\text{NO}$ (Hall et al. 1967) and 208 pm in $\alpha\text{-UO}_3$ (Greatorex et al. 1972). The mean value from 180 crystal structure data is 177 pm. There seems to be no clear relationship between equatorial coordination and axial bond lengths in the uranyl(VI) entity (Denning 1983). With exception of the above already mentioned compounds, deviations from linearity are $\leq 5^\circ$. Bond lengths of equatorial ligand oxygens with central uranium vary between 235 pm and 255 pm. Sterically demanding ligands like halogenide ions (with exception of fluoride) prefer tetragonal coordination. Coordination with by one bidentate ligand with „short bite“ is usually pentagonal as e.g. in $\text{UO}_2(\text{CH}_3\text{COO})_2 \cdot 2\text{H}_2\text{O}$. Bidentate coordination with two ligands and coordination angle close to 70° (e.g. oxalate) however prefer likewise pentagonal coordination.

Coordination by two bidentate ligands with „short bite“ is usually associated with hexagonal coordination around uranyl(VI) as e.g. in $\text{UO}_2(\text{NO}_3)_2(\text{TEP})_2$ (Kanellakopoulos et al. 1993) as is in case of three bidentate „short bite“ ligands e.g. in $(\text{NH}_3)_4\text{UO}_2(\text{CO}_3)_3$ (Graziani et al. 1972), $\text{K}_3\text{NaUO}_2(\text{CO}_3)_3$ (Mazzi & Rinaldi 1960, Mazzi & Rinaldi 1961) or $\text{RbUO}_2(\text{NO}_3)_3$ (Barclay et al. 1965).

2. The Electronic Structure of UO_2^{2+}

Spectroscopic investigations of a compound in the UV-Vis region can be rationalized and systematized by a model of the electronic structure of this compound. The uranyl ion is a molecular unit and therefore a considerable number of parameters enter in a numerical description of its electronic structure. Beside electronic transitions, vibrational and rotational transitions as well as their mutual coupling have to be taken into account. The spectroscopic properties of the uranyl(VI) ion UO_2^{2+} have been intensively investigated during development of the US atomic bombs in the framework of ‘Manhattan project’. These spectroscopic investigations are summarized by Dieke & Duncan (1949) and Rabinowitch & Belford (1964).

Discussion of the electronic structure of the UO_2^{2+} entity was lasting and discrepant. The number of electronic transitions, the energetic sequence of bonding and non-bonding orbitals

as well as the cause of the very weak oscillator strength of the low energy electronic transition have been controversially discussed. Different mutually exclusive interpretations have been offered (Jørgensen & Reisfeld 1982, Denning 1992). A selection of contributions will be briefly abstracted in the following. Due to the great number and variety of contributions, the selection is inevitably subjective.

A simple model considering only σ bonds (Eisenstein & Pryce 1955) was extended by π -bonds (M^cGlynn & Smith 1961a). MO calculations based on combination of U(VI) and O(II) valence orbitals result in six symmetry adapted molecular orbitals with following symmetries in $D_{\infty h}$: (U-7s, U-6d₀, O-2p₀) : σ_g , (U-f₀, O-2p₀) : σ_u , (U-5f _{\pm 1}, O-2p _{\pm 1}) : π_u and (U-6d _{\pm 1}, O-2p _{\pm 1}) : π_g . The uranium valence orbitals 5f _{\pm 2}, 5f _{\pm 3} and 6d _{\pm 2} form non-bonding orbitals of symmetry δ_u , ϕ_u and δ_g , resp. The bonding orbitals σ_g , σ_u , π_g and π_u accept twelve valence orbitals that are formally 2p electrons of O(II). The resulting ground state symmetry is total symmetric $^1\Sigma_g^+$. The treatment of the electronic structure with approaches and methods of increasing sophistication resulted in differing orders of molecular orbitals in the ground state. From analyses of absorption and emission spectra four (Volod'ko et al. 1966) to twelve (Schwarz 1985) electronic transitions were concluded. From theoretical analysis, Jørgensen concluded 14 and 56, resp. electronic transitions depending on the actual highest occupied molecular orbital (Jørgensen 1979, Jørgensen & Reisfeld 1982).

The causes for the very low oscillator strength of the lowest energy electronic transition have been disputed for a long time. By extensive low-temperature single crystal spectroscopic investigations using polarized light, Zeeman splitting and isotopic shift experiments, a rather complex structure of the low energy electronic transition of the uranyl entity has been revealed. The current state of the art is further improved by the increasing power of numerical methods and computers. The following section abstracts influential contributions from literature, published after establishing uranium as the third element of the 5f actinide series and homologue of neodymium at about 1950 (Hahn 1962, Seaborg 1967).

2.1 Chronological Survey of Contributions Dealing with the Electronic Structure of UO_2^{2+}

The assumption of empty 5f orbitals contributing to bonding in the linear O-U-O entity as well as within central uranyl and ligands (Glueckauf & M^cKay 1950, Katzin 1950, Connick & Hugus 1952) gave rise to a first and qualitative insight into the properties of uranyl(VI). A simplified semi-quantitative model on basis of a MO treatment of orbitals within the UO_2^{2+} entity was suggested by Eisenstein & Pryce (1955). This model rendered possible an interpretation of magnetic properties in actinyl(VI) ions UO_2^{2+} , NpO_2^{2+} , PuO_2^{2+} and AmO_2^{2+} . Only σ bonding between sp_z hybridized oxygen atoms in axial position to uranium were taken into account. Symmetric linear combination of both O-sp_z hybrid orbitals is bonded to 6d₀/7s-hybrid orbital of uranium, while its asymmetric combination is bonded to U-5f₀ orbital. These σ bonds are filled with four electrons of UO_2^{2+} . The neglect of possible π bonding contributions is discussed. By applying this simple model to magnetic properties of UO_2^{2+} , the

magnitude of the weak paramagnetism of U(VI) could be understood to result from angular momentum of non-bonding $5f_{\pm 1}$ character mixed into the HOMO.

Coulson & Lester (1956) discuss f orbital hybridization of uranyl valence orbitals as a possible description for ligand interaction in equatorially hexagonal coordinated $[\text{UO}_2(\text{NO}_3)_3]$. Such a description was found possible only if f orbitals are included into the hybridization scheme.

Jørgensen (1957) interpret weak absorption bands of uranyl(VI) in the range 485 - 380 nm and 350 - 310 nm as a result of Laporte forbidden electronic transitions from ligand orbitals to empty 5f orbitals of central uranium. He emphasized importance of spin-orbit interaction in molecules containing heavy atoms like uranium and consequently excluded a spin forbidden transition.

McGlynn & Smith (1961a) propose an electron configuration of the uranyl(VI) ground state. One electron MO energy levels of UO_2^{2+} were calculated from Slater orbital type overlap integrals of oxygen and uranium atomic orbitals. A total symmetric singlet $^1\Sigma_g^+$ with electron configuration $(\sigma_u^+)^2 < (\sigma_g^+)^2 < (\pi_u)^4 < (\pi_g)^4$ was found. The axial bond is formally a triple bond however with a π_g bond of almost negligible strength. The weakness of the electronic transition is explained by a spin forbidden singlet-triplet transition. A total of five electronic transitions have been identified.

Belford (1961) investigates contributions of 6d- and 5f-orbitals to π bonding in UO_2^{2+} based on the MO model of Eisenstein & Pryce (1955). Several bond schemes were found to satisfactorily explain the weak paramagnetic susceptibility, including some schemes that do not consider 5f orbitals at all. Therefore, f orbital contribution to bonding in uranyl(VI) is not proven.

Belford & Belford (1961) study bond strength in uranyl by numerical calculation of σd -, πd -, σf - and πf overlap integrals of uranium with p orbitals of oxygens. Overlap integrals of σd - and πd reveal considerable contributions to bonding. Overlap integrals of π orbitals were found of equal or higher strength compared to σ integrals. Possibilities for strong $f\sigma$ bonds are discussed.

Jezowska-Trzebiatowska & Bartecki (1964) investigate vibrational fine structure of UO_2^{2+} electronic transition in organic solvents and aqueous solutions. They conclude three electronic transitions to levels of a split triplet state.

Israéli (1965) extended and modified the work of McGlynn & Smith. (1961a). That researchers started from UV-Vis spectra of uranyl nitrate in aqueous solutions. Absorption by nitrate in the range 350 - 200 nm covered bands of uranyl and introduced inconsistency into the interpretation given by McGlynn & Smith (1961a). Israéli reported further electronic transitions at 34500 cm^{-1} , 42600 cm^{-1} and 53000 cm^{-1} . A total of seven electronic transitions were found. The ground state sequence of MO orbitals is $(\sigma_g^+)^2 < (\sigma_u^+)^2 < (\pi_u)^4 < (\pi_g)^4$.

Newman (1965) discussed relativistic effects on overlap integrals in uranyl(VI) electronic ground state. Relativistic treatment was found to increase π overlap integrals. On basis of calculated relativistic overlap integrals a tentative ground state configuration $[(e_{1g})^4 < (a_{1g})^2 < (e_{1u})^4 < (a_{2u})^2] : ^1A_{1g}$ (in D_{3d}) was proposed.

Volod'ko et al. (1967) investigate spectroscopic properties of U(VI) solids and solution species with well-defined symmetry. Correlation of integral absorption in the range 500 - 350 nm and symmetry of equatorial coordination was observed. For non-centric coordinations C_s and D_{6h} integral absorption is increased. Based on experimental results and analysis of results and inconsistencies in (M^cGlynn & Smith 1961a, 1961b), four excited electronic states were identified. Classification of electronic levels in D_{6h} symmetry was proposed and discussed relative to the interpretation given by (M^cGlynn & Smith 1961a).

Newman (1967) analyzed 20 K low temperature spectra of $CsUO_2(NO_3)_3$ single crystals on basis of previously given interpretations (Belford 1961a, M^cGlynn & Smith 1961a, M^cGlynn 1961b, M^cGlynn et al. 1961, Newman 1965). Singulet-triplet intervals are found of a magnitude comparable or smaller than spin-orbit coupling.

Bell & Biggers (1965, 1967, 1968) analysed UV-Vis and emission spectra of $UO_2^{2+}(aq)$ in 3 M $NaClO_4$ (0.014 M H^+) solution. The spectra were deconvoluted digitally into 24 Gaussian bands in the range 179.5 nm - 500 nm. Variation of each Gaussian band as a function of pH and temperature were analyzed. No mirror-image relationship between absorption and emission spectra is observed. Bell & Biggers (1968) interpret absorption and emission spectra by seven electronic transitions where two low energy transitions were observed as singulet-triplet transition. The author emphasized that no suitable electronic model exists for this interpretation.

Sanwal & Pant (1969) outline that spectroscopic investigations of solids and solutions suggest several electronic transitions give rise to the low energy electronic transition of uranyl(VI). On basis of extensive spectroscopic investigations at ambient temperature and 80 K, evidence for at least seven electronic transitions in the range 485 nm to 255 nm is reported. A summary of inconsistencies in the model of (M^cGlynn & Smith 1961a) is given. An excited triplet state is excluded.

Görller-Walrand & Vanquickenborne (1971, 1972) discuss the electronic structure of uranyl(VI) on basis of absorption spectra of 25 uranyl(VI) coordination compounds with defined symmetry. (Görller-Walrand & de Jagere 1972a, 1972b, Görller-Walrand & Vanquickenborne 1972, Görller-Walrand & de Jagere 1973). Contributions of electron electron repulsion (e^2/r_{12}), spin orbit coupling (H_{so}), axial field (V_{ax}) and equatorial field ($V_{\ddot{a}q}$) decrease in the order $V_{ax} > e^2/r_{12} \approx H_{so} > V_{\ddot{a}q}$. Görller-Walrand et al. assume a LUMO derived from the configuration (in $D_{\infty h}$) $(\sigma_u^+, \sigma_g^+, \pi_u, \pi_g)^{11} (\phi_u, \delta_u)^1$. As a result 14 different excited states are possible. From group theoretical analysis the effect of coordination on each of the excited states is evaluated and compared to spectroscopic results. Excited triplet states contradict the results of this analysis and are excluded. The low transition moment of the

characteristic low energy transition of uranyl(VI) is interpreted by a Laporte forbidden transition. The HOMO is found with σ_u^+ symmetry. The UV-Vis spectrum of uranyl(VI) is determined by transitions $\phi_u \leftarrow \sigma_u^+$ and $\delta_u \leftarrow \sigma_u^+$.

Brint & McCaffery (1973) interpret magnetic circular dichroism and absorption spectra of $(\text{Bu}_4\text{N})\text{UO}_2(\text{NO}_3)_2$ in a polymer matrix at 10 K. As the most likely arrangement of occupied MOs, $e_{1g} < a_{1g} < a_{2u} < e_{1u}$ (D_{3h}) is given. The low energy electronic transition results from six transitions to triplet states ${}^3E_{1g}$ and ${}^3E_{2g}$.

Jørgensen & Reisfeld (1975) interpret the low extinction coefficient of uranyl(VI) by an intramolecular Laporte forbidden transition from π_u -HOMO to 5f orbitals. The high contribution of spin orbit coupling to the overall energy of the molecule is pointed out, that outweighs the energy difference between different defined spin states. Thus, interpretation of the electronic structure of uranyl(VI) by a Russell-Saunders scheme is not suitable.

Veal et al. (1975) correlate the split of U-6p_{3/2} components of the 6p- spin doublets with axial U-O bond lengths in XPS spectra of 13 U(VI) solids. The splitting increases with increasing U-O distance. These experimental findings are corroborated by theoretical calculations.

Boring et al. (1975) discuss semi-ab initio MSX_α -SCF calculations of UO_2^{2+} electronic ground states at three different axial U-O bond lengths. They also emphasize importance of relativistic effects that could not be taken into account in their study. A ${}^1\Sigma_g^+$ ground state resulted directly from the calculation. The energetic sequence of occupied MOs is $\sigma_g < \pi_u < \sigma_u < \pi_g$. U-6p and O-2s orbitals were included into the MO treatment, in agreement with results of Veal et al. (1975). MOs being mixed with U-6p orbitals also show considerable O-2s participation. These orbitals therefore may not be treated as inert core electrons and must be included into an electronic structure calculation.

Ellis, Rosén & Walch (1975) calculate the electronic ground state both relativistically and non-relativistically by application of discrete variational (DV) method. A ground state sequence $\pi_u < \pi_g < \sigma_g < \sigma_u$ is obtained in both cases. Inclusion of U-6p and O-2s orbital contributions are significant.

Walch & Ellis (1976) investigate influence of equatorial ligands (point charge model) on the electronic structure of uranyl(VI) by relativistic Dirac-Slater MO calculations. Influence of equatorial ligands resulted in an increase of the energy difference between ground and first excited state. Calculations of the optical transition result in a very small energy gap of only 4000 cm^{-1} compared to the experimental value of 20 000 - 22 000 cm^{-1} . Inclusion of contributions due to the equatorial ligands widened the calculated HOMO-LUMO distance to 9800 cm^{-1} , somewhat closer to the experimental value.

Denning et al. (1976a) report extensive spectroscopic investigations of $\text{Cs}_2\text{UO}_2\text{Cl}_4$ single crystals at 4.2 K using polarized light, ${}^{18}\text{O}$ isotopic substitution of axial oxygens and Zeeman

effect measurements. Twelve electronic transitions were observed in the range 20 000 cm^{-1} to 29 000 cm^{-1} . Arguments in favour of a σ_u HOMO are forwarded.

Yang et al. (1978) investigate the electronic structure of uranyl(VI) by relativistic SW- X_α -method. A comparison between non-relativistic and relativistic calculation shows that contributions of U-6p/O-2s orbitals are mainly caused by relativistic effects. The four highest occupied MOs are not significantly influenced by inclusion of relativistic effects and can be correlated with their non-relativistic counterparts: $1\pi_g > 3\sigma_u > 3\sigma_g > 2\pi_u$. Comparison of calculated relativistic energy levels by XPS results of (Veal et al. 1975) show satisfactory agreement. HOMO-LUMO difference however is only 0.3 eV. This small difference is explained by neglect of influences due to equatorial ligands.

Jørgensen (1979) analyze the consequences of a transition from π_u -HOMO to non-bonding ϕ/δ -f orbitals in uranyl(VI). 56 excited states are possible. Strong spin orbit coupling leads to a mixture of angular moments of f orbitals. Only moments parallel to the O-U-O bond characterize a state. Discussions of possible singlet-triplet states therefore are void.

Denning et al. (1979b) present a detailed study of the uranyl(VI) electronic structure. Analysis is based on experimental results of (Denning et al. 1976a, Denning et al. 1979a) and theoretical MO calculation. These non-relativistic calculations result in a σ_u -HOMO and in a Laporte forbidden transition.

Tatsumi & Hoffmann (1980) discuss extended Hückel calculations of MoO_2^{2+} and UO_2^{2+} to explain the linear trans geometry in uranyl. This trans geometry differs from the bent cis geometry of MoO_2^{2+} . The preference of trans geometry is not caused by participation of 5f orbitals but by contributions of the filled „non-valence“ 6p orbitals. Interaction between σ_u^+ and $6p_z$ valence orbitals results in destabilization of σ_u^+ . This orbital thus becomes HOMO. Destabilization by interaction with z components of 5f orbitals results in a stabilization of uranyl in linear geometry. This stabilization mechanism is not available for transition metals lacking f orbitals. Hence, transition metals prefer cis geometry.

Wood et al. (1981) calculate one electron energy levels of UO_2^{2+} , UO_2^+ and UO_2 by relativistic MS- X_α -SCF method. Experimental results of (Veal et al. 1975, Denning et al. 1976, 1979a,b) are taken into consideration. Calculations resulted in an ordering of energy levels in agreement with experimental observations as well as a plausible HOMO-LUMO energy difference.

Wadt (1981) compares isoelectronic structures UO_2^{2+} with linear geometry and ThO_2 with bent geometry on basis of numerical calculations. Linear geometry of UO_2^{2+} is observed even under neglect of U-6p participation, thus contradicting interpretation given by (Tatsumi & Hoffmann 1980). The explanation suggested is a different energetic ordering of empty 6d and 5f orbitals: $5f < 6d$ in U(VI) and $6d < 5f$ in Th(IV). Interaction of 6d orbitals is found responsible for bent ThO_2 structure.

Pyykkö & Lohr (1981) investigate the effect of a relativistic calculation on MO orbital energies by a relativistic parametrized extended Hückel (REX) method. REX results are compared to (Walch & Ellis 1976); a close agreement is observed. U-6p orbital participation in bonding is negligible. Their influence is indirect: they shift the σ_u combination of O-2p atomic orbitals to higher energies. The uranyl HOMO becomes essentially 5f MO (86.7% 5f).

Jørgensen (1982) comments at length the discussion of UO_2^{2+} electronic structure calculations. The considerable 5f contribution to the HOMO (Pyykkö & Lohr 1981) results in a low energy transition of mainly f character - in contrast to previous interpretations (Rabinovitch & Belford 1964, Burrows & Kemp 1974) seeing this transition as an electron transfer transition. The consequences of a σ_u -HOMO (Denning et al. 1976, Denning et al. 1979a,b) instead of a π_u -HOMO (Jørgensen 1979) are discussed. Influence of U-6p orbitals on the energy level of σ_u valence orbitals is emphasized. The considerable discrepancies in available electronic structure calculations are pointed out.

Görrler-Walrand et al. (1982) interpret absorption and MCD spectra of $\text{Cs}_3\text{UO}_2\text{F}_5$ crystals at 4 K. Transition moments in D_{5h} crystal field symmetry are discussed. At least eight electronic transitions are identified. A correlation with electronic levels is proposed. A close agreement with results of (Denning et al. 1979a,b) is observed.

DeKock et al. (1984) calculate the electronic structure of UO_2^{2+} by relativistic LCAO-MO Hartree-Fock-Slater method. It is shown that influence of (non-relativistic) U-6p and O-2s hybridization alone is not sufficient to give rise to a σ_u -HOMO. Relativistic destabilization of 5f contribution (71% U-5f) in σ_u results in a σ_u (S1U in relativistic treatment) HOMO. A good agreement in experimental and calculated HOMO-LUMO energy difference is obtained. Influence of tetrahedral equatorial coordination is studied for $\text{UO}_2\text{F}_4^{2-}$. Ligand orbital participation in HOMO (65 % F-2p) is found considerable.

Larsson & Pyykkö (1986) compare results obtained by various calculation methods. Far-reaching agreement is reported on UO_2^{2+} linearity, character of HOMO and LUMO as well as axial U-O bond length. Influence of equatorial ligands reduces LUMO ungerade character and results in an increase of transition moments.

Barker et al. (1987) present investigations of $\text{Cs}_2\text{UO}_2\text{Cl}_4$ by two photon absorption spectroscopy together with theoretical analysis. A satisfactory agreement of calculated and experimentally derived electronic states is shown. Critical comparison with the work of (Pyykkö & Lohr 1981, DeKock et al. 1984) is given. Importance of ligand influence on character of MO proposed by (DeKock et al. 1984) is found untenable.

Ryzhkov & Gubanov (1990) investigate bonding in solids $\gamma\text{-UO}_3$, $\text{Cs}_2\text{UO}_2\text{Cl}_4$ and UO_2F_4 and solution species $\text{UO}_2(\text{NO}_3)_2 \cdot 2\text{H}_2\text{O}$ by DV-(discrete variational) Dirac-Slater and Hartree-Fock approximations. Influence of relativistic effects is investigated by comparison with non-relativistic treatment. Relativistic treatment results in a wider HOMO LUMO gap. In case of nitrate complex non-relativistic calculation indicates a mixture of 5f orbitals and O-2p orbitals

and consequently a mixture of HOMO and LUMO while relativistic treatment calculates an energy gap of about 1.2 eV.

Krupa et al. (1994) discuss interactions between equatorial ligands and the uranyl(VI) group in UO_2Cl_2 for absorption and emission spectra at 77 °C. Evidence for 6d participation in excited states is forwarded. The Laporte rule affects σ_u -ground state transitions to these states to a lesser extent; thus these transitions are more probable.

Cornehl, Heinemann, Marcalo, Pires de Matos & Schwarz (1996) apply coupled cluster method (CCSD) to validate experimental thermodynamic data of ‘bare’ uranyl(VI) ion UO_2^{2+} . A Hartree-Fock frontier orbital scheme is shown in Fig. 2.1. Orbitals $1\delta_u$ and $1\phi_u$ are non-bonding orbitals localized at the uranium atom. The other orbitals are bonding combinations of U-7s, U-6d and U-5f as well as O-2s and O-2p atomic orbitals.

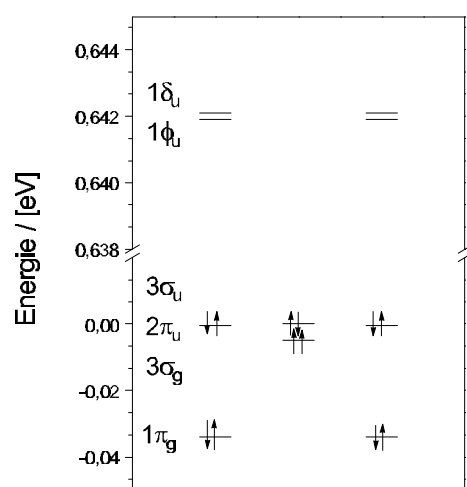


Fig. 2.1 : Hartree-Fock frontier orbital scheme of $^1\Sigma_g^+$ ground state of uncoordinated UO_2^{2+} ion (Cornehl et al. 1996).

determine properties of the uranyl group. Effect of equatorial ligands is secondary and influences electronic transitions by reducing the ungerade character of σ_u -orbitals with subsequent increase of oscillator strength in non-centric coordinations (Görller-Walrand & Vanquickenborne 1972). The unusual strength of the UO_2^{2+} entity results from its triple bond character (Denning et al. 1979b).

2.2 Summary

Electronic structure of UO_2^{2+} entity is currently understood by occupied molecular orbitals with a σ_u -HOMO. Character of this σ_u -HOMO is mostly O-2p. LUMO orbital is formed by an empty 5f_φ orbital. The characteristic low-lying electronic transition takes place from ground state σ_u -MO to non-bonding f orbitals. Transition therefore is ungerade-ungerade and Laporte-forbidden. This transition is characterized by a manifold of electronic states resulting from interaction of an occupied 5f orbital and an energy gap in the ground state structure. The field of axial oxygens

3. Spectroscopic Properties

3.1 UV-Vis Absorption Spectroscopy

The UV-Vis absorption spectrum of the free uranyl ion is given in fig. 3.1 in the range 500 nm to 220 nm. The spectrum shows a weak absorption band in the range 480 nm and 330 nm with a characteristic fine structure as well as a nearly continuous spectrum beyond 330 nm without characteristic features. Above 480 nm no further absorption band was observed and the characteristic weak absorption band is associated with the lowest lying electronic transition. Considerable attention was concentrated on this part of the uranyl(VI) spectrum (Dieke & Duncan 1949, Rabinowitch & Belford 1964).

The characteristic fine structure of the low energy absorption spectrum consists from a nearly regular sequence of bands (Dieke & Duncan 1949), resulting from coupling of electronic transitions with symmetric stretching vibration of the uranyl(VI) group (Jones 1958, DeJagere & Görrler-Walrand 1969). This part of the UV-Vis spectrum is shown in Fig. 3.2.

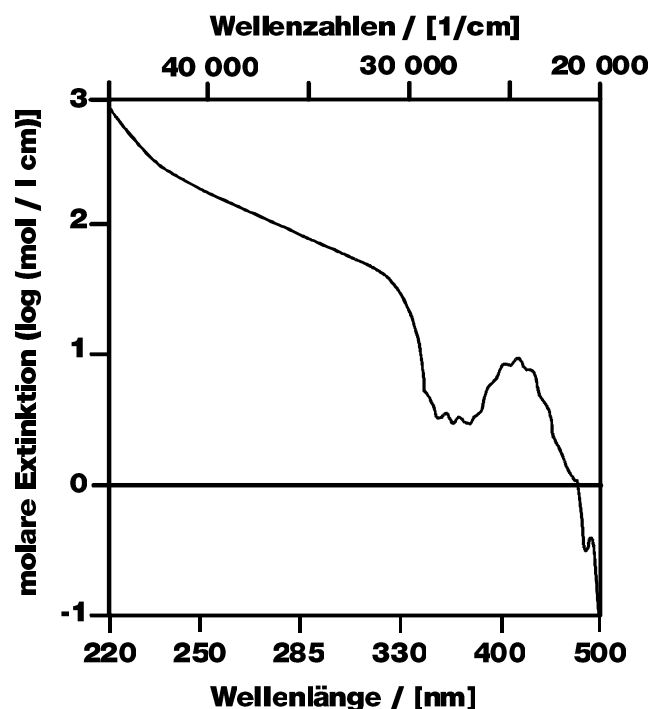


Fig. 3.1 : UV-Vis spectrum of free uranyl(VI) ions in the range 500 nm to 220 nm (McGlynn & Smith 1961a).

The absorption maximum is found at 413.8 nm and a molar extinction coefficient of $9.7 \pm 0.2 \text{ l mol}^{-1} \text{ cm}^{-1}$.

Intensity of electronic transitions is usually compared on basis of the oscillator strength. The oscillator strength f is a dimensionless figure proportional to the area under the absorption band. The absorption spectrum of the uranyl(VI) ion exhibits an unusually weak oscillator strength (Jørgensen & Reisfeld 1982). From figure 3.2 an oscillator strength $f \approx 10^{-4}$ in the range 330 nm to 580 nm is calculated. The oscillator strength therefore is of the order of $4f-4f$ transition of lanthanides (Carnall 1979) and about one order of magnitude less than typical oscillator strengths found for $5f-5f$ transitions of actinides (Carnall & Rajnak 1975). Oscillator strengths of allowed transitions are of typical order $10^{-1} - 10^{-3}$, Laporte-forbidden spin allowed

transitions have typically $f = 10^{-3} - 10^{-4}$ and for spin forbidden transitions f is in the range $10^{-4} - 10^{-8}$ (Sýkora & Sima 1990). The oscillator strength of the free uranyl ion therefore corresponds to oscillator strengths of both spin forbidden as well as Laporte forbidden electronic transitions (cf. Table 3.1). This low oscillator strength in the order of $f-f$ transitions

is unusual for a molecular that formally does not have f electrons at all. In the oxidation state +VI the electron configuration of uranium is $[\text{Rn}] 7s^0 6d^0 5f^0$ (cf. section 1.2).

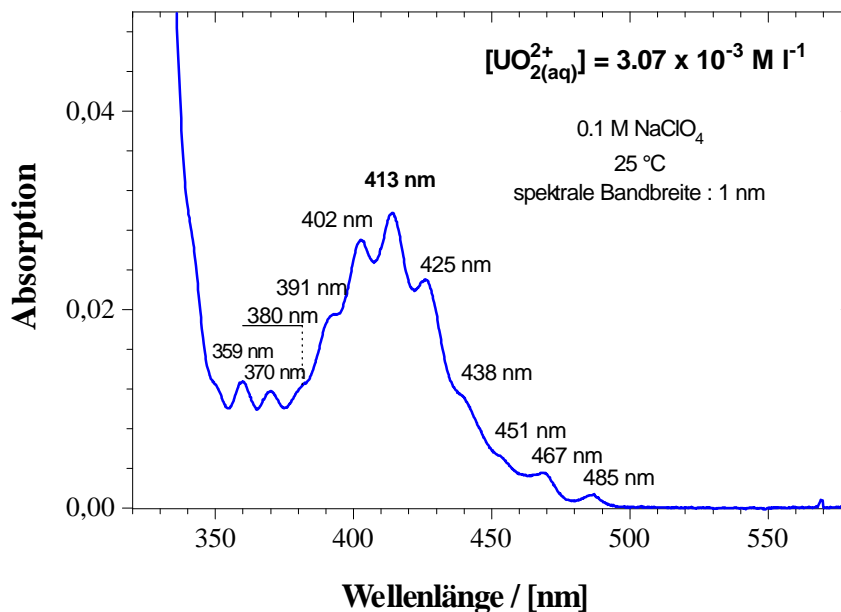


Abb. 3.2 : UV-Vis spectrum of free uranyl ion in 0.1 N NaClO_4

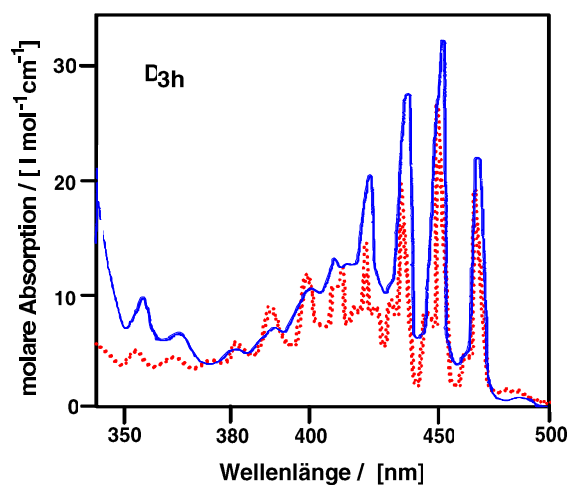


Fig. 3.3 : Typical UV-Vis spectrum of coordination geometry D_{3h} (Görrler-Walrand & Jagere (1972a)). solid : solution species $[\text{UO}_2(\text{NO}_3)_3]^-$. dashed : $\text{NaUO}_2(\text{CH}_3\text{COO})_3$ at 77 K

In literature, close agreement in the spectra of a uranium(VI) coordination in solids at low temperatures and the same coordination in solutions has been pointed out (Volod'ko et al. 1967, Görrler-Walrand et al. 1972a,b, 1973). Intensity and position of electronic transitions seems to be mainly governed from the geometry of equatorial coordination and only to a lesser extend by the chemical nature of the ligands. Each coordination geometry is reported to exhibit a characteristic spectrum while the chemical nature of the ligand is of minor influence.

Coordination geometries lacking a center of inversion, e.g. in case of hexagonally coordinated solution species $\text{UO}_2(\text{NO}_3)_3^-$ and $\text{NaUO}_2(\text{CH}_3\text{COO})_3$ solid (both symmetry D_{3h}) (fig. 3.3) result in an increase in the molar absorption compared to geometries with center of inversion. Those compounds have molar absorptions typically of. $10 \text{ l mol}^{-1} \text{ cm}^{-1}$.

Table 3.1 : Oscillator strengths f of spin- and Laporte forbidden electronic transitions in actinide-, lanthanide- and transition metal complexes

<u>metal ion</u>	f	<u>transition</u>	ϵ [$\text{l mol}^{-1} \text{ cm}^{-1}$]	<u>wavelength</u>	<u>Ref.</u>
UO_2^{2+}	$1.7 \cdot 10^{-4}$	Laporte forbidden	9.7	413.8 nm	Meinrath 1998c
Am^{3+}	$4 \cdot 10^{-4}$	Laporte forbidden	410	503.2 nm	Meinrath 1991
Cm^{3+}	$5 \cdot 10^{-5}$	Laporte forbidden	55.3	396.0 nm	Carnall & Rajnak 1975
Tb^{3+}	$7.5 \cdot 10^{-5}$	Laporte forbidden	0.3	350 nm	Carnall 1976
$\text{Co}(\text{NH}_3)_6^{3+}$	$4 \cdot 10^{-6}$	spin forbidden	0.23	770 nm	Jørgensen 1963
"	$9 \cdot 10^{-4}$	Laporte forbidden	56	472 nm	Jørgensen 1963
LMCT	0.8	allowed	20 000		Sýkora & Sima 1990

LMCT : ligand to metal charge transfer

Solution species and solids with pentagonal symmetry D_{5h} , e.g. $\text{UO}_2\text{F}_5^{3-}(\text{aq})$ and $\text{K}_3\text{UO}_2\text{F}_5(\text{s})$, exhibit characteristic spectra similar to those of $\text{UO}_2^{2+}(\text{aq})$. Molar absorptions of this non-centric coordination is not increased and correspond to molar absorptions of centric symmetries D_{2h} and D_{4h} with ϵ_{max} about $10 \text{ l mol}^{-1} \text{ cm}^{-1}$.

3.2 Emission Spectroscopy

The uranyl ion is luminescent in solutions at room temperature as well as in a great number of solid phases. This luminescence property has caused major attraction devoted to uranium salts and solutions about the turn of the last century. Results of this interest are e.g. discovery of Stokes shift 1852/53 (Stokes 1852, Stokes 1853) and discovery of radioactivity by Becquerel in 1896. Spectroscopic investigations during the 'Manhattan' project were directed primarily to photochemical methods of isotopic enrichment. The huge amount of spectroscopic material collected during 'Manhattan Project' is summarized in two monographs (Dieke & Duncan 1949, Rabinovitch & Belford 1964).

3.2.1 Emission Spectrum

Due to the luminescence emitted by the uranyl(VI) ion by its electronic decay from an electronically excited state, the uranyl ion was considered a 'model case of inorganic photochemistry' (Balzani et al. 1978). Current understanding of the electronic structure of uranyl(VI) indicates that the luminescence is fluorescence, not phosphorescence.

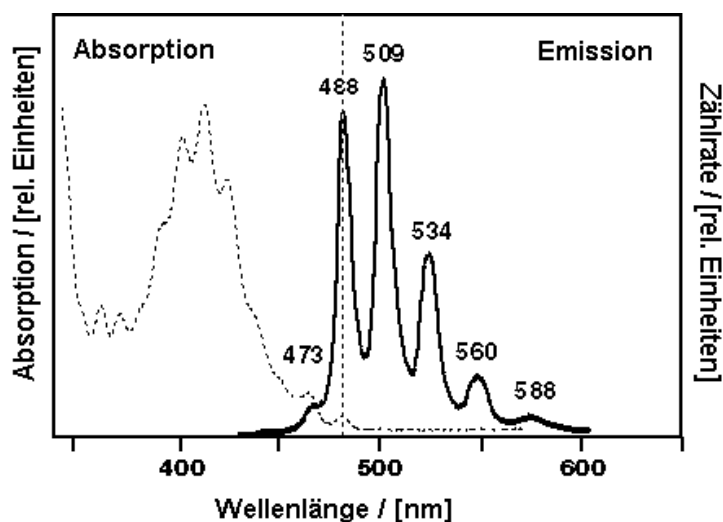


Fig. 3.4 : Emission spectrum (solid) and absorption spectrum (dashed) of free uranyl ion in 0.1 M HClO₄ at 25 °C. Wavelengths given in nm. (Fluorescence spectrum of (Kato et al. 1994)).

The emission spectrum of free uranyl(VI) ion in 0.1M NaClO₄ at 25 °C is given together with its absorption spectrum in fig. 3.4. Absorption and emission spectrum exhibit common bands at 488 nm (emission) / 485 nm (absorption) and 473 nm (emission) / 467 nm (absorption). The absorption band at 488 nm corresponds to the low energy transition to the lowest lying vibronic state of the first excited electronic state, while the emission band at 473 nm corresponds to a transition from an excited vibronic level of the fluorescent state to the electronic ground state ('hot band')

3.2.2 Life Time

The life time of excited uranyl(VI) ion in aqueous solution depends on a series of factors. These factors are e.g. temperature, medium, presence of ligands and quenchers (Benson et al. 1975, Burrows & Kemp 1974). Some data on the life time of the uranyl(VI) fluorescence under various conditions are summarized in tables 3.2 and 3.3. Data in tables 3.2 and 3.3 strikingly illustrate dependence of fluorescence life time from surrounding conditions like temperature and medium. This dependency of fluorescence life time from its electronic environment offers the possibility to use uranyl(VI) as a sensor for processes in solution. This

application in turn requires detailed understanding of influences determining the emission process of uranyl(VI) ion and its life time.

Table 3.2 : life time of uranyl(VI) fluorescence in solution under various conditions

life time [μ s]	conditions	reference
1.24	0.02 M NaClO ₄ , H ₂ O	Hill 1974
2.38	0.02 M NaClO ₄ , D ₂ O	Hill 1974
0.98	0.02 M UO ₂ (NO ₃) ₂ , RT.	Burrows 1990
3	D ₂ O	Kropp 1967
2.5	0.2 M NaClO ₄ , 20 °C, pH 2	Zheng et al. 1986
5.5	0.2 M NaClO ₄ , 5 °C, pH 2	Zheng et al. 1986
1.21	0.1 M UO ₂ (NO ₃) ₂ , pH 1.9	Burrows 1990
1.9 ± 0.2	0.1 M HClO ₄ , RT.	Meinrath et al. 1993
2.1	0.1 M HClO ₄	Moriyasu et al. 1977
8.1 ± 0.6	1.0 M HClO ₄ , RT.	Meinrath et al. 1993
6.8	1.0 M HClO ₄	Moriyasu et al. 1977
1.7 ± 0.1	3.0 M NaClO ₄	Park et al. 1990
11.7	1.0 M H ₂ SO ₄ , 22 °C	Yokoyama et al. 1973
12.7 ± 0.8	1.0 M H ₂ SO ₄ , RT.	Meinrath et al. 1993
10.8	1.0 M H ₂ SO ₄	Moriyasu et al. 1977
10 ± 4	0.67 H ₃ PO ₄ , 28 ± 1 °C	Matsushima et al. 1974
232.1 ± 0.5	1.0 M H ₃ PO ₄ , RT.	Meinrath et al. 1993
187	1.0 M H ₃ PO ₄	Yokoyama et al.1975

RT. : room temperature

Table 3.3 : temperature dependence of fluorescence life time of uranyl(VI) in aqueous solution of 0.02 M UO₂(NO₃)₂ at pH 3 (Formosinho & Miguel 1984)

temperature [°C]	life time in [μ s]
9	2.5
12	2.3
15	2.0
20	1.6
26	1.1
36	0.8
50	0.6

3.2.3 Photochemistry; Quenching by Water and Carbonate

Uranyl(VI) has a rather varied photochemistry. Excited uranyl(VI) is both a good oxidizing and reducing species. Redox reactions in solution take a large share in the photochemistry of U(VI) (Balzani et al. 1978). Taking the standard potential E_0 of reaction



and the low lying excited state at about 2.54 eV ($20\,600 \text{ cm}^{-1}$) results in a reduction potential of excited uranyl of about 2.7 V, an oxidation power comparable to F_2 . Comparison of collision rates e.g. with solvent molecules of typically 10^{12} s^{-1} (Porter 1983) and life times of excited uranyl ions in table 3.2 indicates that e.g. many organic substances can react photochemically with excited uranyl(VI). Examples are oxidation of methanol (Ledwith et al. 1973), aliphatic alcohols (Matsushima 1972, Azenha et al. 1989) and benzaldehyde (Matsushima et al. 1972). Formation of dihalide radicals X_2° ($\text{X}=\text{Cl}, \text{Br}, \text{I}, \text{SCN}$) was reported in solutions of the ions Cl^- , Br^- , I^- and SCN^- (Yokoyama et al. 1974, Burrows & Pedrosa de Jesus 1976, Moriyasu et al. 1977, Burrows 1990). Photochemistry of uranyl(VI) has been summarized in more detail by (Greatorex et al. 1972, Balzani et al. 1978, Jørgensen & Reisfeld 1982, Güsten 1983).

In the framework of present study, two reactions of excited uranyl(VI) are of prominent interest. These reactions are first the reaction with the water molecule itself, second the reaction with CO_2 and its dissociation products HCO_3^- and CO_3^{2-} .

3.2.3.1 Quenching by Water

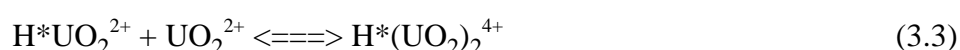
The life time of uranyl(VI) fluorescence shows an isotopic effect as consequence of a solvent change from H_2O to D_2O by a factor of 2 (cf. table 3.2) (Hill et al. 1974). Radiationless relaxation of excited trivalent lanthanide ions however have a much stronger isotopic effect (Haas & Stein 1972), in case of e.g. Eu^{3+} by a factor of 54. This effect has been explained in case of the lanthanides photophysically by resonance of solvent vibronic levels that are higher in case of D_2O compared to H_2O and hence less effective quenchers. To interpret the comparatively weak isotopic effect of uranyl(VI), chemical quenching is usually assumed instead of a photophysical effect (Benson et al. 1975).

Abstraction of hydrogen from water molecules is considered as quenching reaction of excited uranyl(VI) in water. This reaction is interpreted by different mechanisms (Moriyasu et al. 1977, Marcantonatos 1977, Marcantonatos 1980, Formosinho et al. 1984). As evidence for the hydrogen abstraction reaction, two effects are usually given: the above mentioned small isotopic effect of deuterated water on fluorescence life time (cf. table 3.2), and the variation in fluorescence decay time constants as function of pH. While emission of uranyl(VI) ion at low pH (ca. $< \text{pH } 2$) is monoexponential, decay becomes biexponential after raising pH to about 3. Occurrence of biexponential decay however could not yet be predicted and the understanding

of fluorescence behaviour as function of pH thus has been hampered considerable. The pH dependence is explained in literature by different mutually exclusive mechanisms taking hydrogen abstraction as a reaction of central importance.

Moriyasu, Yokoyama & Ikeda (1977) suggest that abstraction of hydrogen by an excited uranyl ion from H_3O^+ is slower than from H_2O and hence explains both the pH dependence of fluorescence life times and observation of biexponential decay curves.

Marcantonatos (1980) discusses hydrogen abstraction by excited uranyl(VI) $^*\text{UO}_2^{2+}$ according to



by formation of a fourfold positively charged coordination compound formed by a uranyl(VI) ion in excited state with a ground state uranyl (exciplex).

Formosinho, Da Graça & Burrows (1984) explain biexponential decay by reversible intersystem crossing between two states of excited uranyl. The reaction kinetics in both cases are found with high energy of activation. Hence, hydrogen abstraction is assumed to play an important role in the mechanism.

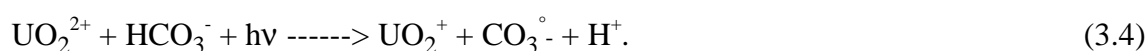
3.2.3.2 Quenching by Carbonate

The carbonate radical $\text{CO}_3^{\circ-}$ exhibits a broad absorption band between 500 nm and 700 nm with a maximum at 600 nm ($\epsilon = 1860 \text{ l mol}^{-1} \text{ cm}^{-1}$) (Behar et al. 1970). It is formed according to



(Neta et al. 1988).

Flash light photolysis of $2 \cdot 10^{-3}$ molar U(VI) solution containing 10^{-2} M NaHCO_3^- resulted in a broad band centred at about 580 nm. The band is interpreted as evidence for formation of $\text{CO}_3^{\circ-}$ radicals (Burrows & Kemp 1974) according to



This observation indicates that carbonate is a possible quencher of uranyl(VI) fluorescence. For reduction potentials of the couple $\text{CO}_2 / \text{CO}_2^{\circ-}$, standard potentials between -2.0 V and -1.9 V are given (Wardman 1989). Quenching by CO_2 therefore is possible, however has not been reported yet. No data are available in literature for the redox couple $\text{CO}_3^{2-} / \text{CO}_3^{\circ-}$.

U(V) is not stable in water and disproportionates according to



Reaction 3.5 is a slow process involving breaking of covalent bonds. Therefore kinetics is slow. Oxidation of UO_2^+ by photochemically produced radicals OH° and $\text{CO}_3^{\circ-}$ therefore is possible and may explain that neither in water nor in carbonate containing solutions formation of U(IV) has been observed after irradiation with light.

Quenching by oxygen has not been observed (Benson et al. 1975, Allen et al. 1978, Güsten 1983) despite the fact that the standard potential of reduction for the couple $\text{O}_2 / \text{O}_2^{\circ-}$ is only about -0.33 V. Concentration of oxygen in aqueous solution is probably too low.

3.2.4 Summary

Fluorescence life time of the excited uranyl(VI) ion depends on a series of influences, e.g. temperature, medium, ligand concentration and presence of quenching substances. These influences are partly difficult to control. The complicated relationship of influencing parameters has led to several mutually exclusive interpretations of uranyl(VI) aqueous solution behaviour. (Formosinho & Da Graça 1984, Park 1990). Comparability of results from different sources therefore is limited. It has to be kept in mind that interpretation of fluorescence behaviour is related to understanding of the electronic structure of uranyl(VI). This discussion, too has been rather controversial.

Discrepant informations concerning composition of hydrolyzed uranyl(VI) solutions introduce further uncertainty in interpretation of pH dependence of uranyl(VI) fluorescence. A major number especially of the earlier and influential contributions are based on interpretation of pH dependence of fluorescence behaviour (Benson et al. 1975, Marcantonatos 1978, Deschaux & Marcantonatos 1979, Marcantonatos 1980, Formosinho et al. 1984, Da Graça et al. 1984). Spectroscopic properties, e.g. relation of absorption spectra and coordination geometry, have either not yet been available or have been ignored. Consequently many results reported on this subject are discrepant. These discrepancies can be appreciated by comparing reported quenching constants of metal ions (Yokoyama et al. 1974, Matsushima et al. 1974, Burrows & Kemp 1974) that scatter for several orders of magnitude (Balzani et al. 1978).

There is univocal evidence that uranyl(VI) in diluted perchlorate medium has a fluorescence life time of about 1 - 2 μs . Temperature, pH value, concentration of potential quenchers and ligands are understood as important influencing factors.

4. Hydrolytic Behaviour of Uranium(VI)

The hydrolytic behaviour of uranium(VI) has intensively been studied since about 1940. This interest is mainly motivated by the importance of uranium in nuclear technologies. Prospection, mining, processing, nuclear fuel production, reprocessing and disposal of nuclear wastes needs a detailed understanding of uranium(VI) in aqueous solutions. In case of hexavalent actinides, onset of hydrolysis is observed already at pH 4. In concentrated solutions above 10^{-3} M U(VI), where uranium(VI) forms oligomeric hydrolysis species, hydrolysis is observed even at pH 3. For the formally pentavalent actinyl ions, e.g. Np(V), onset of hydrolysis is observed only at pH > 9, for the trivalent actinides, e.g. Am(III), at pH > 6.

But relative importance of hydrolysis for an understanding and prediction of its aqueous solution behaviour in technical applications only in part explains the large number of studies directed to hydrolysis of hexavalent uranyl. An additional factor are the oligomeric species formed by uranyl(VI) at elevated concentrations. As will be outlined in the sequel and focused on in the central part of this report, the precise number and composition of oligomeric species actually formed is not yet clear. Furthermore, uranyl(VI) displays fascinating spectroscopic properties, e.g. fluorescence emission. This fluorescence has directed attention to uranium since 1843 when Brewster discovered this property. A further factor is the rather unusual stable hexavalent form of a linear O-U-O unit with surprising kinetic and thermodynamic stability. Similar properties are only to be found with the artificial elements NpO_2^{2+} , PuO_2^{2+} and AmO_2^{2+} . About 5% of all known minerals involve uranium, the vast majority are formed by hexavalent uranium. But for only half a dozen minerals, experimental thermodynamic data has been reported.

To illustrate current discrepancies within our knowledge of uranium(VI) hydrolysis, the recommended data from two recent reviews are given in table. 4.1. It is obvious that both reviews give widely different appraisal, however based on about the same literature data. Discrepancy is not only on certain formation constants but even on the very existence of certain species. It is evident that current situation demands for further investigations.

However it is also evident that mere repetition of studies already available in literature is most probably not very helpful. As a matter of fact, more than 30 studies out of a total of 41 studies reported in the open literature have been done by the same method, that is by potentiometric titration. Other methods applied are solvent extraction, spectroscopic methods or solubility studies.

A critical analysis of U(VI) hydrolysis has to give conclusive answer to the selection of parameters in interpreting the experimental data in terms of statistical evaluation. Furthermore, critical assessment of the results in terms of its capability to predict solution behaviour is necessary.

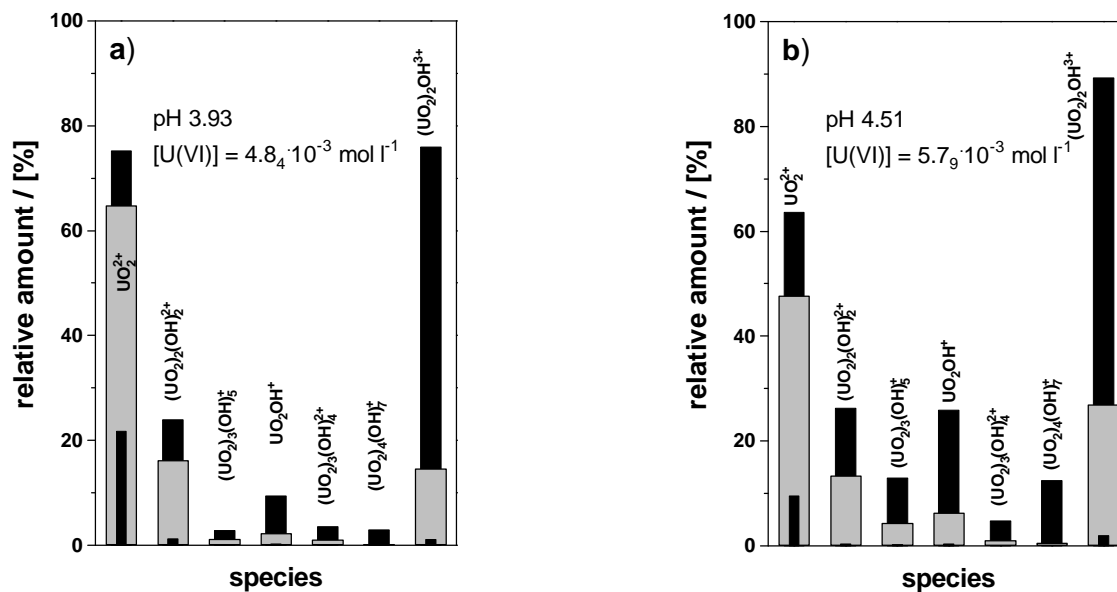
Table 4.1: Comparison of recommended hydrolysis species, their respective formation constants and comments given in (IAEA 1992) and (NEA 1992).

species	IAEA (1992)	NEA (1992)
	lg K° / comment	lg K°
$(\text{UO}_2)_2(\text{OH})_2^{2+}$	-5.54 ± 0.04	-5.62 ± 0.04
$(\text{UO}_2)_3(\text{OH})_5^+$	-15.44 ± 0.10	-15.55 ± 0.12
UO_2OH^+	-5.76 ± 0.10	-5.2 ± 0.3
$\text{UO}_2\text{OH}_2^\circ$	-13.00 ± 0.25	< -10.3
$(\text{UO}_2)_2\text{OH}^{3+}$	-4.06 ± 0.15	-2.7 ± 1.0
$(\text{UO}_2)_3(\text{OH})_4^{2+}$	species not firmly established	-11.9 ± 0.3
$(\text{UO}_2)_4(\text{OH})_7^+$	species not firmly established	-21.9 ± 1.0
$\text{UO}_2(\text{OH})_3^-$	existence in doubt	-19.2 ± 0.4
$(\text{UO}_2)_3(\text{OH})_7^-$	---	-31 ± 2
$\text{UO}_2(\text{OH})_4^{2-}$	only one data/erroneous interpretation	-33 ± 2

It has to be stated explicitly that before the investigations described in the following have been started, no method to assess composition of hydrolysed U(VI) solutions by experimental methods has been advised. The only possibility to assess composition of hydrolysed U(VI) solutions currently available is by calculation based on formation constants summarized in table 4.1. However it is obvious that the discrepancies within the data is by far too large to expect at least some reliability. even for solutions at elevated concentrations above 10^{-4} M U(VI).

Even if a decision is made for one of the both data sets, conclusive results may not be expected. The IAEA data set does not allow correction of ionic strength. For NEA data set, methods for ionic strength correction in terms of Specific Interaction Theory (Scatchard 1936) are recommended. In fig. 4.1a,b, calculation results for species composition of hydrolyzed U(VI) solutions is given. The calculations are based on data and methods recommended by NEA review data (NEA 1992). The conditions selected are almost simple: aqueous perchlorate solutions at an ionic content $\mu=0.1$ M, pH 3.93 (fig. 4.1a) and pH 4.51 (fig. 4.1b), resp. with total uranium concentrations of $4.84 \cdot 10^{-3}$ M (fig. 4.1a) and $5.79 \cdot 10^{-4}$ M (fig. 4.1b). Included into fig. 4.1a,b are the 95% confidence limits obtained from NEA data.

It is evident from fig. 4.1 that no conclusion can be drawn on the likely solution composition from prediction by recommended data. Within 95% confidence limit a species can either be completely absent or a prevailing solution species. This fact is most strikingly illustrated for the $(\text{UO}_2)_2\text{OH}^{3+}$ species. It is straight forward to expect even wider margins if additional species, e.g. sulfato species, were included.



Figs. 4.1a,b : Bar diagrams giving percentual amounts of species in two representative hydrolyzed U(VI) solutions at different pH and total uranium concentration. The composition is predicted by data and methods from (NEA 1992). Mean values are given by grey bars. Black bars representing minimum (front) and maximum (back) species amount predicted within the 95% confidence limit of the recommended data.

The need for a direct method to assess solution composition of hydrolyzed U(VI) solutions is strongly underlined by figs. 4.1a,b. The search for such a method will be focused on in the following. This method will be based on UV-Vis spectroscopic investigations of U(VI). As outlined in the preceding chapters, the spectroscopic properties of U(VI) offer a wide field of unresolved questions. Therefore, the evaluation of single component spectra of well defined solution species is of considerable interest to contribute to fundamental aspects of U(VI) spectroscopy.

Detailed analysis of literature data however leads to the conclusion that the study must be accompanied by careful statistical treatment of experimental evidence. The major means of this statistical treatment will be non-parametric statistics (Bates & Watts 1988, Lord 1945), resampling algorithms like Jackknife and Bootstrap (Efron 1981, Efron & Gong 1983), chemometrics (Malinowski 1991, Otto 1997) and statistical tests like Dixon's Q test (Dixon 1950, Rorabacher 1991). These methods will be briefly introduced together with their application. The reader is however advised to check with the original literature.

4.1 UV-Vis Absorption Spectroscopy of Hydrolysed U(VI) Solutions

A total of 26 UV-Vis absorption spectra of hydrolyzed U(VI) solutions are collected in 0.2 nm steps using quartz cuvettes with pathlength of 1 cm. Signal-to-noise ratio of these spectra is improved by averaging multiple scans. The location of these solutions in the pH-Ig (U(VI)) diagram is shown in fig. 4.2.

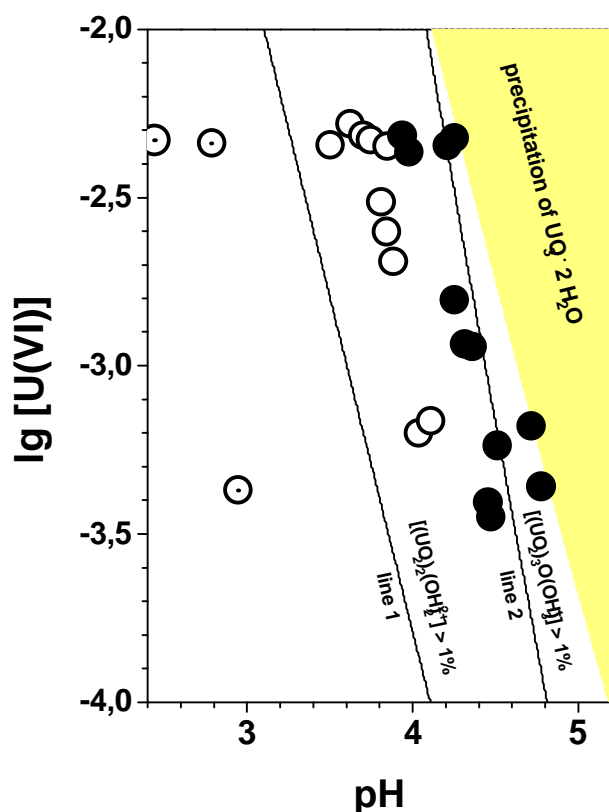


Fig. 4.2 : Uranium(VI) concentrations and pH of 26 samples.

To illustrate the experimental observations, eleven of totally 26 spectra are shown in fig. 4.3. The differences in symbols and colours of figs. 4.2 and 4.3 already take into account results of the subsequent data analysis and are of no significance at present.

Fig. 4.3 further illustrates the need for careful statistical treatment since the spectra are rather weak and do not show a major peak shift that would allow separation of individual species contributions on basis of features characteristic for a certain species. Hence the techniques chosen to approach this problem are advanced chemometric

Since the solution behaviour of U(VI) is interpreted by the assumption that only solution species affect the observed behaviour, occurrence of precipitation effects had to be avoided carefully. Therefore, solubility limits under given conditions have been studied intensively (Meinrath et. al. 1993, Meinrath & Kimura 1993a, Meinrath & Kimura 1993b, Meinrath et al. 1996). The stability limit of the respective solid phase $\text{UO}_3 \cdot 2 \text{H}_2\text{O}$ is given in fig. 4.2 by the yellow area. As can be seen from fig. 4.2, solutions are undersaturated with respect to schoepite $\text{UO}_3 \cdot 2 \text{H}_2\text{O}$.

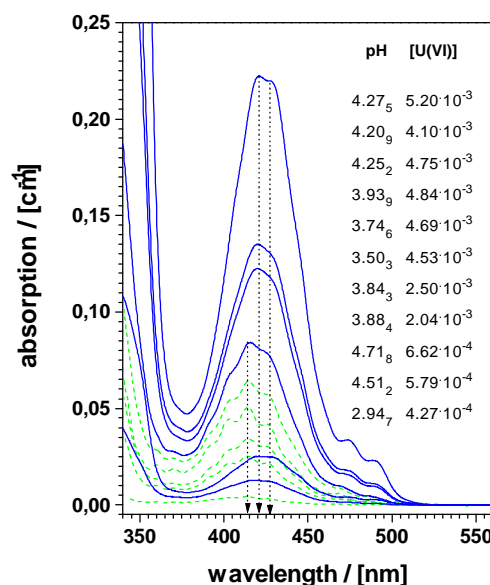


Fig. 4.3 : Selected experimental UV-Vis spectra of hydrolysed U(VI) solutions in the pH range 2.9 to 4.8.

techniques. These chemometric techniques, especially the various methods of factor analysis, offer a series of advantages that are most favourable in given context:

- a) Factor analysis is a model free technique. Thus no a priori assumptions are necessary to analyse a given system.
- b) Factor analysis implicitly takes into account the statistical nature of experimental data. Suitable statistical procedures to cope with this nature are available.
- c) The results of data analysis and decisions made on basis of the numerical analysis are expressed in figures. Therefore, personal bias can be avoided.
- d) Factor analysis treats multiple observations simultaneously. Simultaneous treatment uncovers inconsistency in both data and data analysis that might go unnoticed during a case-to-case spectral deconvolution.

4.2 Factor Analysis

A suitable definition of factor analysis is given by Malinowski (1991) : „Factor analysis is a multivariate technique for reducing matrices of data to their lowest dimensionality by use of orthogonal factor space that yield predictions and/or recognizable factors and analyzes simultaneously multiple observations“.

FA is applicable to data formed by sums of product functions $x_{ik} = \sum y_{ij} z_{jk}$. Such data can be expressed by matrix formulation as $X = Y Z$ and submitted to far-reaching data analysis and modelling. In the following, UV-Vis spectra are analyzed. An experimentally observed absorbance a_{ik} at the wavelength i in solution k is, within the validity range of Beer's Law, a sum of the products of molar absorption ϵ_{ij} of n species with its concentration c_{jk} in the k -th sample according to eq. 4.1:

$$a_{ik} = \epsilon_{i1} c_{1k} + \epsilon_{i2} c_{2k} + \dots + \epsilon_{in} c_{nk} \quad (4.1)$$

The matrix A of absorbances a_{ik} measured at a range of wavelengths i in several solutions k of the same chemical system under varying conditions can be expressed by matrix formulation as $A = E C$, where E is a column matrix of the molar absorbances ϵ of each species at the measured wavelengths and C a row matrix of the concentration c of each species in the individual solutions. Evaluation of the matrix E is of great interest, because the columns of E contain the single component spectra of the relevant species.

Factor analysis aims first at the determination of number n of factors contributing significantly to the absorbance matrix A by application of abstract factor analysis (AFA), yielding abstract factor matrix E' and C' . The abstract factor matrix E' is composed of the column eigenvectors of A , while C' is composed of the row eigenvectors of A . Second, the abstract factor matrices are analyzed by target rotation (Rozett & McLaughlin Petersen 1975, Malinowski 1991, Hopke 1989, Otto 1997) to yield physically interpretable matrices E composed of n columns of single component spectra of U(VI) hydrolysis species and C composed of n rows of species concentrations in each solutions. Third, both spectra and species concentrations are interpreted in terms of a chemical model and analyzed statistically to yield an estimate on the quality of the complete analysis. Finally, the resulting single component spectra are validated by peak deconvolution of mixed species spectra.

The complete procedure is given in the flow sheet fig. 4.4.

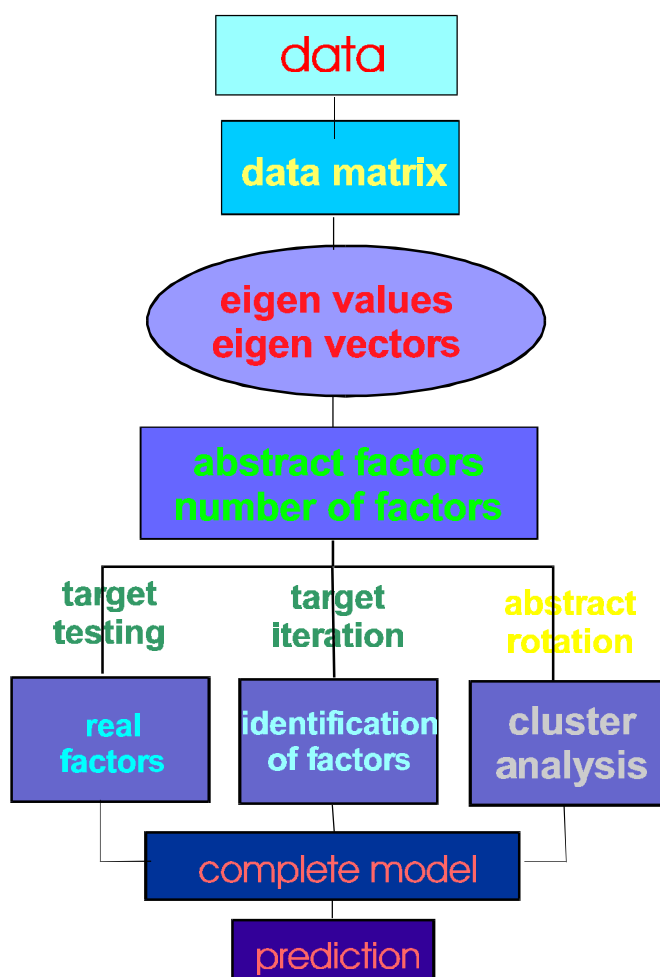


Fig. 4.4 : Conceptual flow sheet of factor analysis procedure

The data matrix A is constructed from 181 UV-Vis absorption data from an experimental spectrum in 1 nm steps in the range 340 nm to 520 nm thus including the steep absorption edge

towards the UV region. The spectral data was arranged in 26 columns, each column holding spectral data of one of the 26 spectra. This experimental data matrix was submitted to AFA.

As shown in the conceptual flow sheet fig. 4.4, the first step of AFA decomposes the experimental data matrix into its eigenvectors and eigenvalues. There are several equivalent techniques to perform this task, e.g. Jacobi rotation (Schönhage 1961), non-linear iterative least squares algorithm (Wold 1966) and Singular Value Decomposition (Golub & Reinsch 1970). By these techniques, observed variances are interpreted by a set of mutually orthogonal vectors (the eigenvectors of matrix A), where each vector is chosen to extract successively as much of the data variance as possible. In this work, SVD algorithm is used for determination of eigenvectors and their eigenvalues λ . A real data matrix A_{rc} , of r rows and c columns with $r \geq c$, is decomposed according to Eq. 3:

$$A_{rc} = U_{rc} S_{cc} V_{cc}^T \quad (4.2)$$

into a unitary matrix U of the column eigenvectors of A, a unitary transposed matrix V of the row eigenvectors of X and a diagonal matrix S, composed of the roots of the eigenvalues of A and elements $s_{ij} = 0$ ($i \neq j$). SVD extracts the roots of eigenvectors in decreasing relevance. The associated diagonal values s_{ii} with $s_{ii}^2 = \lambda_i$ ($\lambda_i = i$ -th eigenvalue) are ordered with decreasing magnitude. It is straightforward to identify

$$U_{rc} S_{cc} = E^\ddagger \quad (4.3)$$

$$V_{cc} = C^\ddagger \quad (4.4)$$

Data matrices E^\ddagger and C^\ddagger contain the requested information, however in an mathematical abstract form and associated with random error and bias.

If experimental data could be obtained unaffected by random errors and bias, AFA would result in a limited number of non-zero eigenvalues in S_{cc} corresponding to the dimensionality of the data matrix, that is the number of factors contributing to the experimental data under investigation. However, experimental data can hardly be obtained without random errors and bias. Therefore, all eigenvalues λ_i are non-zero, albeit usually quickly approaching very small values with increasing i. Decision on the dimensionality of the data space therefore has to be based on statistical tests. Only the n largest eigenvalues λ and the associated column and row eigenvectors are contributing significantly to the experimental variance. The remaining c-n eigenvalues λ° and the associated eigenvectors form the so-called null space or error space (indicated by $^\circ$) and are excluded from the further analysis. Forming matrices E' and C' from the first n row and column eigenvectors only allows calculation of a matrix A' , where random errors and bias are reduced by omitting summation over the null-space (Hopke 1989). Therefore, A' differs from A by the amount of removed random error and bias. The eigenvalues can be understood as a measure of the residual variance not explained by the abstract factors. Therefore, the magnitude of eigenvalues with respect to the unavoidable noise in the data offers access for statistical analysis. Here, several techniques are available.

4.3 Abstract Factor Analysis

The result of abstract factor analysis (AFA) are summarized in Table 4.2 for the first 6 of 26 eigenvalues obtained from application of SVD to the experimental data matrix A.

Table 4.2 : Results of AFA for the first 6 of 26 eigenvalues of data matrix A

λ	uncertainty in eigenvalue (3σ)	RE	χ^2	χ^2 expectation values
1.3468468	0.001023	$9.173 \cdot 10^{-3}$	43599	676
0.0192484	0.000699	$8.132 \cdot 10^{-4}$	2187.3	625
0.001105	0.000675	$3.105 \cdot 10^{-4}$	1456.1	576
0.0000981	0.000645	$2.013 \cdot 10^{-4}$	308.1	529
0.0000033	0.000299	$1.136 \cdot 10^{-4}$	131.9	484
0.0000008	0.000735	$8.083 \cdot 10^{-5}$	31.1	441

Table 4.2 gives the eigenvalues in the first column. It is shown that the eigenvalues rapidly decrease in magnitude. The remaining 20 eigenvalues are even of lower magnitude and are therefore omitted from table 4.2. Included into table 4.2 are the results of three statistical test commonly applied. These tests need an estimate on the average noise in the data. This estimate has been obtained in the present study from an analysis of base line noise and from previous analysis of carbonate complexation of uranium(VI) by UV-Vis spectroscopy (Meinrath 1997b) and set to $\sigma = 3 \cdot 10^{-4} \text{ cm}^{-1}$. However, there is an independent method for assessing an estimate of data noise, the so-called SCREE test (Cattell 1966). This test will be introduced below and shown to corroborate the conclusions from baseline analysis and spectral deconvolutions.

The second column gives uncertainty in eigenvalue (Hugus & El-Awady 1971). The uncertainty in eigenvalue is estimated from an analysis of error propagation in eigenvalue analysis. Calculation is based on the correlation matrix $D = A A^T$, where A^T is the transposed A matrix. Thus, by comparison of the eigenvalues with their uncertainty, the number of significant eigenvalues and therefore the rank of matrix A is the borderline where the uncertainty gets larger than its eigenvalue. This borderline is $n > 3$ in table 4.2. This criterion therefore advocates three significant eigenvalues and therefore three species in solution.

From Theory of Error (Malinowski 1977) figures of merit summarized in table 4.3 can be derived for the root mean square error (or 'real error' in the data matrix) RE, the imbedded error IE and the error XE extracted from the original data matrix X due to omission of the error eigenvectors. These types of error can be calculated from the error eigenvalues λ^o , the rows r and columns c of the respective data matrix A and the number n of significant eigenvalues as obtained from AFA according to Eqs. 4.5 -4.7:

$$IE = \left| \frac{n \sum_{j=n+1}^c \lambda_j^o}{rc(c-n)} \right|^{\frac{1}{2}} \quad (4.5)$$

$$XE = \left| \frac{\sum_{j=n+1}^c \lambda_j^o}{rc} \right|^{\frac{1}{2}} \quad (4.6)$$

$$RE = \left| \frac{\sum_{j=n+1}^c \lambda_j^o}{r(c-n)} \right|^{\frac{1}{2}} \quad (4.7)$$

Table 4.3 : Root mean square error RE, imbedded error IE and extracted error XE as a function of the number n of relevant factors for the first eight factors of matrix A

number n of factors	RE	IE	XE
1	$9.173 \cdot 10^{-3}$	$2.452 \cdot 10^{-3}$	$8.839 \cdot 10^{-3}$
2	$8.132 \cdot 10^{-4}$	$3.074 \cdot 10^{-4}$	$7.529 \cdot 10^{-4}$
3	$3.105 \cdot 10^{-4}$	$1.437 \cdot 10^{-4}$	$2.752 \cdot 10^{-4}$
4	$2.013 \cdot 10^{-4}$	$1.076 \cdot 10^{-4}$	$1.702 \cdot 10^{-4}$
5	$1.136 \cdot 10^{-4}$	$6.789 \cdot 10^{-5}$	$9.109 \cdot 10^{-5}$
6	$8.083 \cdot 10^{-5}$	$5.292 \cdot 10^{-5}$	$6.110 \cdot 10^{-5}$
7	$7.171 \cdot 10^{-5}$	$5.071 \cdot 10^{-5}$	$5.071 \cdot 10^{-5}$
8	$6.279 \cdot 10^{-5}$	$4.746 \cdot 10^{-5}$	$4.110 \cdot 10^{-5}$

The root mean square error RE is a measure of the difference between pure data, unaffected by random errors and bias, and the raw experimental data. The imbedded error IE is a measure of the mean square error between the pure, error- and bias-free data and the data reproduced by matrix multiplication of E' and C'. Finally, extracted error XE is a measure for the diffe-

rence between the reproduced data and the raw data. Table 4.3 indicates the distribution of different types of error as a function of factors assumed to contribute significantly to the variance of the data matrix A. It has been shown further, that RE is always larger than XE and the amount of imbedded error that is not extractable by FA is always larger than zero (Malinowski 1977). The differences in RE between different selections of n give the amount of error taken out by the additional factor(s). As can be seen, this difference is always $> 3 \cdot 10^{-4}$ for 1-3 factors. A fourth factor would carry an average signal of only $1.1 \cdot 10^{-4} \text{ cm}^{-1}$. It would be very difficult to extract information out of such a weak spectroscopic signal. Therefore, the conclusion on three significant factors in the given system is further supported.

The value of XE for three significant factors in table 4.3 indicates an improvement of the experimental data by an average of $2.7 \cdot 10^{-4}$ absorption units per data point due to AFA. It is equally evident from table 4.3 that AFA is able to improve the experimental data, however the imbedded error IE criterion estimates that an average of $1.4 \cdot 10^{-4}$ absorption units of random errors and bias remain in the data reproduced from the first three row and column eigenvectors.

Bartlett's (1950) χ^2 criterion is also calculated from the correlation matrix $D = A A^T$. The eigenvalues λ are the p roots for which eq. 4.8 holds

$$|D - \lambda| = 0, \quad (4.8)$$

where D is a correlation matrix of p variables. For the determinant |D| holds $|D| = \lambda_1 \lambda_2 \dots \lambda_p$.

The test quantity is the χ^2 value

$$\chi^2 = - (n - p + 0.5) \ln D_{p-k} \quad (4.9)$$

where n gives the number of independent observations less one, p gives the degree of freedom and k the number of eigenvalues already tested. The quantity D_{p-k} is calculated by eq. 4.10

$$D_{p-k} = |D| / \left\{ I_1 I_2 \dots I_k \left[\frac{p - I_1 - I_2 \dots I_k}{p - k} \right]^{p-k} \right\} \quad (4.10)$$

Thus, comparing χ^2 with the desired probability level of the tabulated χ^2 distribution, the null hypothesis can be tested for each number of factors. In table 4.2, the χ^2 value is rearranged to make degree of freedom to the test criterion. Hence, a number of factors is considered significant if the value given as χ^2 is larger than the squared degree of freedom, given as χ^2 expectation value in the last column. It is evident that the χ^2 criterion likewise advocates three factors.

As a final test, the SCREE test (Cattell 1966) is given in fig. 4.5. The SCREE test is a plot of the residual percent variance remaining in the data matrix after removing variances explained by the larger eigenvectors. For given data matrix A, the SCREE test is shown in fig. 4.5.

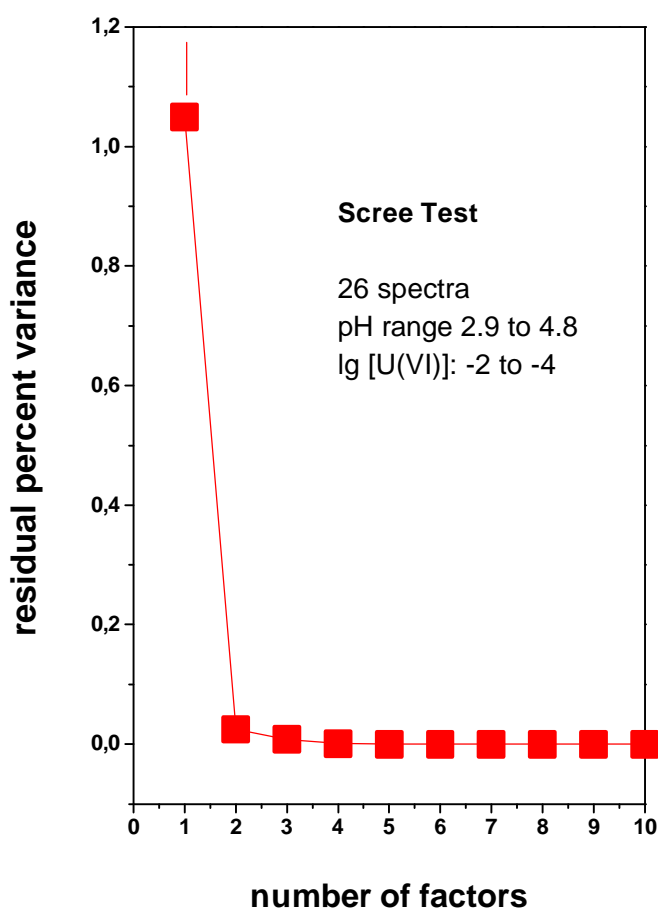


Fig. 4.5 : Residual percent variance as a function of factors (eigenvectors) included into reproduction of the absorption matrix A (SCREE test) (Cattell 1966, Cattell 1978).

By multiplication of a row eigenvector $E_1^\#$ and a column eigenvector $C_1^\#$ vector a matrix $D_{1rc}^\# = E_1^\# C_1^\#$ is obtained. The variance in $D_1^\#$ can be removed from the experimental data matrix A, resulting in a new data matrix $A_1^\#$ that does not contain variance explained by matrix $A_1^\#$; hence $A_1^\# = A - D_1^\#$. Of course, the experimental variance of the second largest column and row eigenvectors can be removed from $A_1^\#$ in a similar way, thus creating matrix $A_2^\#$. The residual variance of matrices $A_n^\#$ can be expressed by the eigenvalues obtained from AFA. This residual variance RV is given by eq. 4.11:

$$RV(A_n^\#) = \sum_{k=n+1}^{k=p} I_k, \quad (4.11)$$

with p giving the total number of eigenvalues, here 26.

If RV is normalized by the total sum of eigenvectors the residual percent variance (RPV) is obtained. This residual percent variance is given in fig. 4.5 as a function of the number of eigenvalues removed from data matrix A. The SCREE test suggests a borderline between statistically significant eigenvalues and eigenvalues due to noise for that value n, for which the RPV curve levels out. In the present case, this decision can be based on linear regression. Those eigenvalues are taken as significant only rising above the 95% confidence limit given by the regression line of points n to p calculated by the well-known procedure of Working and Hotelling (1929). This point is found at n=3 from fig. 4.5. The SCREE procedure therefore takes the three largest eigenvalues as significant, while the remaining $p-3 = 23$ eigenvectors and eigenvalues are considered as noise.

Hence, the result from AFA is a matrix A_3 calculated from the first three eigenvalues and eigenvectors by $A_3 = U_{13} S_{33} E_{3c}$. This implies that instead of 181×26 data points, only 181×3 data points have to be handled in the further data treatment and that bias and noise has been eliminated from the data analysis. Hence, AFA smoothes the experimental data and eases the data analysis.

4.4 Identification of Single Component Spectra

The three factors obtained from AFA however are obtained in a mathematically abstract form and void of physical significance. For illustration the first six abstract factors are shown in fig. 4.6.

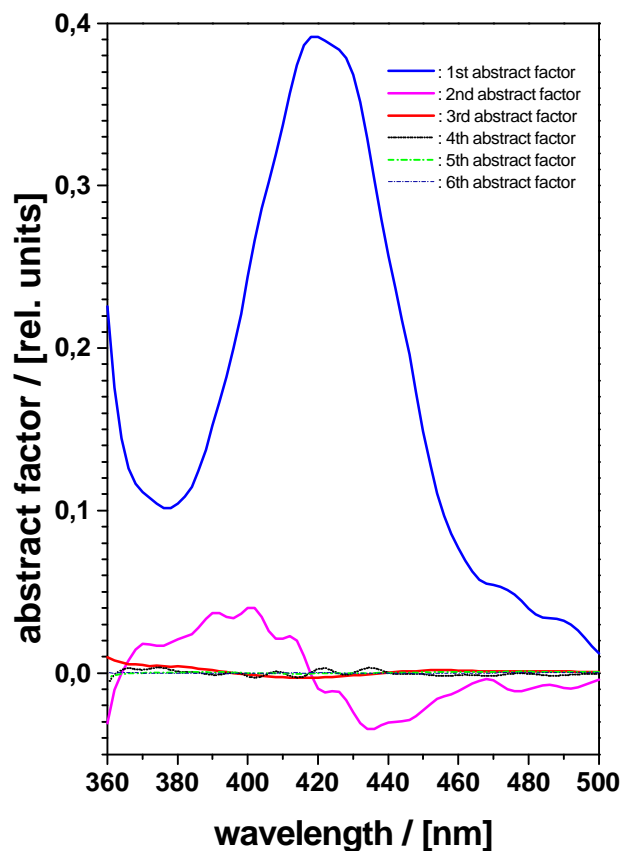


Fig. 4.6 : First six abstract factors. The first three factors only are considered significant.

4.4.1 Identification of the Second Factor

From chemical reasoning it is immediately evident that one factor is the absorption spectrum of the $\text{UO}_2^{2+}(\text{aq})$ ion. In order to get an unbiased estimate on the second factor, the data matrix A was reduced by an iterative procedure for eliminating columns (spectra) with the aim to reduce the third eigenvalue to insignificance. The resulting two-factor matrix D_2 is composed of ten of the 26 spectra. In fig. 4.2, these samples are indicated by open circles.

Further analysis concentrates on the matrix D_2 composed of these ten two-factor spectra. Matrix D_2 is submitted to AFA. The abstract factor matrix is then reduced to matrix $D_2^\ddagger = E^\ddagger C^\ddagger$ of the first two row and column eigenvectors, resp. The further analysis concentrated on the identification of the second factor, because the first factor is already recognized as the $\text{UO}_2^{2+}(\text{aq})$ UV-Vis spectrum. A uniqueness test (Malinowski 1991, Hopke 1989) indicated, that there are no absorptions at wavelengths specific for either of the both factors. Key Set Factor Analysis (Malinowski 1982) therefore is not applicable to separate the both components. An estimate for the yet unknown second component therefore is obtained by repeatedly subtracting an arbitrary amount of a UO_2^{2+} spectrum from a certain two-factor spectrum. The only constraint applied in this procedure was the non-negativity of absorbances in the resulting second-factor test spectrum. By this procedure, sets of possible second factor spectra are obtained. These spectra are then submitted to Target Factor Analysis (TFA) and Target Iteration (Rozett & McLaughlin Petersen 1975, Malinowski 1991, Hopke 1989, Roscoe & Hopke 1981). TFA is a least squares procedure searching the best fit of a suspected factor to a data matrix. One of the benefits of TFA is to improve the targeted factor towards the needs of the data matrix and even to give estimates for unmeasured data points (Malinowski 1991).

To test a suspected factor s_i (e.g. a suspected single component spectrum), a rotation matrix T is needed that rotates the eigenvectors of the abstract matrices E' and C' , which are void of physical meaning, into meaningful vectors. The rotation matrix T can be composed vector by vector, a process called target testing. For a suspected factor s_i (test vector), the transformation vector t_i is obtained from eq. 4.12:

$$t_i = \{D^T D\}^{-1} D^T s_i = D^+ s_i \quad (4.12)$$

where D^T indicates transposed D matrix, D^{-1} indicates the inverse of D matrix and $\{D^T D\}^{-1} D^T = D^+$ is known as the pseudo inverse of D (Peters & Wilkinson 1970).

The result of this procedure is given in fig. 4.7, presenting the spectrum of the second factor as a result of TFA. It is compared to the well-known spectrum of the $\text{UO}_2^{2+}(\text{aq})$ ion. Obviously, the second factor spectrum given in fig. 4.7 is quite similar to the spectrum of dimeric $(\text{UO}_2)_2(\text{OH})_2^{2+}$ from ref. (Meinrath et al. 1993). This finding is not trivial, because until now any reference was made to chemical modelling.

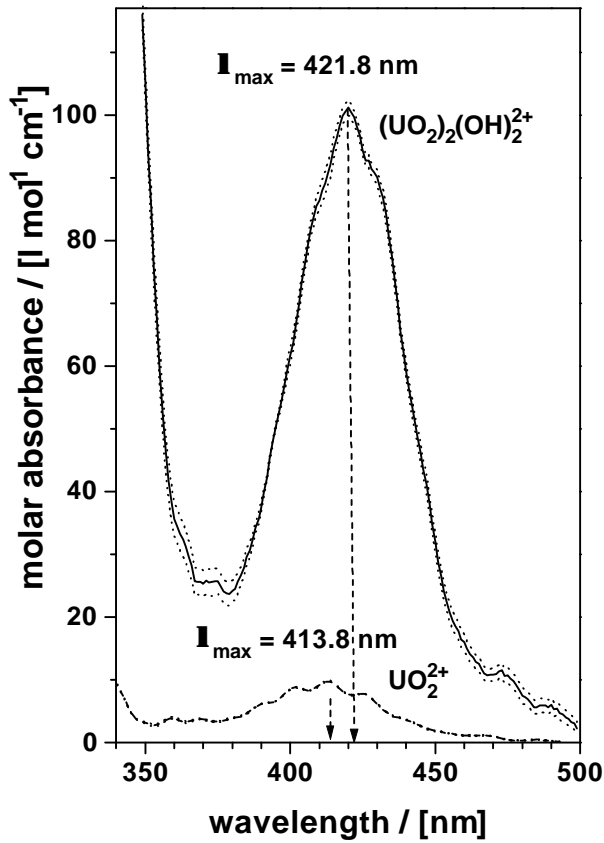


Fig. 4.7 : First two real factors, to be associated with the species $\text{UO}_2^{2+}(\text{aq})$ and $(\text{UO}_2)_2(\text{OH})_2^{2+}$

Target Testing is affected by random errors and bias from both the data matrix and the tested vector s_i . By AFA, errors in the data matrix are reduced. Nevertheless, AFA is not able to generate "pure", error-free data. These errors will also affect a test vector s_i in the Target Transformation eq. 4.12. As estimators for the mutual interaction of matrices E' or C' , test vectors s and predicted vectors x , the following figures of merit have been derived (Malinowski 1978): the apparent error AET in the suspected test vector s :

$$\text{AET} = \left| \frac{\sum_{j=1}^r (s_j - x_j)^2}{r} \right|^{\frac{1}{2}} \quad (4.13)$$

the root mean square error REP in the predicted vector x

$$\text{REP} = \text{RE} (t^T t)^{-\frac{1}{2}} \quad (4.14)$$

and the real error RET in the predicted vector x :

Table 4.4: Estimators RET, AET and REP for the reliability of single component spectra of $\text{UO}_2^{2+}(\text{aq})$, $(\text{UO}_2)_2(\text{OH})_2^{2+}$, $(\text{UO}_2)_3(\text{OH})_5^+$ and $\text{UO}_2\text{CO}_3^\circ$ as well as the value of SPOIL function

species	$\text{UO}_2^{2+}(\text{aq})$	$(\text{UO}_2)_2(\text{OH})_2^{2+}$	$(\text{UO}_2)_3(\text{OH})_5^+$	$\text{UO}_2\text{CO}_3^\circ$
ϵ_{\max}	$9.7 \text{ l mol}^{-1} \text{ cm}^{-1}$	$101 \text{ l mol}^{-1} \text{ cm}^{-1}$	$474 \text{ l mol}^{-1} \text{ cm}^{-1}$	$36 \text{ l mol}^{-1} \text{ cm}^{-1}$
λ_{\max}	413.8 nm	421.8 nm	429.0 nm	400 nm (sh)
(sh:shoulder)				
Matrix A:				
RET	0.05	1.0	4.1	19.6
AET	0.23	1.3	5.8	19.8
REP	0.22	0.8	4.1	2.0
SPOIL	0.22	1.3	(1.0)	10
Matrix B:				
RET	0.15	0.8	8.1	17.56
AET	0.36	1.3	3.0	17.9
REP	0.39	1.0	8.7	3.1
SPOIL	0.4	0.8	0.9	5.6

$$\text{RET} = \left| \frac{\sum_{j=1}^r (x_j - \bar{X}_j)^2}{r} \right|^{\frac{1}{2}} \quad (4.15)$$

The AET parameter estimates effects of Target Transformation on the tested vector s itself. If the suspected factor s is a true factor of the factor space spanned by the matrix E^* (Eq. 4.12), the difference between suspected vector s and predicted vector x will be minimal.

The root mean square error REP estimates interaction between matrix E^* and the vectors s and x , the latter both vectors represented by the norm of the transformation vector t . The real error in the predicted vector RET encompasses as unmeasurable quantity the pure, error-free predicted vector x . However, if the estimators AET and REP are evaluated, RET can be estimated from eq. 4.16:

$$\text{RET} = \sqrt{\text{AET}^2 - \text{REP}^2} \quad (4.16)$$

By eq. 4.16, an estimate on the absolute error in the test vector with respect to its compatibility with the data matrix can be obtained.

In Table 4.4, these estimators are summarized for target testing of single component spectra of $\text{UO}_2^{2+}(\text{aq})$, $(\text{UO}_2)_2(\text{OH})_2^{2+}$ and $\text{UO}_2\text{CO}_3^\circ$ with maxima of molar absorptions: $\epsilon_{413.8} = 9.7 \text{ l mol}^{-1} \text{ cm}^{-1}$ of $\text{UO}_2^{2+}(\text{aq})$, $\epsilon_{421.8} = 101 \text{ l mol}^{-1} \text{ cm}^{-1}$ of $(\text{UO}_2)_2(\text{OH})_2^{2+}$ and $\epsilon_{400.0} = 36 \text{ l mol}^{-1} \text{ cm}^{-1}$ of $\text{UO}_2\text{CO}_3^\circ$ (Meinrath 1997b). The data is tested for two data matrices. Matrix A is composed of all 26 spectra, while data B contains only those spectra that are not two component spectra used to evaluate the single component spectrum of the $(\text{UO}_2)_2(\text{OH})_2^{2+}$ species. Therefore, matrix B does not contain experimental evidence used to derive this spectrum.

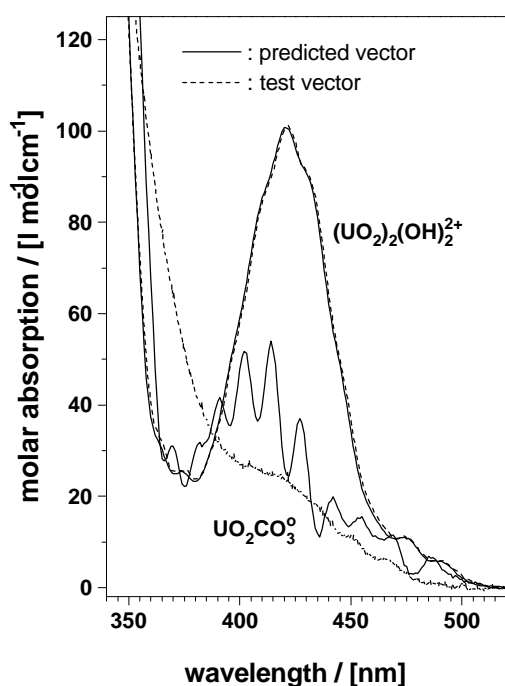


Fig. 4.8 : Effect of target testing on single component spectra $(\text{UO}_2)_2(\text{OH})_2^{2+}$ and $\text{UO}_2\text{CO}_3^\circ$.

Recently, spectroscopic evidence is forwarded that $\text{UO}_2\text{CO}_3^\circ$ is detectable in aqueous U(VI) solution at free carbonate concentrations as low as $\lg [\text{CO}_3^{2-}] > -11$ [Meinrath et al. 1996). In the present case, free carbonate concentrations $\lg [\text{CO}_3^{2-}] \approx -11$ are calculated for solutions at about pH 4.8. Because of the high tendency of U(VI) to form carbonato complexes even at extremely low free carbonate concentrations, $\text{UO}_2\text{CO}_3^\circ$ has been included into the target testing procedure. The poor performance of the $\text{UO}_2\text{CO}_3^\circ$ test vector is evident from table 4.4. The AET is about 50% of the molar absorption at 400 nm. This becomes also evident from the comparison between test vector (the single component spectrum) and the predicted vector of $\text{UO}_2\text{CO}_3^\circ$ in fig. 4.8. The tested vector is strongly distorted. The values of RET and REP in table 4.4 also indicate that the single component spectrum of $\text{UO}_2\text{CO}_3^\circ$ is not part of the vector space spanned by the experimental spectra of either matrix A or matrix B.

The picture looks different for the single component spectra of $\text{UO}_2^{2+}(\text{aq})$ and $(\text{UO}_2)_2(\text{OH})_2^{2+}$. The respective AET estimators in table 4.4 indicate good reproduction of the

test vectors when fitted to the vector space of the experimental data. Furthermore, the estimators AET, RET and REP are of similar magnitude for each test vector, thus indicating that none of the test vector contains gross errors that would affect the validity of the target testing procedures as well as the subsequent analyses. The single component spectrum of $\text{UO}_2^{2+}(\text{aq})$ has been obtained from a single-species solution at high concentration. Its quality is indicated by the small value of RET. The similarity of AET and REP indicates that the main error in the predicted vector originates from the data matrix. The situation is different for the single component spectrum of $(\text{UO}_2)_2(\text{OH})_2^{2+}$. The absolute error in the test vector RET is larger. However, the estimators RET, AET and REP have to be judged relative to the molar absorption ϵ_{max} .

A further helpful estimator is the so-called SPOIL function that indicates the effect of reproducing the data matrix by predicted vector instead of the abstract eigenvectors in E^* . Malinowski (1978) has suggested the SPOIL function as a crude estimate for the acceptability of a predicted vector. SPOIL estimators < 1.5 indicate highly acceptable predicted vectors, while $\text{SPOIL} > 4.5$ indicates only poorly acceptable predicted vectors. From table 4.4, all SPOIL estimates fall into the highly acceptable class with exception of the $\text{UO}_2\text{CO}_3^\circ$ single component spectrum. Therefore, interference of carbonato species in the present study can be excluded with good confidence.

Spectral contributions due to species $\text{UO}_2^{2+}(\text{aq})$ and $(\text{UO}_2)_2(\text{OH})_2^{2+}$ are fully acceptable as relevant factor in the given chemical system. In fig. 4.8, both the test and predicted vector of the single component spectrum of $(\text{UO}_2)_2(\text{OH})_2^{2+}$ are given, the respective rotation vector t_{22} (eq. 4.12) being derived from matrix B. The test vector and the predicted vector are nearly coinciding. Therefore, this single component spectrum is independently validated by data different from those it has been derived from. Furthermore, results are not much different for matrix A, as is indicated by the numerical data given in table 4.4.

4.4.2 Identification of the Third Factor

From these three factors that are found to span the data space of matrix A, two factors are therefore identified and verified by statistical criteria. The following discussion will concentrate on the identification of the third factor.

Several strategies can be adopted to identify the yet unknown single component spectrum of the third factor. A simple iterative procedure is as follows: Select some arbitrary three-component spectra and estimate the chemical composition of the solutions from the known analytical data and some guessed formation constants. Then, by simple matrix operation from

$$Q = Y Z \quad (4.17a)$$

where Q is the absorption matrix composed of n experimental absorption spectra, Y is the yet unknown matrix of single component spectra and Z is the matrix of guessed species

concentrations. Matrix Y, which can be considered as a crude first approximation to the single component spectra matrix E, is obtained by

$$Z^{-1} Q = Y. \quad (4.17b)$$

The assumed number of species n determines the number of spectra to be used in matrix Q.

Since two single component spectra, $\text{UO}_2^{2+}(\text{aq})$ and $(\text{UO}_2)_2(\text{OH})_2^{2+}$, are already known, an iterative procedure can be started that varies the formation constants for calculation of solution compositions in Z in order to minimize the differences between known and estimated single component spectra of UO_2^{2+} and $(\text{UO}_2)_2(\text{OH})_2^{2+}$ in Y.

The various approximations of the single component spectrum of $(\text{UO}_2)_3(\text{OH})_5^+$ thus derived are submitted to Target Iteration as described above. The resulting third-factor spectrum is shown in fig. 4.9.

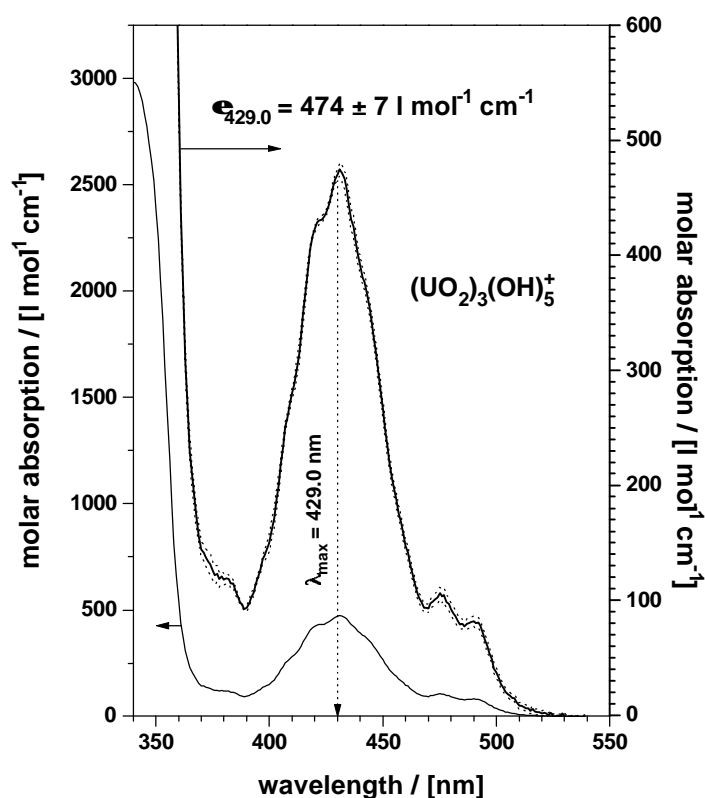


Fig. 4.9 : Single component spectrum of the species $(\text{UO}_2)_3(\text{OH})_5^+$. Dotted lines represent 99% confidence limits.

A molar absorption of $474 \pm 7 \text{ l mol}^{-1} \text{ cm}^{-1}$ at 429.0 nm is found for the low-energy electronic transition, much higher than observed for the $(\text{UO}_2)_2(\text{OH})_2^{2+}$ species of $101 \pm 2 \text{ l mol}^{-1} \text{ cm}^{-1}$. The increase in the molar absorption due to oligomerization of $\text{UO}_2^{2+}(\text{aq})$ to the hydrolysis products is still considerable when normalizing molar absorptions to the number of uranyl(VI) groups per species: 9.7 ($\text{UO}_2^{2+}(\text{aq})$) : 50.5 ($(\text{UO}_2)_2(\text{OH})_2^{2+}$): 158 ($(\text{UO}_2)_3(\text{OH})_5^+$).

By application of the iterative procedure eq. 4.17, it is found that interpretation of the experimental data in the given pH and U(VI) concentration range by a four-species model ($\text{UO}_2^{2+}(\text{aq})$, UO_2OH^+ , $(\text{UO}_2)_2(\text{OH})_2^{2+}$ and $(\text{UO}_2)_3(\text{OH})_5^+$) will either result in negligible UO_2OH^+ concentrations or negative molar absorptions.

4.5 Statistical Treatment

By using the single component spectra of UO_2^{2+} , $(\text{UO}_2)_2(\text{OH})_2^{2+}$ and $(\text{UO}_2)_3(\text{OH})_5^+$, the transformation matrix T can be established from combining the transformations vectors t_{10} , t_{22} and t_{35} of $\text{UO}_2^{2+}(\text{aq})$, $(\text{UO}_2)_2(\text{OH})_2^{2+}$ and $(\text{UO}_2)_3(\text{OH})_5^+$, resp.:

$$T = [t_{10} \ t_{22} \ t_{35}] \quad (4.18)$$

Using the transformation matrix $T = [t_{10} \ t_{22} \ t_{35}]$, the abstract two-factor matrices E' and C' can be transformed into physically meaningful absorption and concentration matrices E containing the estimated single component spectra of the three species and C containing the estimated concentrations of each of these species in the 26 solutions by eq. 4.19 with results summarized in table 4.5:

$$A' = E C = E' T T^{-1} C' \quad (4.19)$$

The application of matrix T in Target Factor Analysis eq. 4.19 yields single component spectra matrix E and concentration matrix C simultaneously. From experimentally determined pH values in each solution and individual species concentrations in each sample, obtained in the columns of matrix C, formation constants of the respective solution species can be calculated. The quality of the factor analysis can further assessed by comparing measured total U(VI) concentrations with those calculated by summing over the species concentrations obtained in matrix C.

It is obvious from the last column (Δ [%]) of table 4.5 that the over-all agreement between calculated and measured total concentrations is satisfactory with a few distinct exceptions. These exceptions are in the data obtained at pH 4.27₅ and pH 4.77₆, where the deviations given by in column Δ [%] indicate extraneous data.

In both data sets, the uncertainty given for $[\text{UO}_2^{2+}(\text{aq})]$ is >1000 %, thus indicating that the spectral contributions due to $\text{UO}_2^{2+}(\text{aq})$ are beyond significance. However, due to the small molar absorption of the $\text{UO}_2^{2+}(\text{aq})$ species, it may nevertheless carry a considerable U(VI) concentration that is missed in the added concentrations of $[\text{U(VI)}]_{\text{calc}}$.

In fig. 4.10, the UV-Vis spectrum at pH 4.27₅ is shown together with the spectral contributions of the individual species. The dashed lines represent 99% confidence limits. It is evident from fig. 4.10 that the spectral contribution of $\text{UO}_2^{2+}(\text{aq})$ is too small to be reliably assessed. As a consequence, formation constants $\lg K'_{35}$ from these both solutions has been

Table 4.5: Individual species concentrations (1σ uncertainty in [%]), calculated and measured U(VI) total concentrations with their percent difference Δ [%]

pH	$[\text{UO}_2^{2+}(\text{aq})]$	$[(\text{UO}_2)_2(\text{OH})_2^{2+}]$	$[(\text{UO}_2)_3(\text{OH})_5^+]$	$[\text{U(VI)}]_{\text{calc}}$	$[\text{U(VI)}]_{\text{meas}}$	Δ [%]
2.44 ₃	$4.77 \cdot 10^{-3}$ (1.4)	-	-	$4.77 \cdot 10^{-3}$	$4.68 \cdot 10^{-3}$	2
2.78 ₆	$4.78 \cdot 10^{-3}$ (1.0)	-	-	$4.78 \cdot 10^{-3}$	$4.58 \cdot 10^{-3}$	4
2.94 ₇	$4.01 \cdot 10^{-4}$ (5.8)	-	-	$4.01 \cdot 10^{-4}$	$4.27 \cdot 10^{-4}$	6
3.50 ₃	$4.32 \cdot 10^{-3}$ (0.7)	$9.33 \cdot 10^{-5}$ (3.6)	-	$4.51 \cdot 10^{-3}$	$4.53 \cdot 10^{-3}$	1
3.62 ₂	$4.59 \cdot 10^{-3}$ (0.5)	$1.99 \cdot 10^{-4}$ (1.4)	-	$4.98 \cdot 10^{-3}$	$5.23 \cdot 10^{-3}$	5
3.70 ₂	$4.03 \cdot 10^{-3}$ (2.3)	$2.59 \cdot 10^{-4}$ (4.2)	-	$4.55 \cdot 10^{-3}$	$4.83 \cdot 10^{-3}$	6
3.74 ₆	$4.50 \cdot 10^{-3}$ (3.7)	$2.38 \cdot 10^{-4}$ (8.2)	-	$4.98 \cdot 10^{-3}$	$4.69 \cdot 10^{-3}$	4
3.81 ₀	$2.54 \cdot 10^{-3}$ (1.1)	$1.45 \cdot 10^{-4}$ (2.3)	-	$2.82 \cdot 10^{-3}$	$3.07 \cdot 10^{-3}$	6
3.84 ₃	$2.10 \cdot 10^{-3}$ (1.9)	$1.54 \cdot 10^{-4}$ (3.1)	-	$2.41 \cdot 10^{-3}$	$2.50 \cdot 10^{-3}$	4
3.84 ₇	$3.62 \cdot 10^{-3}$ (1.7)	$3.83 \cdot 10^{-4}$ (1.9)	-	$4.39 \cdot 10^{-3}$	$4.49 \cdot 10^{-3}$	2
3.88 ₄	$1.83 \cdot 10^{-3}$ (1.4)	$8.27 \cdot 10^{-5}$ (3.8)	-	$2.00 \cdot 10^{-3}$	$2.04 \cdot 10^{-3}$	2
4.03 ₆	$6.35 \cdot 10^{-4}$ (3.1)	$1.17 \cdot 10^{-5}$ (20.1)	-	$6.58 \cdot 10^{-4}$	$6.31 \cdot 10^{-4}$	4
3.93 ₉	$3.68 \cdot 10^{-3}$ (1.0)	$5.06 \cdot 10^{-4}$ (0.8)	$4.49 \cdot 10^{-6}$ (5.0)	$4.71 \cdot 10^{-3}$	$4.84 \cdot 10^{-3}$	3
3.98 ₀	$3.02 \cdot 10^{-3}$ (2.8)	$5.47 \cdot 10^{-4}$ (1.8)	$4.14 \cdot 10^{-6}$ (12.8)	$4.24 \cdot 10^{-3}$	$4.31 \cdot 10^{-3}$	2
4.20 ₉	$2.34 \cdot 10^{-3}$ (3.1)	$7.93 \cdot 10^{-4}$ (1.1)	$5.80 \cdot 10^{-5}$ (0.8)	$4.10 \cdot 10^{-3}$	$4.51 \cdot 10^{-3}$	9
4.25 ₂	$2.78 \cdot 10^{-3}$ (6.7)	$8.18 \cdot 10^{-4}$ (2.7)	$7.37 \cdot 10^{-5}$ (1.6)	$4.64 \cdot 10^{-3}$	$4.75 \cdot 10^{-3}$	2
4.25 ₄	$1.16 \cdot 10^{-3}$ (7.9)	$1.22 \cdot 10^{-4}$ (8.8)	$1.06 \cdot 10^{-6}$ (5.4)	$1.41 \cdot 10^{-3}$	$1.57 \cdot 10^{-3}$	9
4.27 ₅	$1.23 \cdot 10^{-5}$ (>1000)	$1.40 \cdot 10^{-3}$ (1.5)	$1.95 \cdot 10^{-4}$ (0.6)	$3.39 \cdot 10^{-3}$	$5.20 \cdot 10^{-3}$	35
4.31 ₆	$8.70 \cdot 10^{-4}$ (5.7)	$1.34 \cdot 10^{-4}$ (4.4)	$7.81 \cdot 10^{-6}$ (4.0)	$1.16 \cdot 10^{-3}$	$1.16 \cdot 10^{-3}$	0
4.36 ₁	$9.20 \cdot 10^{-4}$ (9.3)	$1.38 \cdot 10^{-4}$ (7.4)	$1.58 \cdot 10^{-5}$ (3.4)	$1.24 \cdot 10^{-3}$	$1.14 \cdot 10^{-3}$	9
4.37 ₈	$5.28 \cdot 10^{-4}$ (6.8)	$6.96 \cdot 10^{-5}$ (6.7)	$5.61 \cdot 10^{-6}$ (4.4)	$7.37 \cdot 10^{-4}$	$6.85 \cdot 10^{-4}$	8
4.45 ₆	$3.51 \cdot 10^{-4}$ (6.9)	$4.04 \cdot 10^{-5}$ (7.0)	$2.77 \cdot 10^{-6}$ (5.4)	$4.40 \cdot 10^{-4}$	$3.93 \cdot 10^{-4}$	10
4.47 ₄	$3.07 \cdot 10^{-4}$ (8.2)	$3.30 \cdot 10^{-5}$ (9.0)	$2.48 \cdot 10^{-6}$ (6.4)	$3.80 \cdot 10^{-4}$	$3.55 \cdot 10^{-4}$	7
4.51 ₂	$3.95 \cdot 10^{-4}$ (6.8)	$7.48 \cdot 10^{-5}$ (4.25)	$4.93 \cdot 10^{-6}$ (3.4)	$5.59 \cdot 10^{-4}$	$5.79 \cdot 10^{-4}$	3
4.71 ₈	$2.83 \cdot 10^{-4}$ (14.6)	$1.38 \cdot 10^{-4}$ (3.8)	$2.35 \cdot 10^{-5}$ (1.1)	$6.12 \cdot 10^{-4}$	$6.62 \cdot 10^{-4}$	7
4.77 ₆	$2.20 \cdot 10^{-7}$ (>1000)	$1.15 \cdot 10^{-4}$ (8.5)	$2.13 \cdot 10^{-5}$ (2.4)	$2.94 \cdot 10^{-4}$	$4.37 \cdot 10^{-4}$	32

evaluated from the concentration of $(\text{UO}_2)_2(\text{OH})_2^{2+}$ and the formation constant $\lg K'_{22} = -6.14_5 \pm 0.08_8$. From this constant and the known concentration of $(\text{UO}_2)_2(\text{OH})_2^{2+}$, an estimation of $[\text{UO}_2^{2+}(\text{aq})]$ can be calculated: $[\text{UO}_2^{2+}(\text{aq})] \approx 3.5 \cdot 10^{-3} \text{ mol l}^{-1}$ for the sample at pH 4.27₅ and $[\text{UO}_2^{2+}(\text{aq})] \approx 3.2 \cdot 10^{-4} \text{ mol l}^{-1}$ for the sample at pH 4.77₆. These contributions are well able to explain the differences between $[\text{U(VI)}]_{\text{calc}}$ and $[\text{U(VI)}]_{\text{meas}}$ in table 4.5.

Factor analysis allows simultaneous treatment of a great number of observations, which in turn is suitable for reliable statistical analysis. The uncertainties given in tables 4.5 and 4.6 have been derived from the residuals between the matrix A of experimental data and the matrix $A' = E C$, calculated on basis of the foregoing factor analysis (Clifford 1973): $\Omega = A - A'$. From the columns ω_i of matrix Ω , an estimator of the residual variance σ_i^2 can be obtained from eq. 4.20:

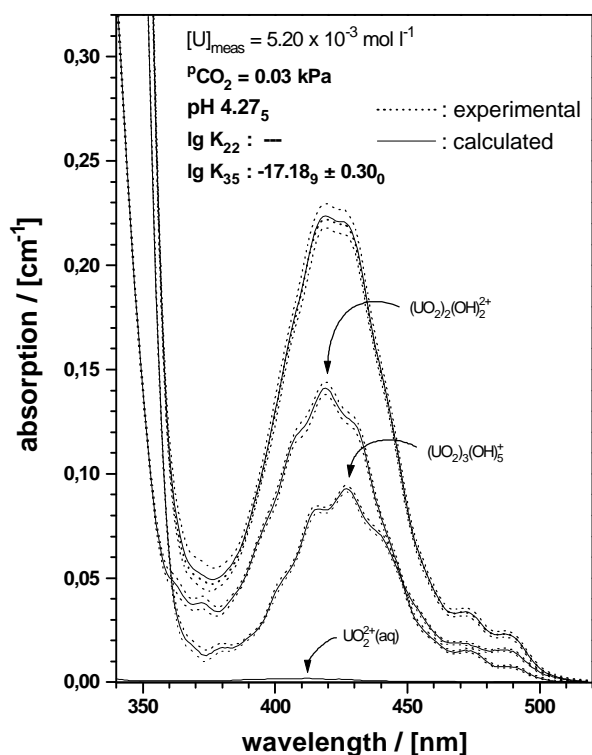


Fig. 4.10 : Spectral deconvolution of the experimental spectrum at pH $4.27_5 \pm 0.03_6$. Dashed lines represent 95% confidence limits in individual species contributions and 99.9% in calculated sum spectrum. The deconvolution is plotted directly from the informations calculated in matrices E and C.

$$\sigma_i^2 = \frac{\omega_i^T \omega_i}{(r - n)}. \quad (4.20)$$

In order to estimate, how these variances transform into estimates of the uncertainties of the concentration matrix C, the variance-covariance matrix Δ of the respective operation is calculated from eq. 4.21

$$\Delta = \sigma_i^2 (E^T E)^{-1} \quad (4.21)$$

The estimators of the standard deviations are given as usual by the square roots of diagonal elements in the variance-covariance matrix Δ . To estimate the uncertainties in the single component spectra, the vectors ω_i in eq. 4.20 are formed by the rows of Ω and r is replaced by c. In eq. 4.21, matrix E is replaced by matrix C (Clifford 1973). The 99% confidence limits given for the single component spectra in figs. 4.7 and 4.9 are calculated by this procedure and

corrected for bias due small sample size by the t-distribution $t_{0.005} = 2.787$ (25 degrees of freedom.).

Table 4.6 : Sample pH (\pm CI), formation constants $\lg K'_{22}$ (\pm CI) including uncertainty from species concentrations (cf. Table 4.5), $\lg K'_{22}$ (pH) including uncertainties from both concentration and pH determination and same data for $\lg K'_{35}$. (confidence intervals CI = 95%)

pH (\pm CI)	$\lg K'_{22}$ (\pm CI)	$\lg K'_{22}$ (pH)	$\lg K'_{35}$ (\pm CI)	$\lg K'_{35}$ (pH)
2.44 ₃ \pm 0.03 ₉	-	-	-	-
2.78 ₆ \pm 0.03 ₅	-	-	-	-
2.94 ₇ \pm 0.02 ₂	-	-	-	-
3.50 ₃ \pm 0.03 ₂	-6.12 ₇ \pm 0.04 ₃	\pm 0.10 ₇	-	-
3.62 ₂ \pm 0.02 ₈	-6.08 ₇ \pm 0.02 ₁	\pm 0.07 ₇	-	-
3.70 ₂ \pm 0.04 ₂	-6.02 ₂ \pm 0.07 ₇	\pm 0.16 ₀	-	-
3.74 ₆ \pm 0.02 ₈	-6.24 ₃ \pm 0.13 ₄	\pm 0.19 ₀	-	-
3.81 ₀ \pm 0.01 ₉	-6.08 ₆ \pm 0.03 ₉	\pm 0.07 ₇	-	-
3.84 ₃ \pm 0.01 ₉	-5.96 ₅ \pm 0.05 ₉	\pm 0.09 ₇	-	-
3.84 ₇ \pm 0.04 ₀	-6.04 ₉ \pm 0.04 ₅	\pm 0.12 ₅	-	-
3.88 ₄ \pm 0.01 ₈	-6.19 ₇ \pm 0.05 ₇	\pm 0.09 ₃	-	-
4.03 ₅ \pm 0.01 ₇	-6.42 ₆ \pm 0.24 ₆	\pm 0.28 ₀	-	-
3.93 ₉ \pm 0.02 ₉	-6.12 ₆ \pm 0.02 ₃	\pm 0.08 ₂	-17.29 ₁ \pm 0.06 ₉	\pm 0.21 ₄
3.98 ₀ \pm 0.02 ₇	-6.00 ₃ \pm 0.06 ₅	\pm 0.11 ₉	-17.27 ₆ \pm 0.18 ₉	\pm 0.32 ₄
4.20 ₉ \pm 0.03 ₈	-6.07 ₉ \pm 0.06 ₃	\pm 0.13 ₉	-16.94 ₀ \pm 0.08 ₇	\pm 0.27 ₇
4.25 ₂ \pm 0.02 ₅	-6.36 ₄ \pm 0.21 ₂	\pm 0.26 ₂	-16.97 ₇ \pm 0.25 ₆	\pm 0.38 ₁
4.25 ₄ \pm 0.01 ₆	-6.30 ₁ \pm 0.14 ₂	\pm 0.17 ₃	-17.29 ₀ \pm 0.19 ₃	\pm 0.27 ₃
4.27 ₅ \pm 0.03 ₆	-	-	-17.18 ₉ \pm 0.23 ₆	\pm 0.41 ₆
4.31 ₆ \pm 0.02 ₁	-6.20 ₃ \pm 0.13 ₆	\pm 0.17 ₈	-17.05 ₅ \pm 0.18 ₃	\pm 0.28 ₈
4.36 ₁ \pm 0.01 ₅	-6.32 ₉ \pm 0.22 ₈	\pm 0.25 ₈	-17.04 ₈ \pm 0.27 ₉	\pm 0.35 ₄
4.37 ₈ \pm 0.01 ₆	-6.26 ₂ \pm 0.17 ₅	\pm 0.20 ₇	-16.98 ₄ \pm 0.21 ₆	\pm 0.29 ₆
4.45 ₆ \pm 0.01 ₆	-6.21 ₆ \pm 0.17 ₉	\pm 0.21 ₁	-17.02 ₃ \pm 0.22 ₇	\pm 0.30 ₇
4.47 ₄ \pm 0.02 ₀	-6.22 ₂ \pm 0.22 ₀	\pm 0.26 ₀	-16.98 ₅ \pm 0.27 ₄	\pm 0.37 ₄
4.51 ₂ \pm 0.01 ₇	-6.16 ₃ \pm 0.15 ₅	\pm 0.18 ₉	-17.20 ₆ \pm 0.20 ₈	\pm 0.29 ₃
4.71 ₈ \pm 0.01 ₉	-6.04 ₈ \pm 0.30 ₁	\pm 0.33 ₉	-17.12 ₅ \pm 0.41 ₄	\pm 0.50 ₉
4.77 ₆ \pm 0.01 ₄	-	-	-17.34 ₄ \pm 0.23 ₆	\pm 0.30 ₆

In table 4.6, confidence intervals of derived formation constants inversely correlate with the respective concentration estimates of $\text{UO}_2^{2+}(\text{aq})$ (cf. table 4.5). This correlation mainly affects the uncertainties in $\lg K'_{35}$, because $\lg K'_{22}$ can be determined at sufficiently high $\text{UO}_2^{2+}(\text{aq})$ concentrations in a two-component system (Meinrath et al. 1993, Meinrath & Schweinberger 1996). The constant $\lg K'_{35}$ however has to be determined in a three-component system at

comparatively low $\text{UO}_2^{2+}(\text{aq})$ concentrations. Nevertheless, the mean values of $\lg K'_{35}$ are quite consistent, thus indicating satisfactory precision of the chemometric approach, while the statistical procedures draw a correct picture of the relations and correlations within the analyzed system.

4.6 Estimation of Uncertainties in pH Values

Calculated formation constants $\lg K'_{22}$ and $\lg K'_{35}$, given in table 4.6 in the second and fourth column, resp., take into account 95% confidence intervals in the evaluated species concentrations given in brackets in table 4.5, while pH is treated as an error-free quantity. Due to the strong dependence of the formation constants of $(\text{UO}_2)_2(\text{OH})_2^{2+}$ and $(\text{UO}_2)_3(\text{OH})_5^+$:

$$\begin{aligned}\lg K'_{22} &= \lg [(\text{UO}_2)_2(\text{OH})_2^{2+}] - 2 \lg [\text{UO}_2^{2+}(\text{aq})] - 2 \text{pH} - 2 \lg \gamma_{\text{H}^+} \\ \lg K'_{35} &= \lg [(\text{UO}_2)_3(\text{OH})_5^+] - 3 \lg [\text{UO}_2^{2+}(\text{aq})] - 5 \text{pH} - 5 \lg \gamma_{\text{H}^+}\end{aligned}$$

on pH with a factor of 2 and 5 resp., it is highly desirable to have an estimate on the uncertainty associated with an individual pH measurement. Unfortunately, procedures recommended by IUPAC for determination of pH (Bates 1981, Covington et al. 1983) are not designed to allow for an estimation of statistical parameters associated with a given measurement. Furthermore, two independent procedures are incorporated into the IUPAC recommendations: the single standard pH scale of the British Standard Institution (BSI) (Covington et al. 1983) and the so-called "bracketing procedure" of NIST (Bates 1981). In given context, BSI definition seems especially unsuitable, because it is incorporating the theoretical Nernstian slope of an electrochemical cell to relate glass electrode potentials to pH values. However, by thermodynamical reasoning, it has been shown that glass electrodes will not exhibit ideal Nernstian behaviour (Baucke 1994). These points have been discussed elsewhere in more detail (Naumann et al. 1994) and are confirmed in this study.

Therefore, an approach based on a multiple point calibration procedure is chosen that has been the laboratory procedure during the past decade. Recently, this procedure has been suggested independently as standard pH calibration procedure (Baucke et al. 1993). A combination glass electrode is calibrated against several pH standards traced back to NIST reference material. The data pairs (mV vs. pH) are interpreted by conventional linear regression and the statistical parameters are evaluated by linear calibration curves (Mandel & Linnig 1957). A detailed outline is given in (Meinrath 1997a).

From statistical treatment of experimental data, unbiased 95% confidence limits are estimated for each pH value and given in the first column of table 4.6. These uncertainties have been included into the estimation of standard deviations for each of the $\lg K'_{22}$ and $\lg K'_{35}$ in the third and fifth column of table 4.6. As shown in the Appendix, variances in pH within the 95%-limits given in the first column of table 4.6 are consistent and correspond to random errors associated with the determination of pH. The precision ξ of pH determination is found to be $\xi = \pm 0.02_5$

pH units. This ξ value is in agreement with values reported for ξ in the literature (Ebel 1978, Schmitz 1994, Davison & Woof 1985, Stapanian & Metcalf 1990, Metcalf 1987).

Comparison of columns $\lg K'_{xx} (\pm CI)$ to columns $\lg K'_{xx} (pH)$ (xx is either 22 or 35) in table 4.6 further shows that uncertainty in pH determination contribute in similar magnitude to the over-all uncertainty in the derived formation constant as does the uncertainty in determination of single species concentrations.

4.7 Evaluation of Formation Constants

The derived formation constants given in table 4.6 are not fitting parameters. Chemometric analysis yields single species concentrations from the inverse of transformation matrix T, derived from least squares procedure on matrix E*. Up to this stage, no chemical model applies. A chemical model is introduced eventually to interpret the data in matrix C. Consistency of formation constants given in table 4.6 therefore is an additional confirmation of present analysis.

From the individual formation constants and their associated uncertainties, mean values and 95% confidence limits can be evaluated by distribution-free order statistics. First, the consistency of data is tested by Q test on extraneous data (Dixon 1950, Rorabacher 1991). Q testing is a commonly applied procedure to test on outlying data, if the data's distribution function is unknown. The tested data are the upper and lower extreme values of $\lg K'_{22}$ and $\lg K'_{35}$, resp in table 4.6. By applying this test procedure, confidence levels are found always larger than 50%. Therefore, to discard any of the tested values as extraneous data is incorrect with high probability. In other words, Q test indicates that the variances observed within the evaluated formation constants in table 4.6 are due to random effects only and gross errors are absent.

To investigate for consistency of derived data, non-parametric statistics (Lord 1947) are used to evaluate confidence limits of the formation constants $\lg K'_{22}$ and $\lg K'_{35}$. Confidence intervals CI are calculated from the range δ of the data and a confidence factor t_{δ} , which is 0.122 (95% confidence interval) for 21 observations and $t_{\delta} = 0.170$ for 14 observations (Lord 1947), according to:

$$CI_{95\%} = \delta t_{\delta(0.95)} \quad (4.22)$$

From eq. 4.22 and the ranges $\delta(\lg K'_{22}) = 0.461$ and $\delta(\lg K'_{35}) = 0.404$, the following unweighted data are calculated:

$$\begin{aligned} \lg K'_{22} &= -6.16_8 \pm 0.05_6 \\ \lg K'_{35} &= -17.12_3 \pm 0.06_9 \end{aligned}$$

An alternative procedure calculates mean values and standard deviations from data sets of varying reliability by weighted means, where the weights are the reciprocals of the squared standard deviation (Korin 1975) given in table 4.6 for each datum. The results are:

$$\lg K'_{22} = -6.14_5 \pm 0.08_8$$

$$\lg K'_{35} = -17.14_2 \pm 0.13_8$$

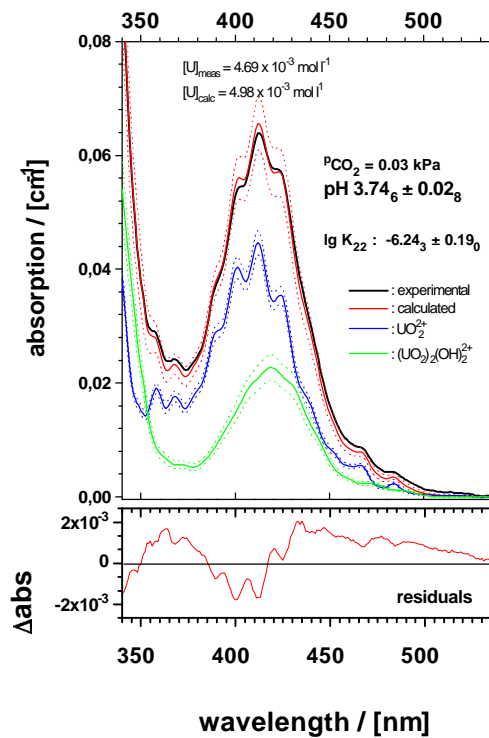
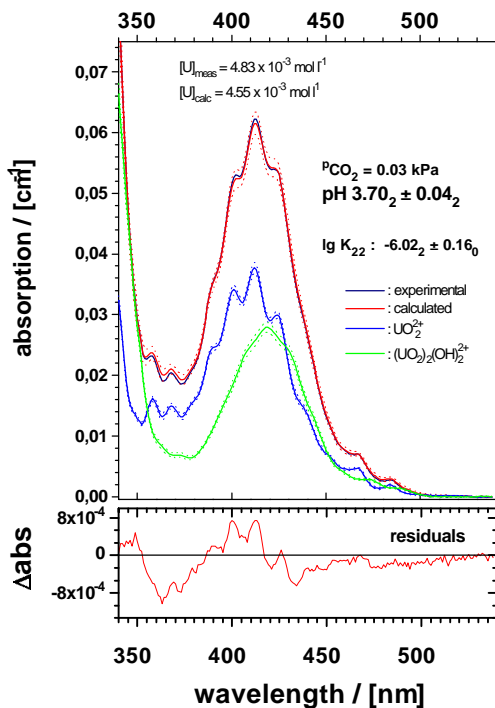
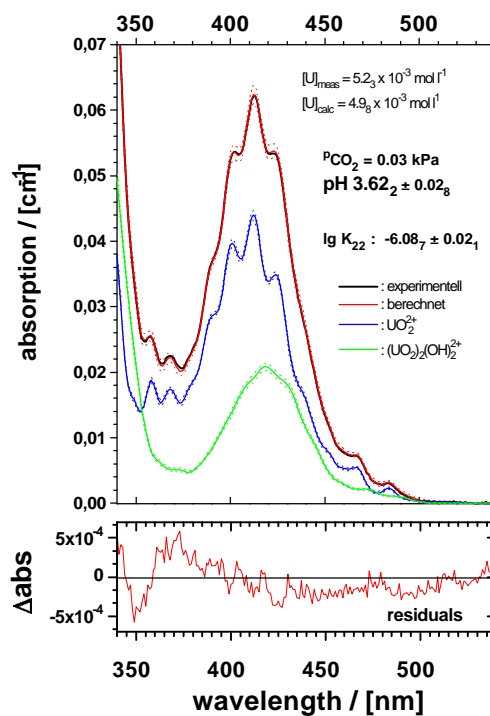
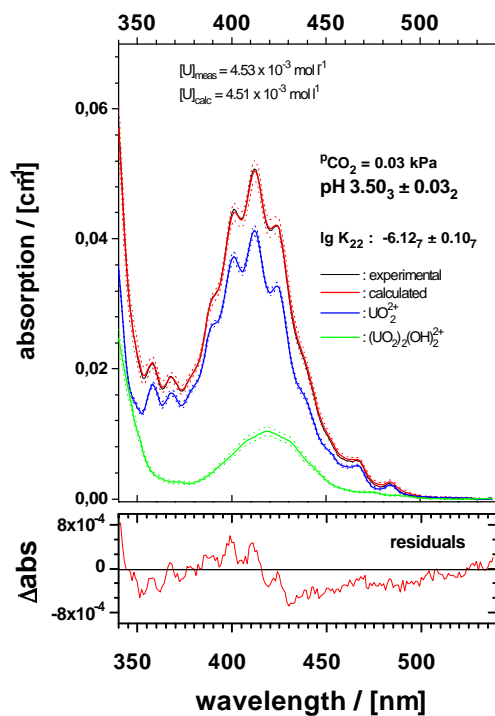
The mean values and 95% confidence limits derived from the both evaluation methods are not significantly different.

Results of the foregoing analysis have been included into figs. 4.2 and 4.3. In fig. 4.3, three-factor spectra are given as blue curves, three-factor spectra in green. The open circles in fig. 4.2 have been identified by factor analysis as two-component spectra, while the dot-centred circles are pure $\text{UO}_2^{2+}(\text{aq})$ spectra. The solid circles are three-component spectra. The lines 1 and 2 are calculated from the formation constants obtained in this study. These lines indicate presence of $(\text{UO}_2)_2(\text{OH})_2^{2+}$ and $(\text{UO}_2)_3(\text{OH})_5^+$ with relative concentrations above 1%. Thus the foregoing analysis lead to a clear picture of hydrolysed U(VI) solutions. As will be outlined in the chapter 6 of this report, this quite unexpected consistency can answer a series of question that have been unresolved problems of U(VI) spectroscopy.

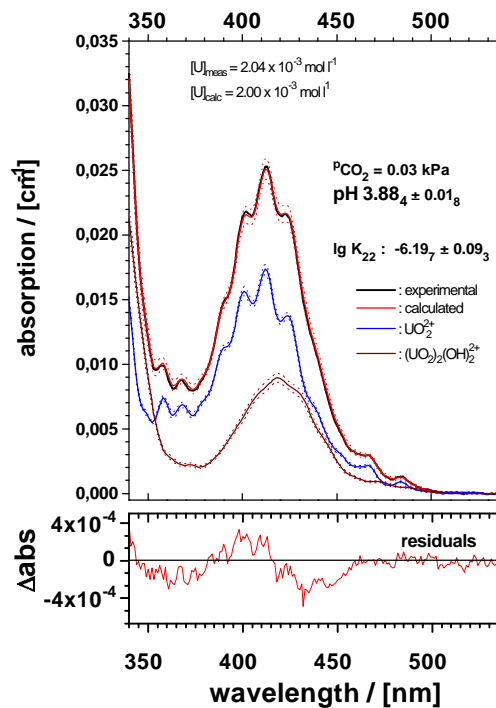
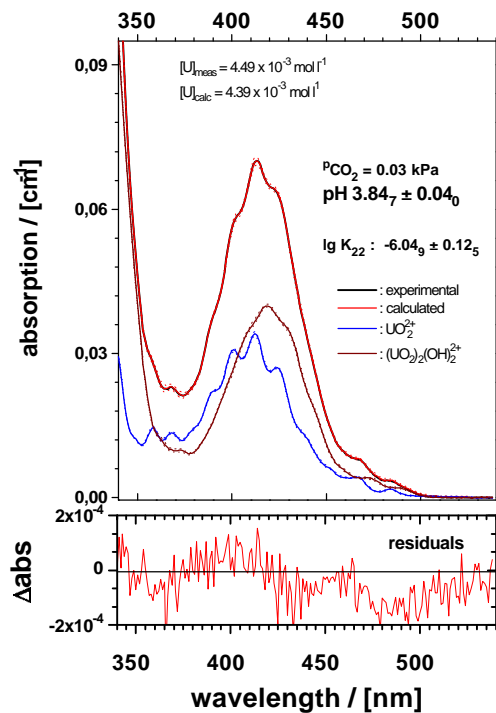
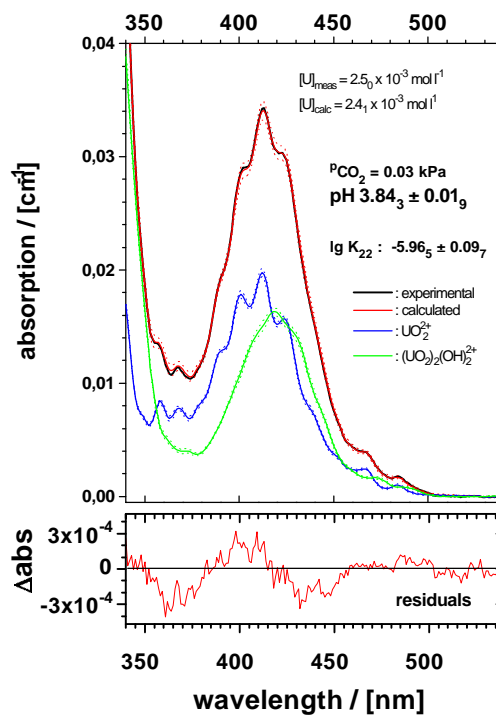
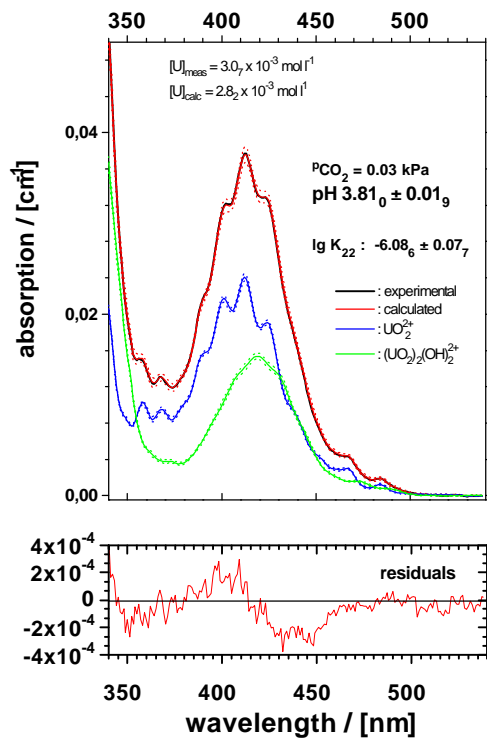
Due to the importance of U(VI) hydrolysis in many fields like nuclear waste disposal, UO_2 pellet corrosion, remediation of areas contaminated by uranium mining and last not least safety analysis of nuclear waste repositories as well as in databases for geochemical modelling, these results are of major importance.

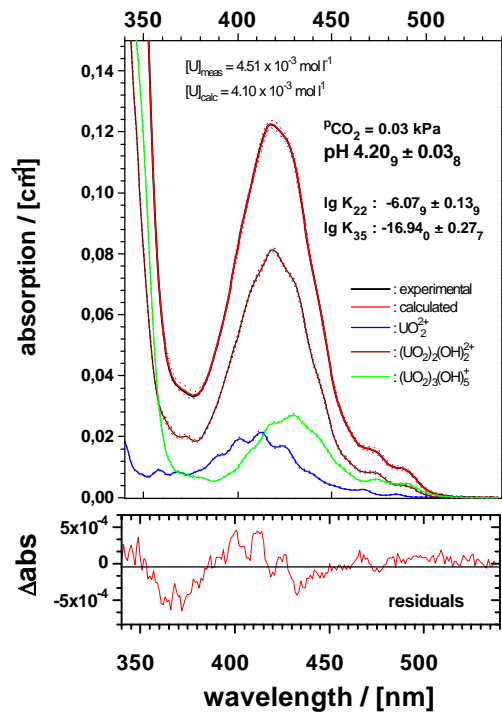
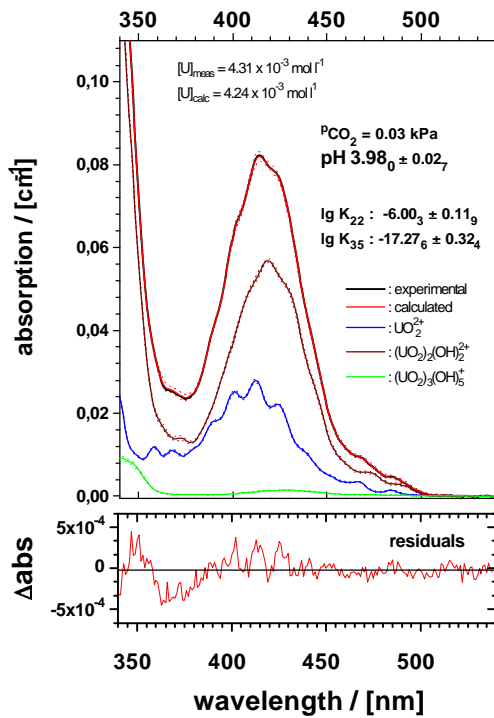
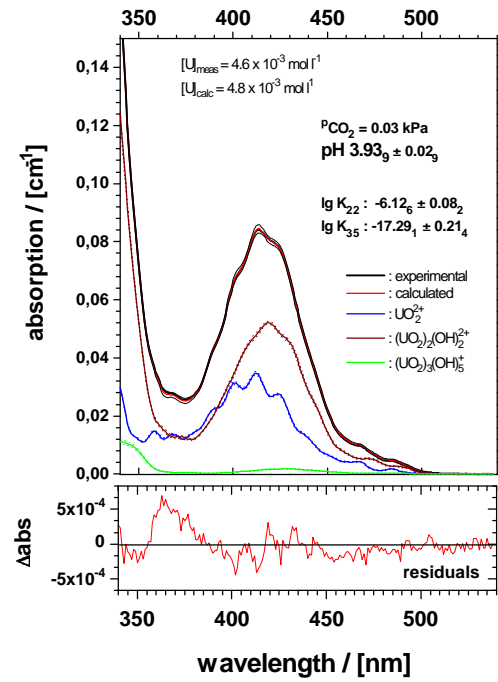
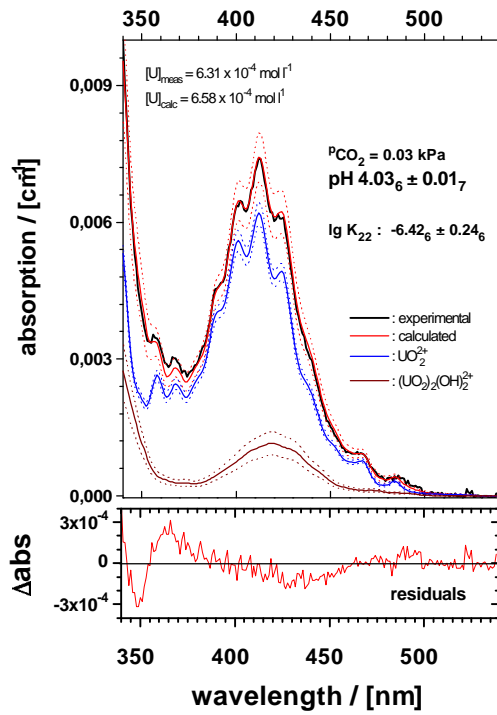
In the following, decisive evidence will be forwarded that these results are sound and consistent.

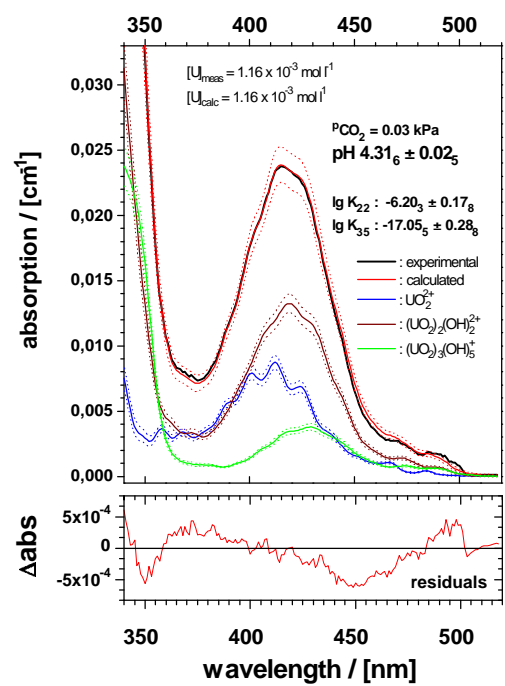
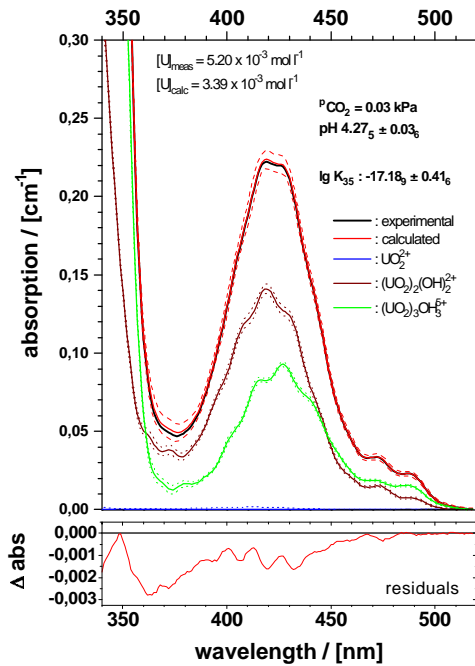
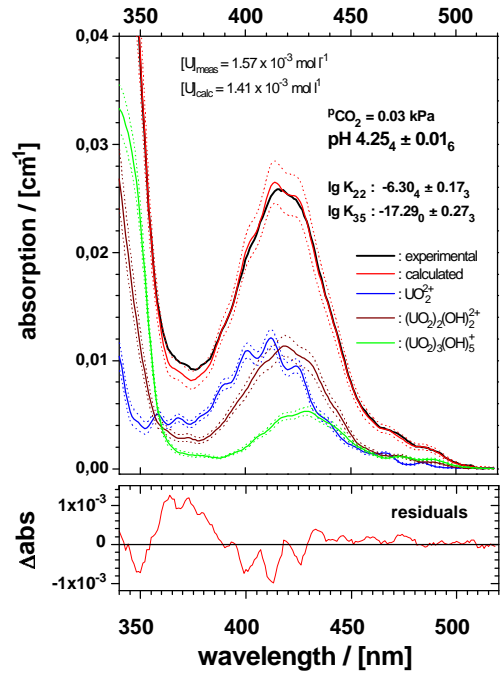
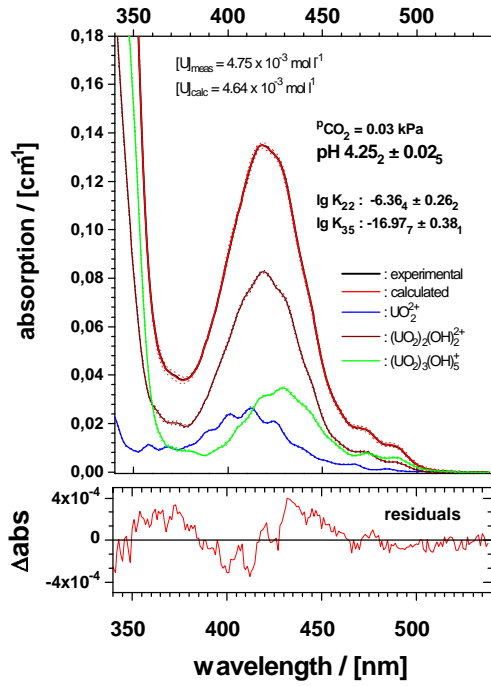
5. Deconvoluted Spectra

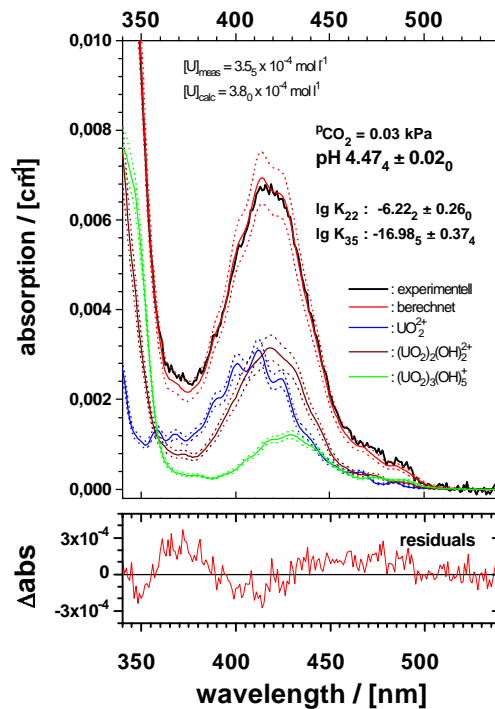
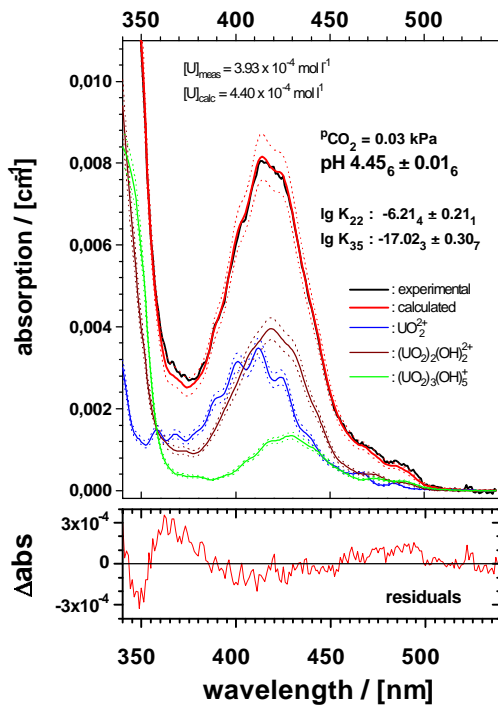
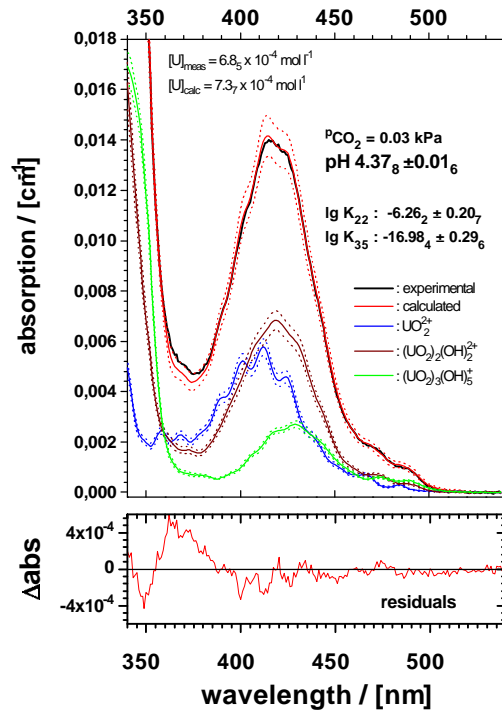
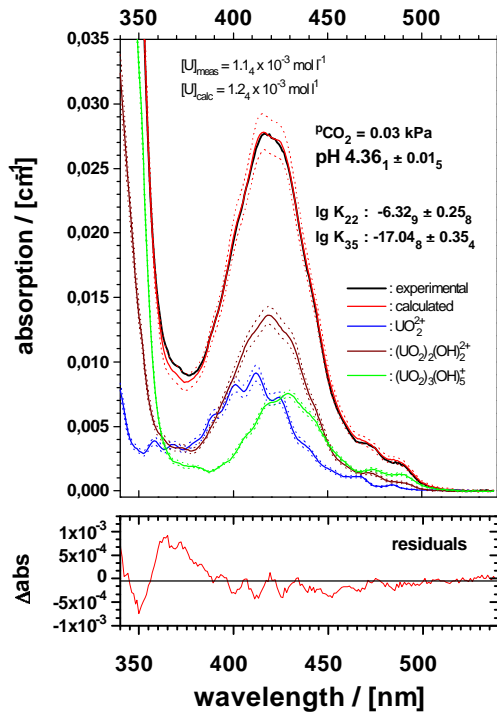


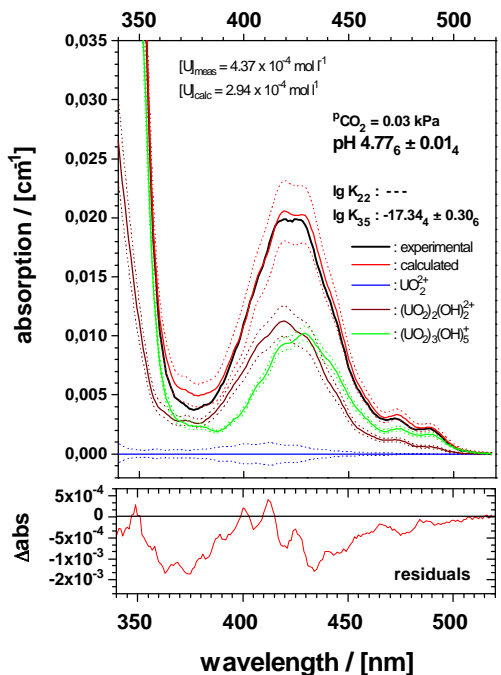
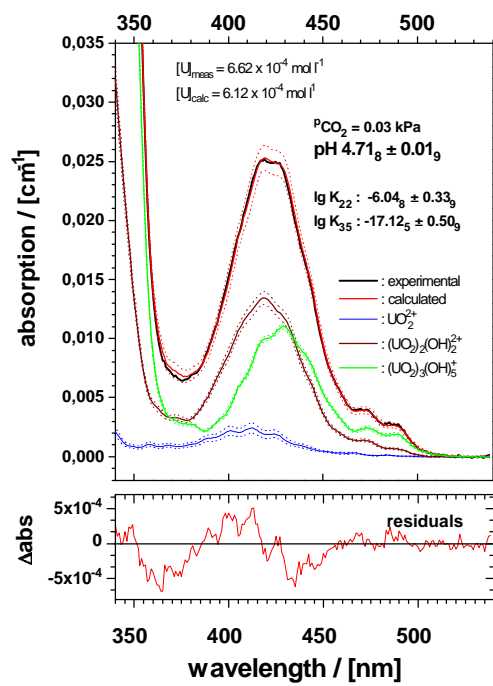
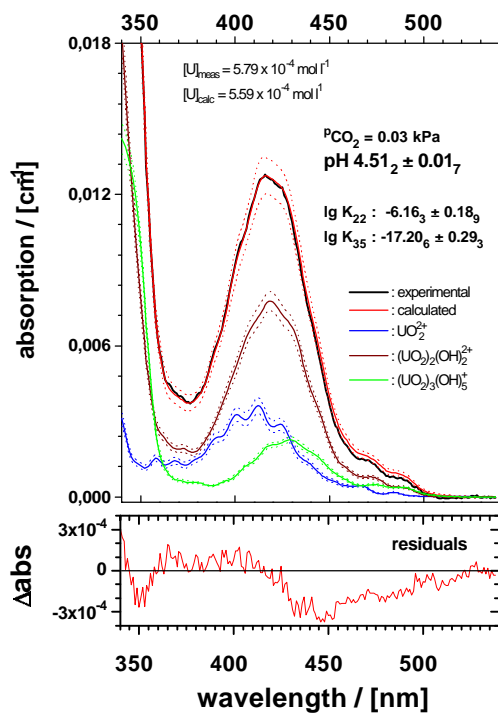
As a first evidence, deconvolution of 23 two- and three-component hydrolysis spectra are given in the following. All parameters of these spectra are given in tables 4.5 and 4.6.











The set of 23 interpreted spectra of hydrolyzed U(VI) solutions proves that only three factors are necessary to quantitatively understand the behaviour. These conditions correspond to the concentration range studied in the overwhelming amount of currently available literature data, especially by potentiometric titrations.

A final validation of these single-component spectra is obtained, if the spectra can be shown to satisfactorily interpret solutions of hydrolyzed U(VI) species under different conditions. This has been demonstrated recently (Meinrath 1998d) in a quantitative manner. Any hint on unexplained experimental variance has been observed despite the fact that the U(VI) concentration range is further extended.

In table 5.1, some experimental conditions studied in selected references are given for illustration. It is evident that investigation of U(VI) hydrolytic behaviour is preferentially studied at elevated U(VI) concentrations, while few data are available for U(VI) concentrations below 10^{-4} M. Only studies at a constant ionic strength of 0.1 M have been included in table 5.1 because a) these studies are compatible with conditions discussed here and b) the pH range accessible for experimental study is probably even more limited at higher ionic strengths due to formation of sparingly soluble uranates. There is agreement in recent literature that $\text{UO}_3 \cdot 2 \text{H}_2\text{O}(\text{s})$, the solubility limiting solid of U(VI) under ambient conditions and $\text{pH} < 7$, readily transforms to a sodium containing uranate at $\text{pH} > 7$ even at low ionic strength of $\mu = 0.1$ M NaClO_4 (Kramer-Schnabel et al. 1992, Meinrath 1997b). Formation of uranates with other cations, e.g. Ca^{2+} , Mg^{2+} or Ni^{2+} is reported (Vochten & Van Haverbeke 1990, Vochten et al. 1991). Thus, in studies at higher concentrations of background electrolytes, the solubility of U(VI) will be further reduced, requiring detailed analysis of these new phases and their specific interaction with the system to be studied.

Table 5.1 : Experimental conditions and methods summarized from some representative studies of U(VI) hydrolysis reported in literature for $\mu = 0.1$ M solutions at 25 °C.

lg [U(VI)] range	pH range	method	conditions	ref.
-2 to -3.5	4 - 4.8	sol.	NaClO_4	Meinrath & Kimura 1993
-2.5 to -4	4 - 4.8	sol.	NaClO_4	Kato et al. 1996
-2.5 to -4.6	4.3 - 5.7	sol.	NaClO_4	Kramer-Schnabel et al. 1992
tracer	5.3 - 7.3	extr.	NaClO_4	A
-3	2.8 - 4.8	tit.	KNO_3	B
tracer	4.5 - 7	extr.	NaClO_4	C
-2.7 to -3	5 - 8.5	tit.	NaClO_4	D
-3 to -3.3	3 - 7	tit.	KNO_3	E
-3	3.8 - 4.7	tit.	NaClO_4	F
-1 to -4	2.5 - 12.5	tit.	NaNO_3	G
-2.7 to -3.7	3.2 - 6	tit.	KNO_3	H
-2 to -3.3	1.9 - 6.1	tit.	NaClO_4	I

sol. : solubility study; extr. : solvent extraction; tit. : potentiometric titration

A: Choppin, G.R., Mathur, J.N. (1991): *Radiochim. Acta*, **52/53**, 25

B: Kotvanova, M.K., Evseev, A.M., Borisova, A.P., Torchenkova, E.A., Zhakarov, S.V.: (1984), *Moskow Univ. Chem. Bull. (USA)*, 37

C: Caceci, M.S., Choppin, G.R. (1983): *Radiochim. Acta*, **33**, 207

D: Maya, L.; (1982): *Inorg. Chem.*, **21**, 2895

E: Overwoll, P.A., Lund, W. (1982): *Anal. Chim. Acta*, **143** (1982), 153

F: Vainiotalo, A., Mäkitie, O. (1981): *Finn. Chem. Lett.*, 102

G: Pongi, N.K., Double, G., Hurwic, J. (1980): *Bull. Soc. Chim. Fr.*, I-347

H: Sylva, R.N., Davidson, M.R. (1979): *J. Chem. Soc. Dalton Trans.*, 465

I: Tsymbal, C. (1969): Report CEA-R-3476, CEA/Saclay

Hence, a series of investigations from different laboratories have been devoted to a precise assessment of $\text{UO}_3 \cdot 2 \text{H}_2\text{O}(\text{s})$ solubility limits in the past half decade. Previous knowledge has been found sparingly and questionable (Meinrath & Kimura 1993). Results are summarized in (Meinrath et al. 1996). By reference to table 5.1, it becomes evident that the 26 solutions given in fig. 4.2 cover the U(VI)-pH region investigated in previous studies and therefore allow for direct comparison. These data furthermore provide a consistent set of evidence that further oligomeric hydrolysis species, e.g. $(\text{UO}_2)_2\text{OH}^{3+}$

The comparison of experimental ranges studied in literature with fig. 4.2 further indicates that conditions investigated in a series of literature studies have lead to supersaturated solutions. To give a striking example, Maya (1982) investigates U(VI) hydrolysis in pH and concentration range within the stability field of the $\text{UO}_3 \cdot 2 \text{H}_2\text{O}$ phase. The marked difference between both the reviews of IAEA (1992) and NEA (1992) as well as the results of present study has to be explained by the different weight the precipitation problem has received during the different evaluations.

Comparison of table 5.1 with fig. 4.2 strongly suggests that species not verified from direct spectroscopic assessment have entered discussion on basis of studies in supersaturated solutions. It has further to be noted that a structure of these additional hydrolysis species has apparently never been discussed. For species verified here by UV-Vis spectroscopy, detailed structural analyses are available (Åberg 1969, Åberg 1970).

Formation constant $\lg K'_{22}$ has been reported rather consistently, ranging between $-5.68 \leq \lg K'_{22} \leq -6.45$. In contrast, formation of $(\text{UO}_3)_3(\text{OH})_5^+$ has been reported with a scatter of more than two orders of magnitude $-15.64 \leq \lg K'_{35} \leq -17.7$ in 0.1 M solutions, despite comparable experimental conditions. Figure 4.2 shows that $(\text{UO}_2)_3(\text{OH})_5^+$ is formed only in minute relative amounts in a pH region close to the saturation limit and therefore can not be detected precisely by concentration dependent methods. UV-Vis spectroscopy is in a more comfortable situation because of high molar absorptions found for these species: $\epsilon_{421.8} = 101 \pm 2 \text{ l mol}^{-1} \text{ cm}^{-1}$ for $(\text{UO}_2)_2(\text{OH})_2^{2+}$ and $\epsilon_{429.0} = 474 \pm 7 \text{ l mol}^{-1} \text{ cm}^{-1}$ for $(\text{UO}_2)_3(\text{OH})_5^+$ to be contrasted with $\epsilon_{413.8} = 9.7 \pm 0.2 \text{ l mol}^{-1} \text{ cm}^{-1}$ found for UO_2^{2+} . The lowest $(\text{UO}_2)_3(\text{OH})_5^+$ concentration speciated in this study was $(1 \pm 0.25) \cdot 10^{-6} \text{ mol l}^{-1}$.

6. Comparison with Fluorescence Spectra

Luminescence of hexavalent uranium in solution and solid state has been known for more than 150 years. Study of luminescence behaviour of the UO_2^{2+} entity has given -direct or indirect- rise to several fundamental discoveries like the Stokes shift or discovery of radioactivity. Uranyl(VI) luminescence is currently understood being a result of the molecular $\text{O}=\text{U}=\text{O}$ structure and the fluorescent state being the lowest lying member of a manifold of a manifold of electron transfer states (Jørgensen & Reisfeld 1982, Denning et al. 1997b).

Application of U(VI) luminescence to speciation of U(VI) however has forwarded discrepant results and interpretations. Especially dependence of fluorescence behaviour on pH is discussed in terms of mutually exclusive interpretations. While in acidic solutions luminescence decay is single-exponential with a emission life time of about 1 μ s, a double-exponential decay has been reported when pH was shifted to about pH 3 (Deschaux & Marcantonatos 1979) with a longer life time of the second decay. Double-exponential decay is interpreted by formation of an exciplex $\text{H}(\text{UO}_2)_2^{4+}$ (Deschaux & Marcantonatos 1979), reversible crossing between two electronically excited states *U and *X (Formosinho et al. 1984) or formation of additional solution species, e.g. UO_2OH^+ (Zheng et al. 1986) or $(\text{UO}_2)_2(\text{OH})_2^{2+}$ (Park et al. 1990, Meinrath et al. 1993), resp. These interpretations are in satisfactory agreement with the respective reported experimental results. To reject any of these interpretations in favour of another is found difficult (Jørgensen & Reisfeld 1982). The present discussion will forward conclusive experimental evidence to reject two of the three interpretations.

In the sequel, correlations between UV-Vis and fluorescence spectra of U(VI) species are reported. Since similar data could not be found in literature, suitable data have been evaluated in exhaustive studies during the past half decade. Carbonato and hydrolysis species have been selected for these studies because the structures of these compounds in solution are available, the UV-Vis spectra are accessible with reasonable effort and spectral features of single component spectra are found characteristic for each species. Both hydroxide and carbonate readily coordinate to the UO_2^{2+} entity and it is known that these coordination is accompanied by drastic spectroscopic changes.

The following discussion therefore not only offers new insight into fundamental properties of U(VI) photophysics but also into the consistency of interpretations adopted for interpretation of the chemical systems under study. Due to restriction of space, only a abbreviated discussion will be given. A complete description of the work will be given elsewhere.

The UV-Vis absorption spectrum of $\text{UO}_2^{2+}(\text{aq})$ is characterized by a broad and unusually weak transition with a maximum at 413.8 nm and integral oscillator strength $f_{10} = 1.4 \cdot 10^{-5}$ (Jørgensen & Reisfeld 1982), superimposed by the symmetric stretching vibration of the linear $\text{O}=\text{U}=\text{O}$ group (Rabinovitch & Belford 1964). This characteristic low energy electronic transition is followed by a steeply increasing absorption continuously extending toward the UV region without characteristic features.

In non-complexing aqueous solutions, fluorescence life time of UO_2^{2+} fluorescence is about 1 μ s at 25 °C. Dependence of the fluorescence life times as well as the emission spectra from temperature and presence of quenchers like inorganic and organic substances, e.g. Fe(III), Cl⁻ and carboxylic acids or alcohols (Güsten 1983) has been studied in detail.

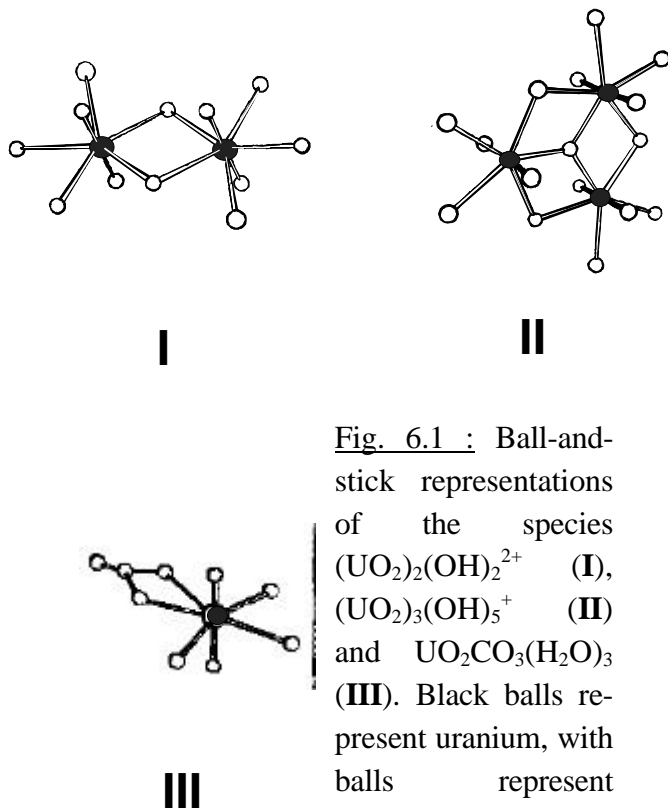


Fig. 6.1 : Ball-and-stick representations of the species $(\text{UO}_2)_2(\text{OH})_2^{2+}$ (**I**), $(\text{UO}_2)_3(\text{OH})_5^+$ (**II**) and $\text{UO}_2\text{CO}_3(\text{H}_2\text{O})_3$ (**III**). Black balls represent uranium, with balls represent oxygen, The carbonate atom is given grey.

Uranium(VI) is forming oligomeric hydrolysis species in aqueous solutions (Sutton 1949, Rush & Johnson 1963) and solution structures of the species are shown in fig. 6.1 (Åberg 1970, Meinrath 1996). It is obvious that the species $(\text{UO}_2)_3(\text{OH})_5^+$ should be given as $(\text{UO}_2)_3\text{O}(\text{OH})_3^+$. To avoid confusion with literature, the former, more common formula is retained. The carbonate species **III** is included. The correct formula $\text{UO}_2\text{CO}_3(\text{H}_2\text{O})_3$ will be abbreviated as $\text{UO}_2\text{CO}_3^\circ$ in the following. A uranyl entity in species **I** - **III** is approximately pentagonally coordinated in the equatorial sphere. In **I**, the average O-U distance is 240 pm. The same holds for **II**, but with 223 pm the central oxygen is closer to uranium than the other oxygens (Åberg 1970). For $\text{UO}_2\text{CO}_3^\circ$, 240 pm - 243 pm have been found as the most likely U-O distances (Meinrath 1996).

Table 6.1: Spectral data of the species UO_2^{2+} , $(\text{UO}_2)_2(\text{OH})_2^{2+}$, $(\text{UO}_2)_3(\text{OH})_5^+$ and $\text{UO}_2\text{CO}_3^\circ$

	UO_2^{2+}	$(\text{UO}_2)_2(\text{OH})_2^{2+}$	$(\text{UO}_2)_3(\text{OH})_5^+$	$\text{UO}_2\text{CO}_3^\circ$
absorption spectrum				
absorption maximum [nm]	413.8	421.8	429.0	400 (sh)
molar absorption [$\text{l mol}^{-1} \text{cm}^{-1}$]	9.7 ± 0.2	101 ± 2	474 ± 7	36 ± 3
integral oscillator strength f per U atom	$1.7 \cdot 10^{-4}$	$1 \cdot 10^{-3}$	$2 \cdot 10^{-3}$	$1.6 \cdot 10^{-3}$
emission spectrum				
life time [μs]	0.9 ± 0.3	2.9 ± 0.4	7 ± 1	35 ± 5
emission maxima [nm]	473, 488 509, 534, 560, 588	499, 519 542, 556	500, 516 533, 554	450(sh), 464 481, 504 532, 548(sh)
Stokes threshold [nm]	488 ± 0.7	479 ± 1	499 ± 1.5	464 ± 0.9

sh: shoulder

Correlations between absorption and emission spectra of compounds **I** - **III** are given in figs. 6.2-6.4. Since an absolute fluorescence intensity measure does not exist, fluorescence intensities are given in relative units and no detailed conclusions concerning relative intensities between different spectra should be drawn from fig. 6.2 - 6.4. Since fluorescence emission depends on the amount of absorbed radiation according to eq. 6.1 (Perkampus 1995)

$$I_{f,\theta} = I_o \cdot \phi_f \cdot 2.303 \cdot \epsilon_\lambda \cdot c \cdot d, \quad (6.1)$$

with

$I_{f,\theta}$: fluorescence intensity at wavelength θ

I_o : intensity of the excitation source

Φ_f : fluorescence quantum yield

ϵ_λ : decadic molar absorption at excitation wavelength λ in $\text{l mol}^{-1} \text{cm}^{-1}$

c : concentration of fluorescent substance in mol l^{-1}

d : path length in cm,

the absorption at wavelength λ has to be known to derive fluorescence quantum yields. Since these informations are enclosed in the absorption spectra, present discussion contributes to the development of fluorescence spectroscopy towards a quantitative method for uranium(VI) speciation.

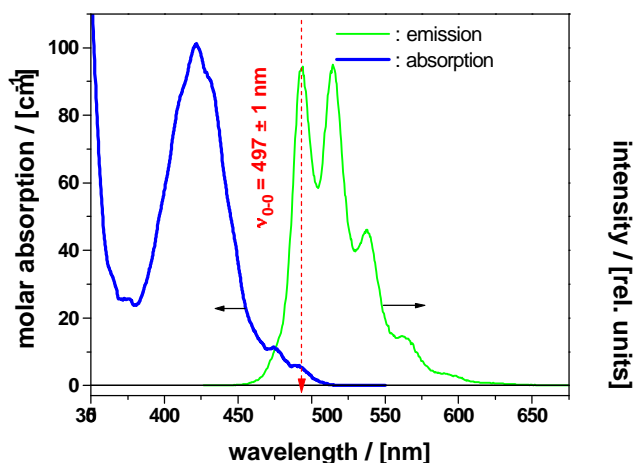


Fig. 6.2 : Comparison of absorption and emission spectrum of $(\text{UO}_2)_2(\text{OH})_2^{2+}$ (**I**). The 0-0 transition is observed at 497 ± 1 nm

An important relationship between electronic absorption and fluorescent spectrum is the coincidence of the vibronic 0-0 transition between electronic ground state and fluorescent excited state. This relationship holds for all four species under study as shown in figs. 3.4 and 6.2 - 6.4 with 0 - 0 transitions at (488 ± 0.7) nm (UO_2^{2+}), (497 ± 1) nm ($(\text{UO}_2)_2(\text{OH})_2^{2+}$), (499 ± 1.5) nm ($(\text{UO}_2)_3(\text{OH})_5^+$) and (464 ± 0.9) nm ($\text{UO}_2\text{CO}_3^\circ$). The standard deviations result from the 1σ uncertainty obtained from statistical treatment of UV-Vis data. A small difference in the 0-0 transition will further result from differences in the atomic coordinates of electronic excited state and ground state.

The overlapping bands at 473 nm for $\text{UO}_2^{2+}(\text{aq})$ in fig. 3.4 are well-known and indicate a „hot“ band. Figs. 6.2 - 6.4 do not indicate any inconsistency within the spectral data obtained for the three species **I** - **III** despite the fact that these data have been derived from separate experiments in different laboratories and evaluated by sophisticated data treatment techniques.

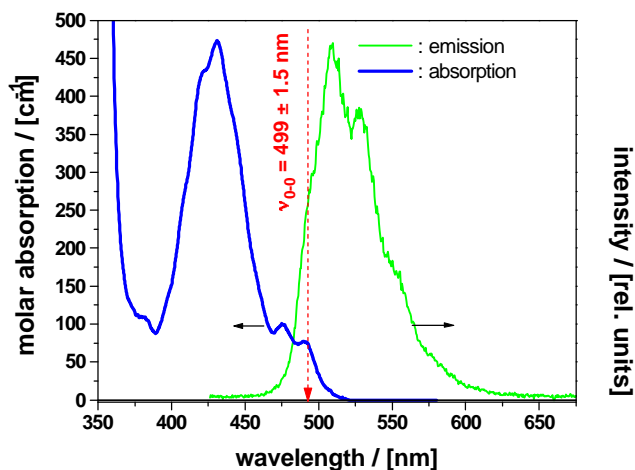


Fig. 6.3 : Comparison of absorption and emission spectrum of $(\text{UO}_2)_3(\text{OH})_5^+$ (**II**). The 0-0 transition is observed at 499 ± 1.5 nm.

Integral oscillator strengths have been estimated from the absorption spectra by interpreting the strong absorption edge towards the UV as tail of a Gauss-shape spectral band. The oscillator strength is obtained from eq. 6.2 (Sykora & Sima 1990):

$$f = 4.32 \cdot 10^{-9} \int \epsilon(\nu) d\nu \quad (6.2)$$

where $\int \epsilon(\nu) d\nu$ represents the integral under the spectral curve as function of the wave number ν . Resulting integral oscillator strengths are included in table 6.1. It is obvious from an inspection of table 6.1 that oscillator strengths are of a similar order of magnitude for the species $(\text{UO}_2)_2(\text{OH})_2^{2+}$, $(\text{UO}_2)_3(\text{OH})_5^+$ and UO_2CO_3^0 when normalized to one U atom : $f_{22} = 1 \cdot 10^{-3}$, $f_{35} = 2 \cdot 10^{-3}$ and $f_{101} = 1.6 \cdot 10^{-3}$, one order of magnitude higher than $f_{10} = 1.7 \cdot 10^{-4}$ for the $\text{UO}_2^{2+}(\text{aq})$ species.

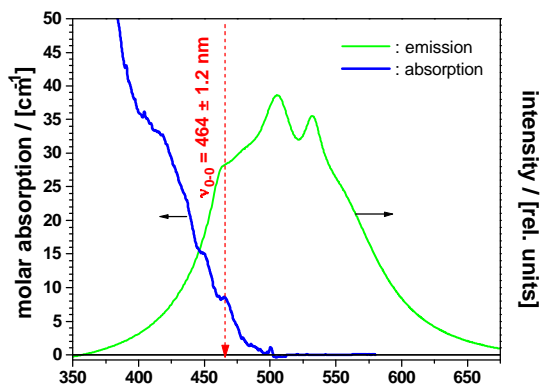


Fig. 6.4 : Comparison of absorption and emission spectrum of UO_2CO_3^0 (**III**). The 0-0 transition is observed at 464 ± 0.9 nm.

Oscillator strengths can be related to fluorescence life times by eq. 6.3 (Jørgensen & Reisfeld 1982) :

$$t = \frac{e_2 \cdot 2.3 \cdot 10^{-8}}{e_1 \cdot P \cdot \Delta E^2} \quad (6.3)$$

ΔE : energy of 0 - 0 transition in eV

e_i : number of mutually orthogonal states in state i

P : oscillator strength of transition between states 1 and 2

Replacing P by f and assuming $e_2 = e_1$, the following fluorescence life times are calculated: $\tau_{10} = 20 \mu\text{s}$, $\tau_{22} = 3.7 \mu\text{s}$, $\tau_{35} = 1.9 \mu\text{s}$ and $\tau_{101} = 2 \mu\text{s}$. The discrepancy between these figures and the experimentally observed life times is obvious (cf. table 6.1).

Low temperature spectroscopic studies of $\text{Cs}_2\text{UO}_2\text{Cl}_4$ crystals with symmetry C_{2h} around the U atom, $\text{CsUO}_2(\text{NO}_3)_3$ crystals with symmetry D_3 of the uranyl unit and $\text{NaUO}_2(\text{CH}_3\text{COO})_3$ with uranyl site symmetry C_3 have shown that the characteristic low energy absorption spectrum of the uranyl is due to transitions to several excited states (Denning et al. 1979b, Denning 1992). For C_{2h} symmetry, 12 electronic origins were identified (Denning 1992, Schwarz 1985), where only the two lowest lying origins correspond to transitions to the fluorescent excited state, being split by 1.6 cm^{-1} . For D_3 symmetry, ten electronic origins could be identified, the lowest being the doubly degenerate origin of the fluorescent excited state. The sodium acetate compound was found more difficult to trace due to strong overlap between electronic origins and vibrational progressions.

The solution species under study in the present work are approximately pentagonally coordinated with approximate uranyl site symmetries of D_{5h} ($\text{UO}_2^{2+}(\text{aq})$) and C_{2v} ($(\text{UO}_2)_2(\text{OH})_2^{2+}$, $(\text{UO}_2)_3(\text{OH})_5^+$, $\text{UO}_2\text{CO}_3(\text{H}_2\text{O})_3$). Hence, transfer of results from the low temperature single crystal studies to room temperature solution species with different site symmetries has to be done with caution. However, the single crystal studies indicate that conclusions of fluorescence life times τ on basis of the integral oscillator strength f are misleading. Realistic estimates of the fluorescence life times by eq. 3 have to be based only on those low energy features of the absorption spectrum of a species corresponding to electronic transitions to the fluorescent state. Therefore, experimental results are also in accord with current understanding of the electronic structure of the UO_2^{2+} entity.

The observation of a fluorescence life time different from that of the $\text{UO}_2^{2+}(\text{aq})$ species has given rise to several different explanations. In a first approach, the second fluorescence life time was interpreted due to formation of an exciplex between excited $^*(\text{UO}_2\text{H})^{2+}$, due to hydrogen abstraction by excited $^*(\text{UO}_2^{2+})$, and a ground state UO_2^{2+} ion, yielding a $^*(\text{U}_2\text{O}_4\text{H})$ species with longer life time (Deschaux & Marcantonatos 1979). This interpretation has been challenged by a different interpretation, assuming reversible crossing between two excited states *U and *X of the UO_2^{2+} ion (Formosinho et al. 1984).

Current understanding, especially the recent assessment of solubility limits in the U(VI)/H₂O system (Meinrath et al. 1996, Meinrath 1998d) indicates that that solutions were considerably supersaturated under the reported conditions. This finding might explain at least in part the poor reproducibility of experimental observations reported by Park et al. (1990). The exciplex theory assumes an analogous behaviour of UO₂²⁺ to aromatic hydrocarbons, where excimer formation is well known. However, since an exciplex dissociates immediately after relaxation, no absorption due to the dimer can be observed. Hence, the exciplex theory is in disagreement with present study, where the ground state absorption has been found to be readily observable.

The reversible crossing theory primarily requires two identifiable states *U and *X. However, no such states could be observed. In contrary, further changes in both emission spectra and fluorescence life time could be observed by extending the range of experimental investigations. These spectra and life times have been shown to correlate well with the species (UO₂)₂(OH)₂²⁺, (UO₂)₃(OH)₅⁺ and UO₂CO₃^o. These observations are also in close agreement with the independent study (Park et al. 1990), indicating satisfactory reproducibility in contrast to the inconsistencies reported on the exciplex theory and the reversible crossing theory.

Nevertheless, the electronically excited states have life times sufficiently long to thermalize to vibronic equilibrium. Typical equilibration times in aqueous solutions at room temperature are in the order 10⁻¹² to 10⁻¹³ s. Thus these states are *thexi* states (thermally equilibrated excited states) that are known to have a chemistry of their own (Sykora & Sima 1990). Numerous photochemical reactions induced by excited U(VI) have been reported, however partly with considerable discrepancy (Balzani et al. 1978). The discrepancies can now be understood as the result of different U(VI) species in the respective solutions and illustrates the need of a detailed understanding of U(VI) solution behaviour in the study of U(VI) photochemical reactions. Excited U(VI) is readily available in nature, e.g. in sea water with average U(VI) concentration of 10⁻⁸ M (Bloch 1980) or in rivers and lakes, where the geogenic U(VI) background is enhanced by phosphate fertilizers (Bloch 1980, Mangini et al. 1979, Veeh et al. 1974). Thus, a clarification of the fluorescence process of U(VI) is of considerable practical interest. Here, photooxidation by U(VI) has been proposed e.g. as possible degradation mechanism of organic substances in sea water or radical generating reactions (Balzani et al. 1978). Hydrolysis and carbonato complexes are prevailing U(VI) species in the natural aqueous environment (Langmuir 1978, Lopatkina 1964). The supposed importance of U(VI) in nature has been a main motivation to chose these species for the present studies.

7. Application in Characterization of Solid-Aqueous Phase Equilibria

In this chapter, the application of spectral informations to solid-aqueous phase equilibria of uranium(VI) will be reported. Compared to the great number of studies by pH titration methods reported in literature, solubility studies are scarce. In fig. 7.1a, solubility data from studies available in literature are given. Included in fig. 7.1 are new solubility data for which spectral data has been collected. These spectral data are given in fig. 7.2.

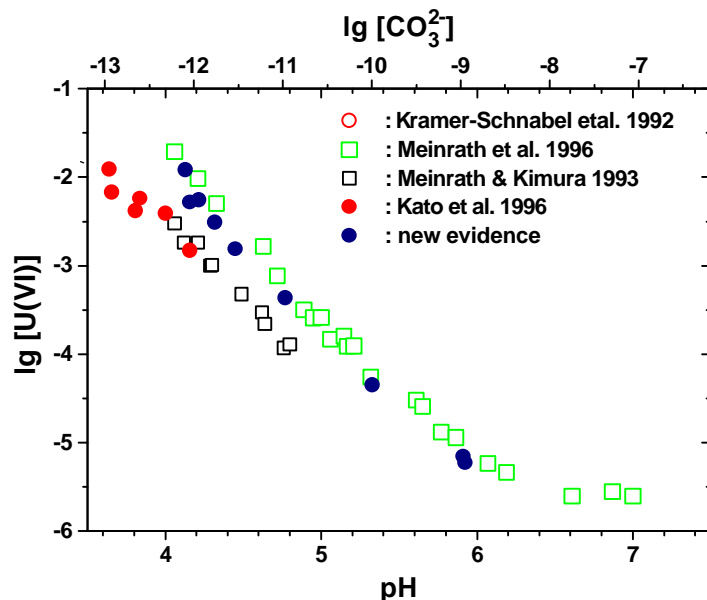


Fig. 7.1a : Solubility data of $\text{UO}_3 \cdot 2 \text{H}_2\text{O}$ as function of pH at $\mu = 0.1 \text{ M NaClO}_4$.

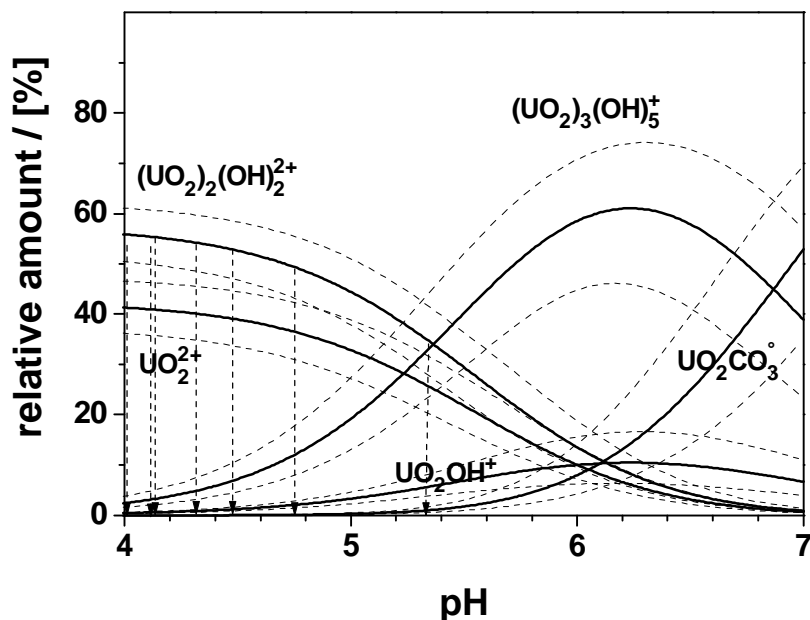


Fig. 7.1b : Species distribution plot of U(VI) in solubility equilibrium with $\text{UO}_3 \cdot 2 \text{H}_2\text{O}(\text{s})$ at 25° at $\mu = 0.1 \text{ M}$ (perchlorate medium). The species are calculated on basis of formation constants $\lg K'_{10} = -6.08 \pm 0.04$, $\lg K'_{22} = -6.14 \pm 0.02$, $\lg K'_{35} = -17.14 \pm 0.07$ and $\lg \beta'_{101} = 9.23 \pm 0.04$ (1σ uncertainties) (Meinrath et al. 1996).

Fig. 7.1b gives relative species concentrations of U(VI) in form of a certain species. Included are the 1σ confidence limits of the respective species, assessed from Bootstrap

resampling algorithms (Efron & Gong 1983, Stines 1990). The arrows give position of spectral data, for which deconvolutions are discussed in the sequel.

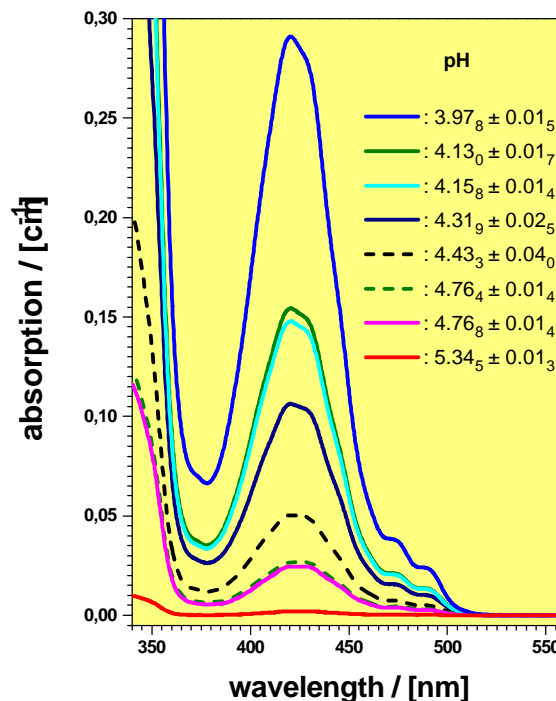


Fig. 7.2 : UV-Vis absorption spectra of solutions in equilibrium with $\text{UO}_3 \cdot 2 \text{H}_2\text{O}$ at $\mu = 0.1 \text{ M HClO}_4$.

Three factors contribute to the relevance of these eight data points. First, the solubility data are long term data in the respect that each data point has been equilibrated with the solid phase for more than three months. Second, the reproducibility of experimental data has been checked for the data points at pH 4.13 and pH 4.75. As can be seen from the 95% confidence limits in pH, the values of $\text{pH } 4.13_0 \pm 0.01_7$ and $4.15_8 \pm 0.01_4$ are not significantly different. For both rechecked data points the differences observed within the spectral information and the solubility data is within the confidence limits obtained from both the solubility data as well as the spectral evaluations. Hence, interpreted spectral data is given in the following figures 7.3 to 7.10. Interpretation is made by the single component spectra of the species UO_2^{2+} , $(\text{UO}_2)_2(\text{OH})_2^{2+}$ and $(\text{UO}_2)_3(\text{OH})_5^+$. The UV-Vis spectra are collected in the range pH 4.0 to pH 5.4. The pH range accessible for direct UV-Vis spectroscopic speciation of U(VI) solutions in equilibrium with $\text{UO}_3 \cdot 2 \text{H}_2\text{O}$ is found rather limited, since above pH 5.5 the solubility is lower than the resolution limit of the UV-Vis spectroscopic method. The term „resolution limit“ is applied deliberately in given context. Due to the comparatively intense absorption spectrum of the $(\text{UO}_2)_3(\text{OH})_5^+$ species, it is well possible to collect spectra above pH 5.5. However, these spectra are not further interpretable by peak deconvolution due to increased noise. Hence, the spectral informations discussed in the sequel are limited to pH values above pH 5.5.

Spectral deconvolution is made by the sequential SIMPLEX (Nelder & Mead 1967). Confidence limits of single components and calculated sum spectrum have been evaluated by canonic analysis (Spendley 1962, Box & Draper 1988). An outline of the procedure in the open literature been given e.g. by Brumby (1982).

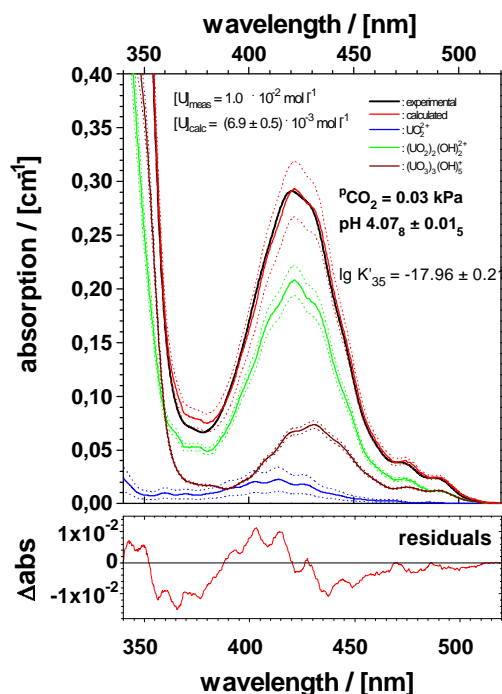


Fig. 7.3 : Deconvoluted UV-Vis absorption spectrum of the solution at pH $4.07_8 \pm 0.01_5$.

Fig. 7.3 gives the spectrum recorded at pH $4.07_8 \pm 0.01_5$. The spectrum is dominated by the contribution of the $(\text{UO}_2)_2(\text{OH})_2^{2+}$ species. The evaluated concentration ratio of this species and the UO_2^{2+} species is about unity: $2.3 \cdot 10^{-3} : 2.06 \cdot 10^{-3}$. This result is encouraging. However, as can be seen from the residual plot, residuals are clearly above $5 \cdot 10^{-4} \text{ cm}^{-1}$. This effect is due to the deviation of fitted sum curve and experimental data in the range 360 nm to 380 nm. This deviation is systematic, but at present state of analysis, no attempt has been made to omit this data range during deconvolution procedure. Furthermore, the UO_2^{2+} species has an only rather small relative spectral contribution. Nevertheless, precise assessment of its contribution would be of outmost interest, because this small contribution carries first a considerable uranium concentration and second carries information relevant for determination of formation constants e.g. of the $(\text{UO}_2)_2(\text{OH})_2^{2+}$ species. Detailed analysis however shows that the spectral contribution of the UO_2^{2+} species is too small to allow concentration assessment with necessary precision. Because the relative contribution of the free uranyl ion will further decrease with increasing pH in both its absolute as well as relative contribution due to decrease in total U(VI) concentration and changes in the species relative contributions. This analysis will be discussed following the analysis of spectral information. Nevertheless, the three single component spectra are well able to interpret the observed spectrum.

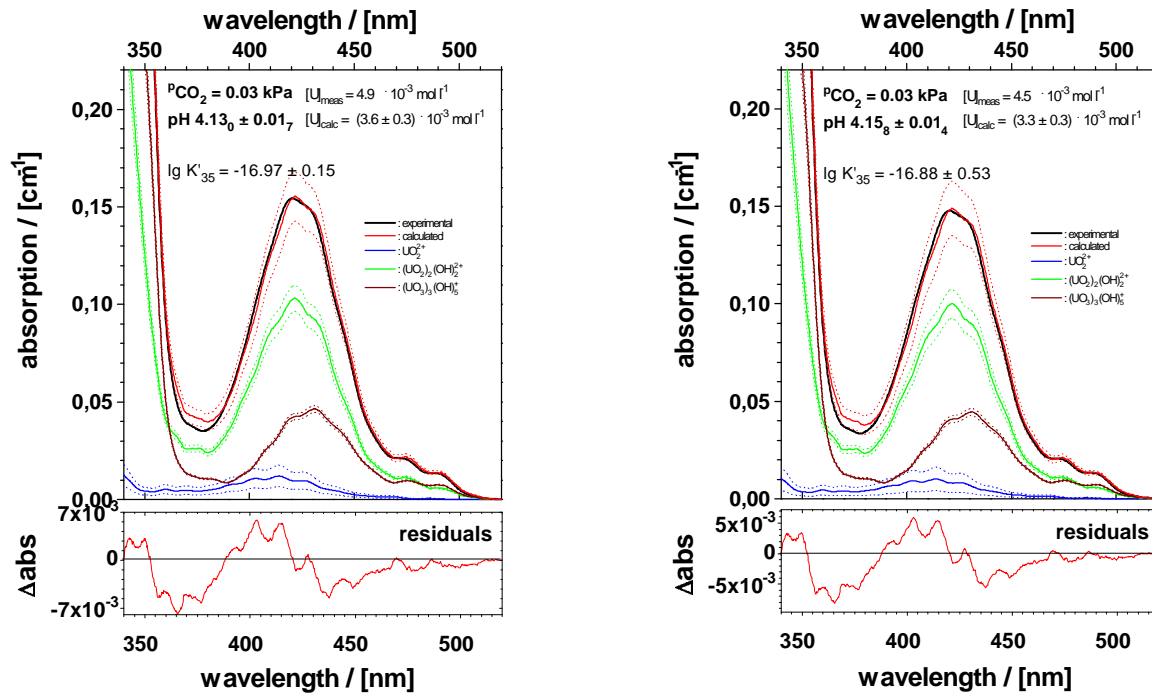


Fig. 7.4/5 : Deconvoluted UV-Vis absorption spectrum at pH $4.13_0 \pm 0.01_7$ and pH $4.15_8 \pm 0.01_4$.

Comparing the absorption spectra at pH $4.13_0 \pm 0.01_7$ and $4.15_8 \pm 0.01_4$ in figs. 7.4/5, the spectra are found very similar. Nevertheless, both spectra have been taken from two different vessels with a time difference of about half a year. Compared to fig. 7.3, the relative contribution of $(\text{UO}_2)_3(\text{OH})_5^+$ are increased but the difference is clearly to be seen. The situation however changes by comparison with fig. 7.6. The spectral contribution of $(\text{UO}_2)_2(\text{OH})_2^{2+}$ are reduced relative to the increased contribution of $(\text{UO}_2)_3(\text{OH})_5^+$ species. The residuals again show the effect of the small difference in the wavelength range 360 nm - 380 nm that adds to the difficulty to assess precise concentration of UO_2^{2+} . Therefore no formation constant of $(\text{UO}_2)_2(\text{OH})_2^{2+}$ is given. The formation constants $\lg K'_{35}$ are calculated on basis of $\lg K'_{22} = -6.14 \pm 0.02$ (1σ standard deviation) obtained in chapter 4.

Fig. 7.6 : Deconvoluted UV-Vis spectrum at pH $4.31_9 \pm 0.02_6$.

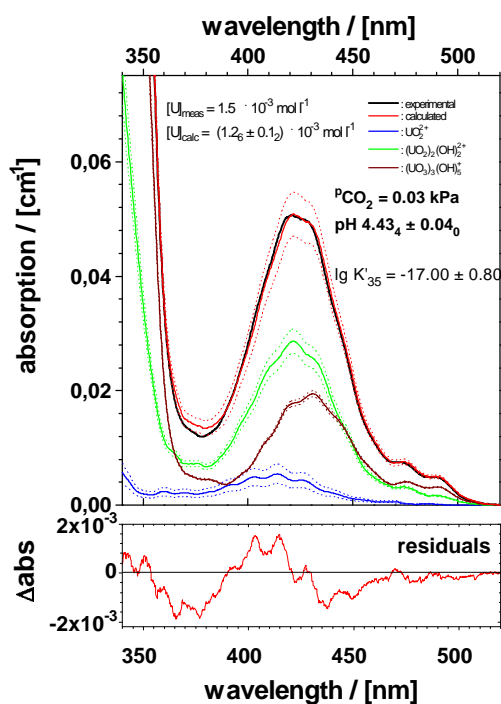
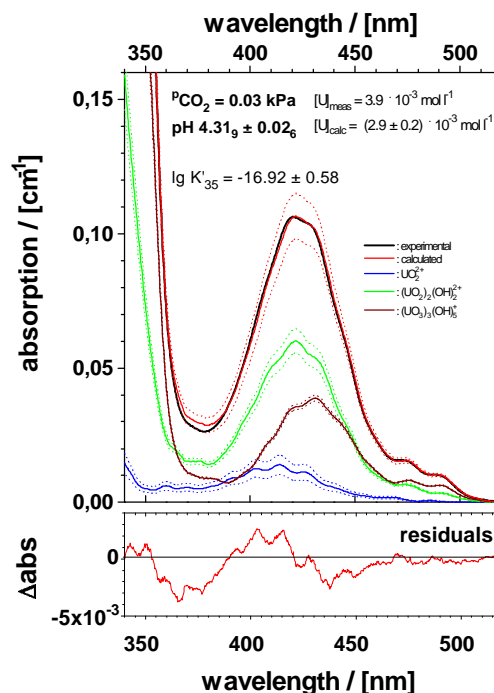


Fig. 7.7 : Deconvoluted UV-Vis spectrum at pH $4.43_4 \pm 0.04_0$.

The observed tendency continues when shifting pH further. The relative contribution of the $(\text{UO}_2)_3(\text{OH})_5^+$ species further increases, while the difference in the wavelength range 360 nm - 380 nm shoes to be systematic and probably a result of different baseline character of the spectrometer used in this study compared to the machine used for collection of spectral evidence in chapter 4.

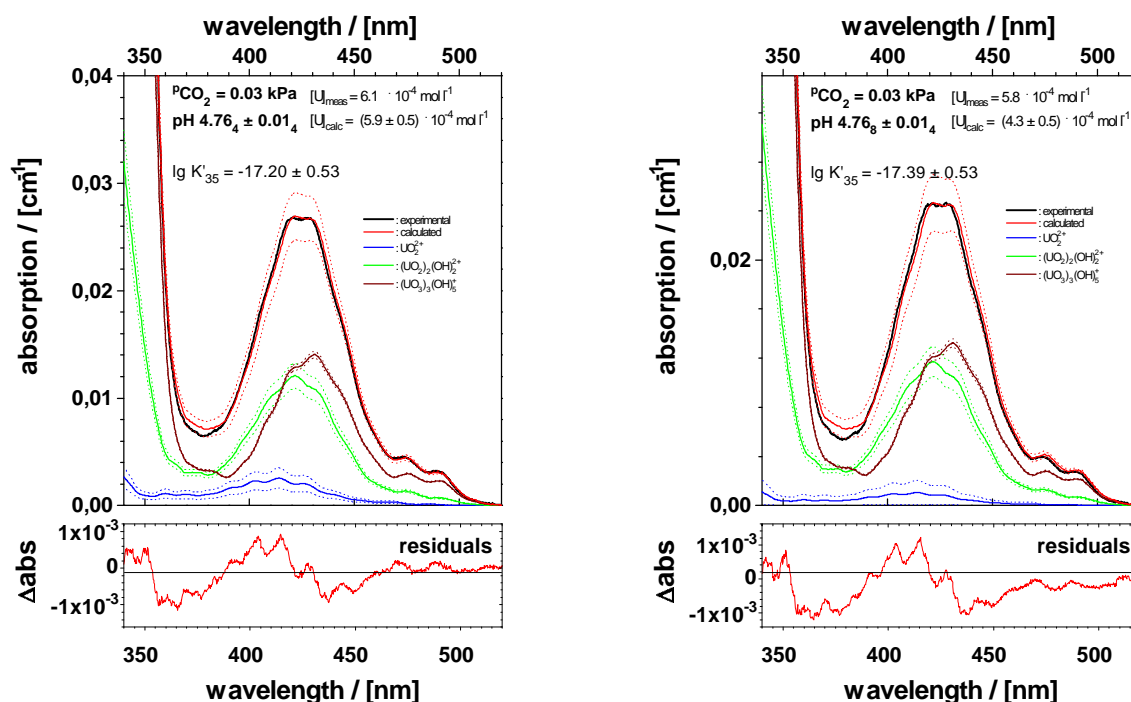


Fig. 7.8/9 : Deconvolution of UV-Vis spectra at $\text{pH } 4.76_4 \pm 0.01_4$ and $\text{pH } 4.76_8 \pm 0.01_4$.

The uncertainty in assessing precise UO_2^{2+} concentrations from spectral deconvolution becomes evident from figs. 7.8/9. While the ratio of the oligomeric species is very close in both spectra, the free uranyl ion concentration varies considerable. Nevertheless, the general tendency is continued: $(\text{UO}_2)_2(\text{OH})_2^{2+}$ decreases, $(\text{UO}_2)_3(\text{OH})_5^+$ increases.

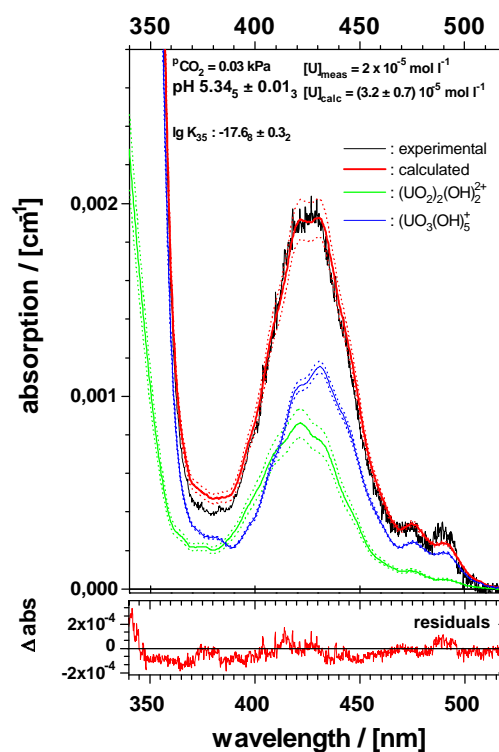


Fig. 7.10 : Deconvolution of the UV-Vis spectrum at $\text{pH } 5.34_5 \pm 0.01_3$.

The deviations between experimental curve and fitted sum spectrum seem considerable. However, it should be noted that maximum absorption of the low energy electronic transition is only $2 \cdot 10^{-3} \text{ cm}^{-1}$. The scatter in the data clearly illustrates that a technical limit has been reached and spectra at even lower concentrations most probably are not interpretable.

Fig. 7.10 shows that the UO_2^{2+} species is absent now. The $(\text{UO}_2)_3(\text{OH})_5^+$ species further dominates the spectra. Following the spectra given in figs. 7.3 to 7.10, the behaviour to be expected from numerical modelling of solubility data and validated by time-resolved laser-induced fluorescence (TRLF) spectroscopy (Kato et al. 1994) is evident. Spectral deconvolution of the individual spectra results in consistent thermodynamic data of the formation constant $\lg K'_{35} \approx -17.00 \pm 0.50$. This data is obtained from the concentration quotients of both $(\text{UO}_2)_2(\text{OH})_2^{2+}$ and $(\text{UO}_2)_3(\text{OH})_5^+$ and the formation constant $\lg K'_{22} = -6.14 \pm 0.05$. The derived data includes all contributing stochastic influences: uncertainty in pH measurement, uncertainty in concentration assessment from canonical analysis and uncertainty from the parameter $\lg K'_{22}$ used to calculate $\lg K'_{35}$ on the 95% confidence level.

In almost all cases the 95% confidence limit of $\lg K'_{35}$ is in the order ± 0.5 . Literature data claims standard deviations in the order ± 0.05 , however under complete neglect of contributing uncertainties, e.g. pH measurement or in concentration assessment. The consideration of all factors contributing to a physical quantity is of utmost importance. This is however a problem that has not yet received the attention it deserves. The use of mean values e.g. in presenting speciation diagrams or in calculating thermodynamic quantities on basis of error affected auxiliary constants is wide-spread.

A full assessment of all contributing errors shows that the major importance of this part of study is the application of single component spectra of relevant U(VI) hydrolysis species in interpretation of solid-aqueous phase equilibria in a quantitative way. As outlined in the first part of chapter 4, such a possibility has not been available previously. As outlined in several communications (Meinrath et al. 1993, Meinrath & Kimura 1993, Meinrath et al. 1996, Meinrath 1997), lack of experimental validation of solution composition has been a major obstacle in understanding both aqueous solution behaviour and photophysical properties of hexavalent uranium.

The discussion given here is by far phenomenological. Especially decisions concerning the number of significant spectral factors (species) is not as straight forward as it might seem from foregoing argumentation. A more detailed statistical treatment of the body of numerical evidence given in this chapter has been presented in (Meinrath 1998d). It has to be noted that determination of statistical properties from experimental data gets increasingly important. This importance is partly resulting from quality control requirements and partly from the requirements of geochemical modelling codes that need an estimate of the uncertainty in each input parameter to obtain an estimate of the overall uncertainty of the model output (Ekberg et al. 1996, Ekberg et al. 1997). Modern concepts of uncertainty analysis, e.g. Latin Hypercube Sampling (Jessen 1975, McKay et al. 1979)), require the distribution function of an input parameter for efficient uncertainty analysis.

8. Assessment of Uncertainties in Determination of pH

The uncertainty associated with experimental determination of pH is a fundamental parameter limiting the precision to which thermodynamic parameters of aqueous solution species can be obtained. To give an illustrative example in eq. 8.1, the thermodynamic formation constant $\lg K_{35}$ of the uranium(VI) hydrolysis species $(\text{UO}_2)_3(\text{OH})_5^+$ depends on pH according to :

$$\lg K_{35}^\circ = \lg \{(\text{UO}_2)_3(\text{OH})_5^+\} - 3 \lg \{\text{UO}_2^{2+}\} + 5 \text{ pH} \quad (8.1)$$

The uncertainty in pH enters in the thermodynamic formation constant $\lg K_{35}$ by a factor of five. The species $(\text{UO}_2)_3(\text{OH})_5^+$ is an oligomeric hydrolysis species of U(VI) and assumed to play an important role e.g in the transport of uranium from uranium production installations to the populations, thus contributing to the health risk of populations in many uranium mining countries of the world. (Meinrath et al. 1996). Performance of geochemical modelling to predict these risk potentials in turn depends on an unbiased estimate of over-all uncertainties to the parameters in the geochemical data bases. Satisfactory thermodynamic description of aqueous solutions consequently strongly depends on the availability of suitable procedures to determine pH values with high accuracy. For practical determination of pH, an operational definition has been adopted by IUPAC, based on comparison of electromotive force (EMF) of a suitable electrode system in the solution of interest with the EMF of the same electrode system in standard buffer solutions (Galster 1991). Standard buffer solutions are proposed by the respective IUPAC commissions (Covington et al. 1983). Widely distributed electrode systems are e.g. glass combination electrodes (Naumann 1994).

Two pH scales are currently proposed by IUPAC: The single standard procedure of the British Standard Institution (BSI) (Covington 1981) and the so-called 'bracketing procedure' of the National Institute of Science and Technology (NIST) (Bates 1981). Both approaches are considered to be mutually exclusive (Baucke et al. 1993). From view-point of determination of thermodynamic data, both calibration procedures are found unsatisfactory. BSI procedure heavily relies on the ideal Nernstian behaviour of the electrode system, which is recently found questionable from thermodynamic analysis of the processes responsible for the electrode response (Baucke et al. 1993, Baucke 1994a, Baucke 1994b). NIST procedure results in different pH values for a given sample solution depending on the choice of 'bracketing' buffer standards. More detailed arguments are given in (Naumann et al. 1994, Baucke et al. 1993).

Recently, a multi-point calibration procedure (MPC) has independently been proposed for approval by IUPAC (Baucke et al. 1993) that has been used by the present author for at least a decade in the framework of determination of thermodynamic constants for hydrolysis and carbonate complexation reactions of metal ions in aqueous systems (e.g. (Meinrath et al. 1996, Meinrath & Takeishi 1993)). The studies not only aim at the determination of accurate mean values of thermodynamic constants, but also on a realistic estimation of confidence limits associated with evaluated parameters. Therefore, the ability to assess the statistical uncertainty for each pH determination is an important criterion in selecting a pH calibration procedure.

Currently however, gross estimation of uncertainties in the determination of pH are more common than detailed assessment. In table 8.1, some typical comments concerning the uncertainty in an experimentally determined pH is given from selected literatures. Assessment of uncertainty in determination of pH is often neglected, sometimes given as a general estimate, while experimental assessment of uncertainty associated with pH determination is found scarce. Furthermore, in the evaluation of over-all uncertainties in thermodynamic constants, contributions from the determination of pH are often neglected, as already discussed in the preceding chapters.

Table 8.1: uncertainty in pH, summarized from selected references

uncertainty in pH	reference	comment
± 0.02	Meinrath & Takeishi 1993	precision
± 0.03	Guiffaut 1994	
± 0.03	Stadler 1988	given as "maximum error"
± 0.02	Büppelmann 1988	6-point calibration
± 0.02	Schmitz 1994	"probably larger"
± 0.02	Harbinson & Davison 1987	
$\pm 0.02_5$	Metcalf 1987	σ of error distribution from 248 measurements by 7 operators
± 0.02	Ebel et al. 1978	from error propagation

A practical pH determination may be affected by a series of possible errors, random errors as well as bias. Some sources of error are summarized in table 8.2.

As outlined in the following, MPC (multi-point calibration) procedure allows assessment of the uncertainty associated with an individual pH-measurement by the statistical concepts of OLS. Practical applicability of an alternative procedure based on a maximum likelihood approach with some principal advantages will be compared to OLS. Discussion will concentrate solely on the prediction of the pH value of an unknown sample based on the MPC procedure. The evaluation of proton activities and concentrations from estimated pH data will not be discussed here. To demonstrate the relevance of results obtained in this study, the effect

of uncertainty in pH to the determination of dissociation constants in the CO₂/H₂O system will be given in the last section of the discussion.

Table 8.2 : some possible sources of bias and noise affecting a pH-measurement (Galster 1991)

residual liquid junction potential
asymmetry potentials
stirring effects
temperature effects (e.g. temperature gradients over the electrode)
clogging of diaphragms
memory effects
filling height of internal solution
electrical noise (shielding of cables)
cross contamination
carbonate exchange (in alkaline calibration buffers)

8.1 Methodology

A random selection of 50 out of about 250 pH measurements with 5-point calibration made during the past half decade is chosen as data set to provide a basis for the following discussion. These measurements have been done in different laboratories by different calibration standards and electrodes. In common to all pH measurements is the use of five NIST traceable pH standard solutions for electrode calibration and sample solutions of 0.1 M perchlorate medium at pH values in the range of pH 2 - 10 and 25° C. The rationale behind this approach is the assumption that the data are affected by random influences in a representative manner. Kolmogorov-Smirnov statistics is applied to compare the empirical distributions with normal distributions (Massey 1951).

From ordinary linear least square regression (OLS), several confidence regions are evaluated for the 50 pH measurements: the OLS confidence limit (OLSCL), the joint parametric uncertainty limit (JPUL) (Schwartz 1980) and the confidence ellipse. From these confidence regions, 1000 normally distributed random variates are drawn by Monte Carlo procedures (Rubinstein 1981). Univariate random numbers are generated by a portable random number generator in Pascal (Press et al. 1989), while random normal variates are generated by algorithms discussed in (Marsaglia & Tsang 1984, Knuth 1981). Characteristics of the computing environment are determined by algorithms from the PARANOIA tool (Karpinski 1985). Linear approximations to the Jacobian matrices are computed by an algorithm of Nash (Nash & Walker-Smith 1987).

8.2 Evaluation Procedure

8.2.1 Ordinary Linear Least Squares Regression

In MPC, an electrode system is calibrated against several pH standard solutions and the mV readings are transferred into a calibration line by a suitable regression technique, where e.g. ordinary least squares (OLS) regression has been proposed (Naumann et al. 1994). From Nernst Law, a linear relationship of the form (8.2) is expected

$$\text{mV} = \alpha + \beta * \text{pH} \quad (8.2)$$

To illustrate the procedure, a numerical example is given in table 8.3.

Table 8.3 : set of typical pH calibration data

pH of standard	mV reading [mV]	OLS residuals [mV]
4.01	182.3	+2.2
4.66	140.5	-1.4
7.00	2.8	-1.7
9.01	-113.5	+0.1
10.01	-171.1	+1.0
OLS parameters :	slope β :	$-58.71 \pm 0.36_7$
	intercept α :	$415.56 \pm 2.68_9$
uncertainties :	confidence ellipse :	$\pm 0.03_9$
	OLSCL :	$\pm 0.06_4$
	JPUL :	$\pm 0.09_0$
	eq. 8.8 :	$\pm 0.03_6$
maximum likelihood parameters :	slope β :	-58.61 ± 0.376
	intercept α :	414.77 ± 2.691

By unavoidable measurement errors, uncertainty creeps into the experimental determination of slope β and intercept α of eq. 8.2. Thus, the calibration data has to be interpreted by a model

$$y_i = \alpha + \beta x_i + e_i ; (i = 1 \dots n) \quad (8.3)$$

where x_i is the pH of the i -th standard, y_i the corresponding mV reading of the pH meter and e_i represents the i -th residual. The residuals e_i are considered as estimates for the true but unknown errors ε_i .

Due to random errors, the estimated parameters α and β will not be equal to the true but unknown parameters. If the errors ε_i are independently and identically distributed with a mean of zero, it is possible to indicate with some specific probability in what region of the parameter space (α, β) the true parameters might reasonably be expected. The standard deviations for slope β and intercept α of the regression line are given by eq. 8.4 - 8.6 (Haswell 1992):

$$\sigma(\beta) = \frac{s_e}{\sqrt{\sum (x_i - \bar{x})^2}} \quad (8.4)$$

$$\sigma(\alpha) = s_e \sqrt{\frac{1}{n} + \frac{\bar{x}^2}{\sum (x_i - \bar{x})^2}} \quad (8.5)$$

$$s_e^2 = \frac{\sum y_i^2 - \alpha \sum y_i - \beta \sum x_i y_i}{n - 2} \quad (8.6)$$

Standard deviations are transformed to ordinary least squares confidence limits (OLSCL) by multiplication with Student's $t_{n-P, \tau}$, ('Student' 1908) where n gives the number of data points, P represents the number of simultaneously estimated parameters and τ gives the desired confidence level. The standard deviations $\sigma(\alpha)$ and $\sigma(\beta)$ are commonly reported parameters that are understood often as a square 68% confidence region of in the parameter space (α, β) . The true confidence region for a linear model function is elliptical in (α, β) (Donaldson & Schnabel 1987) and described for the present linear model by eq. 8.7 (Bates & Watts 1988):

$$2F_{P, n-P, \tau} \cdot s_e^2 = n(\alpha - \bar{\alpha})^2 + 2\sum x_i(\beta - \bar{\beta})(\alpha - \bar{\alpha}) + \sum x_i^2(\beta - \bar{\beta})^2 \quad (8.7)$$

F : Fisher's critical variance ratio for n data points, P parameters and confidence level τ

To show the distribution of the 50 calibrations, confidence ellipses of the 50 measurements in (α, β) are given in fig. 8.1. These ellipses are calculated by eq. 8.7 and enclose the 95% confidence region in (α, β) (mean centred for α). The center point of the ellipse represents the mean $(\bar{\alpha}, \bar{\beta})$, estimated from the respective regression analysis. The ellipse encloses the region (α, β) , where the true parameters might be found with 95% probability. It is obvious from fig. 8.1 that slope β and intercept α are strongly correlated: High slopes β favour low intercepts α and vice versa. Provided the electrode system behaves ideally, it is straightforward to identify the slope β with the theoretical Nernstian slope of $-59.16 \text{ mV pH}^{-1}$. In case of glass electrodes however, ideal behaviour may not be expected and the theoretical slope is commonly found less than expected for an ideal electrode system (Baucke 1994). In the present study, too, the confidence ellipses are not centred at the theoretical Nernst slope of $-59.16 \text{ mV pH}^{-1}$. In all

cases the slopes are above $-59.16 \text{ mV pH}^{-1}$. This observation agrees well with the observations reported by previous authors (Baucke 1994).

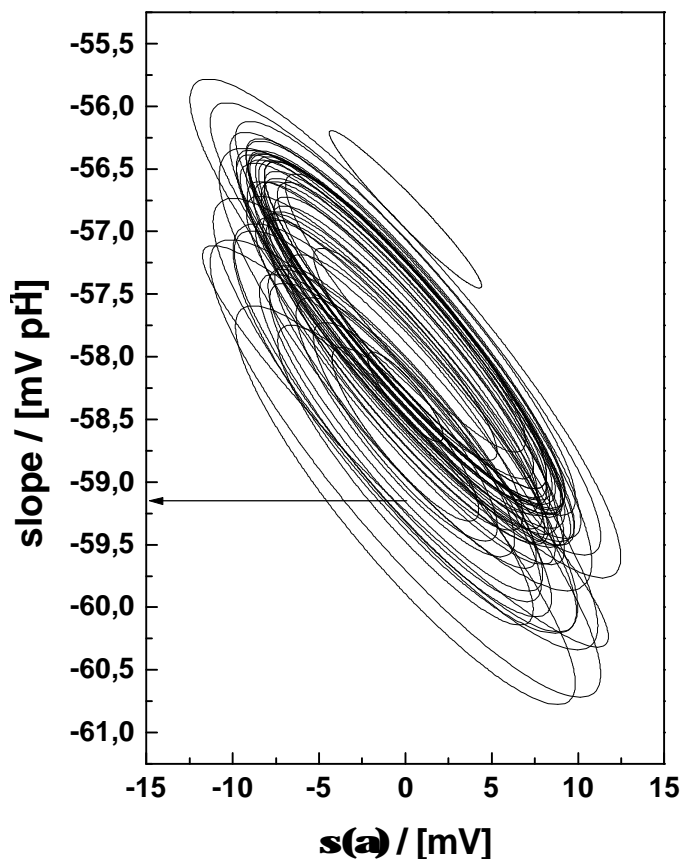


Fig. 8.1 : 95% confidence ellipses of 50 randomly selected 5-point glass electrode calibrations using NIST traceable buffer standards at $25 \text{ }^\circ\text{C}$ (mean centred for intercept α).

A first estimate of the uncertainty associated with a pH value can be obtained directly from the least squares line by eq. 8.8 (Bates & Watts 1988) :

$$s_{y,t} = t_{n-P,t} \cdot s_e \sqrt{1 + \frac{1}{n} + \frac{(x_o - \bar{x})^2}{\sum (x_i - \bar{x})^2}} \quad (8.8)$$

Eq. 8.8 describes a confidence band around the OLS line. The confidence band is bone-shaped with a minimum at $x_o = \bar{x}$ with x being the arithmetic mean of the abscissa data from which the OLS line is derived. The statistical parameters reported in following have been obtained for $\text{pH} = \bar{x}$. The parameter $t_{n-P,\tau}$ represents Student's t for $n-P$ degrees of freedom and the desired confidence level τ . Further estimates of uncertainties are obtained by Monte Carlo simulations, where normal variate random selections are collected from the respective confidence regions in (α,β) . Examples are shown in fig. 8.2a,b for the data given in table 8.3.

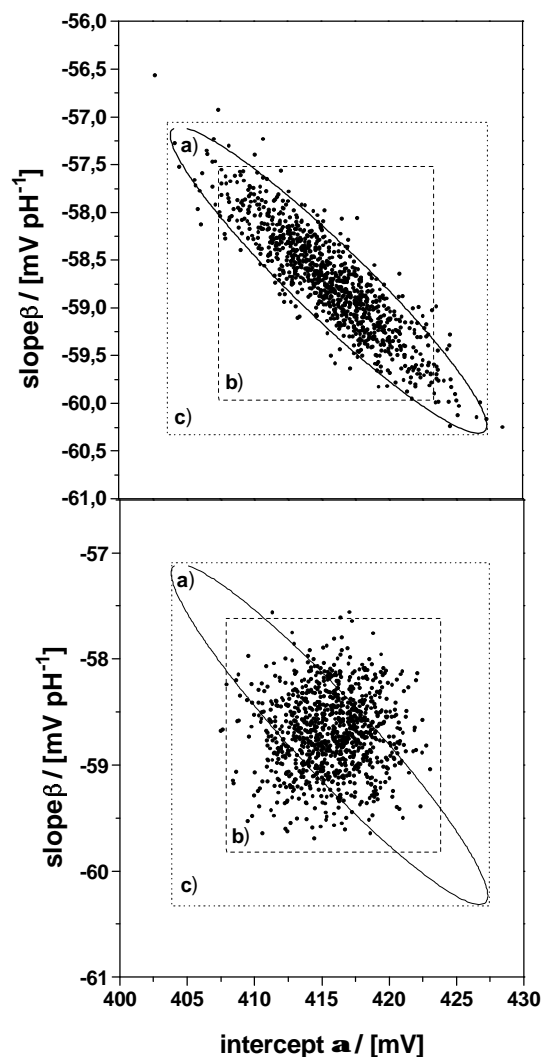


Fig. 8.2a,b : Comparison of 95% confidence regions in (α, β) : a) confidence ellipse, b) square ordinary least square confidence limit and c) joint parametric uncertainty region.

top : location of 1000 normally distributed Monte Carlo samples from the confidence ellipse.
 bottom : location of 1000 normally distributed Monte Carlo samples from the OLSCL region of (α, β) .

When reporting standard deviations, it is implicitly assumed that about 68% of the randomly drawn samples (=simulated measurements) will result in parameters (α, β) within the given limit. For multi-parameter models with mutual correlation of parameters as shown in fig. 8.1 for the parameters (α, β) , this assumption is known to be not valid (Donaldson & Schnabel 1987, Schwartz 1980). Some pairs of (α, β) falling within the 95% confidence ellipse are not included into the square 95% OLSCL obtained from the standard deviations. Taking the data given in fig. 8.2 as a representative example, the square 95% OLSCL (cf. table 8.3) encloses only 88% of the 1000 randomly drawn samples from the confidence ellipse. Hence, the coverage, understood as the ratio of observations actually found within the confidence limit and the theoretically expected number of observations is only about 90% from fig. 8.2. Coverages as low as 80% are found in the present study. The obvious reason for these low coverages are the differences between the shape of confidence areas described by the confidence ellipse and the OLSCL. Fig. 8.2b explains further, that a considerable amount of samples drawn from the OLSCL are outside the parameter space enclosed by the confidence

ellipse. Therefore, mean pH values and standard deviations obtained by Monte Carlo simulations differ for both confidence regions.

Since the statistical uncertainties can not convey the complete picture of the uncertainties in determination of α and β , the use of joint parametric uncertainty limits (JPUL) has been proposed for linear models (Schwartz 1980, Roy & Bose 1953). The confidence interval of i -th parameter P_i is given by eq. 8.9

$$JPUL(P_i) = 2\sqrt{PF_{P,n-P,\tau}} \cdot \sigma(P_i), \quad (8.9)$$

where P gives the total number of parameters simultaneously determined and $\sigma(P_i)$ represents the ordinary standard deviation of the parameter P_i . In fig. 8.2, the JPUL for 95% confidence are indicated. The JPUL is designed to form a rectangle enclosing the confidence ellipse by tangents. The actually observed coverage is always $> 95\%$ and therefore, JPUL are considered to be conservative (Roy & Bose 1953).

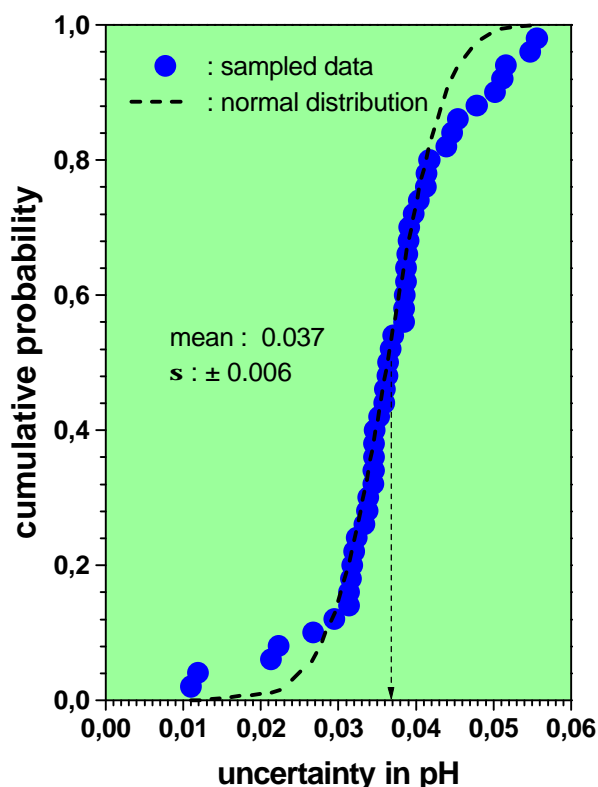


Fig. 8.3 : Comparison the empirical distribution of uncertainties in pH obtained from 1000 Monte Carlo simulations from the 50 confidence ellipses with a normal distribution.

The cumulative distribution of uncertainties obtained for the 50 randomly selected pH measurements by resampling from the confidence ellipse is compared to a normal distribution in fig. 8.3. The fitting criteria is a minimization of Kolmogorov-Smirnov's D (Massey 1951) between empirical and normal distribution. The analysis results in a 0.2% probability that the 50 standard deviations are actually drawn from a normal distribution with mean 0.037 and a

standard deviation of ± 0.006 . This probability seems negligible. On the other hand, there is no reason to expect that the electrode parameters of several different electrodes obtained during a five year period are truly Gaussian distributed. Truly homoscedastic data are rather rarely found from experimental studies. Furthermore, the low probability is mainly caused by deviations in the tails of the distribution. This part is strongly affected by censoring (preferring calibrations with small residuals) and systematic errors during the measurement process. The main systematic measurement error is found to be due to use of carbonate buffers at about pH 10. These buffers are found rather unstable. Without detailed statistical analysis, these most probably erroneous measurements would probably have been accepted into the evaluation of thermodynamic data. After spotting these invalid buffer standards by applying statistical analysis, the buffers were replaced, resulting in improved confidence estimates. The 'spoiled' measurements have nevertheless not been excluded from the present data set to emphasize the need of a detailed statistical assessment of each individual pH measurement.

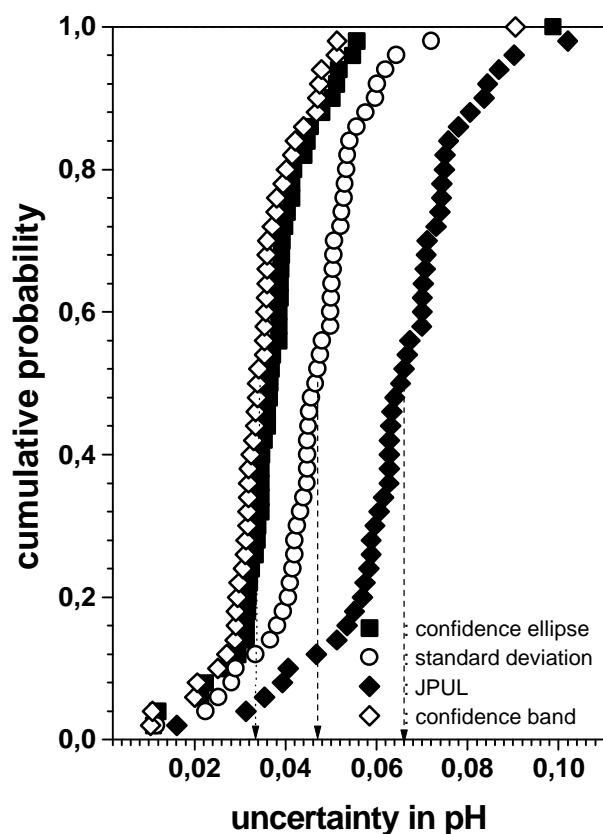


Fig. 8.4 : Comparison of uncertainties obtained from empirical distributions of 1000 normally distributed Monte Carlo simulations from the confidence ellipses, OLSCL and JPUL regions. The distribution of uncertainties calculated by eq. 8.8 is included.

Fig. 8.4 compares the cumulative distributions of uncertainties obtained from the 50 measurements by sampling from the a) confidence ellipse, b) ordinary standard deviations, c) JPUL and d) uncertainties calculated directly from the regression parameters by eq. 8.8. While sampling from the ordinary and JPU intervals results in significantly higher uncertainties, sampling from the confidence ellipse is equivalent with direct calculation by eq. 8.8. If a rough estimation on the precision of the determination of pH by the MPC procedure should be given as a rule of thumb, ± 0.03 pH units would certainly not a too arbitrary choice. This conclusion

may be e.g. compared to results from a round-robin pH study. Seven operators measured 485 pH values of $5.00 \pm 0.05 \cdot 10^{-5}$ M H_2SO_4 solutions using nine different ROSS-type electrodes (Metcalf 1987). The histogram of the 485 (binned) measurements shows considerable skewness toward lower pH, nevertheless a pH of 4.06 ± 0.05 (2σ) is reported. Calibration of electrode systems was made according to the 'bracketing procedure' using standard solutions at pH 7.00 and pH 4.00. Ebel (1978) gave a detailed statistical analysis of the pH measurement using error propagation. Reported uncertainties (1σ) are of the orders ± 0.02 (6-point calibrations). Schmitz (1994) concluded that the uncertainty of pH in diluted solutions is >0.02 pH units. The results from the present study do not offer discrepant conclusions. However, it is to emphasize that the intention of the present discussion is not to derive a universally valid estimate but to appraise several suitable procedures for assessment of uncertainties.

8.2.2 Maximum Likelihood Approach

There are several arguments to question OLS regression for the pH calibration/prediction procedure. First, currently available commercial equipment for determination of pH is capable to measure the EMF of a given solution within ± 0.1 mV, while pH values of standard solutions are given within ± 0.02 pH units. This implies, based on the data in table 8.3, that the uncertainty in the pH buffer standard transfers into an uncertainty of >1 mV, within the order of magnitude reported for residual liquid junction potentials (Galster 1991, Bates 1981). Hence, the assumption that the abscissa values are error-free while all experimental error is concentrated in the ordinate values -a fundamental assumption in regression (Donaldson & Schnabel 1987)- introduces considerable bias. Second, weighted regression maintains this primary assumption of ordinary least square regression and is only helpful, if the specific weights for each calibration point are known (Ripley & Thompson 1987). For equal weights, weighted regression gives the same results as ordinary least squares regression. Third, the calibration/prediction procedure is biased, too, because calibration is based on the assumption that the abscissa data is error-free. In the prediction step however, the ordinate value (in case of pH measurement the mV reading in the sample solution) is assumed to be error-free. This principal difference is of marginal importance in case of laboratory pH measurement in well-characterized solutions under controlled conditions, but becomes of importance e.g. in field measurement of pH for hydrogeological investigations. A statistical approach that avoids these weaknesses is the maximum likelihood approach (Bates & Watts 1988). In the following, the maximum likelihood approach is compared to the OLS approach.

In the maximum likelihood approach, it is assumed that the calibration data represent a random realization of the distribution $\text{pH} = \text{pH}_{\text{true}} + \text{error}$ and $\text{mV} = \text{mV}_{\text{true}} + \text{error}$. Thus, both abscissa and ordinate data are affected by random errors - a major difference to the OLS approach commonly selected. The parameters requested are those that maximize the probability to obtain the experimentally observed data under the constraint, that both abscissa and ordinate data are affected by error. The least squares condition is given by eq. 8.10:

$$L = -\frac{1}{2} \sum (\text{pH}_{\text{obs}} - \text{pH}_{\text{true}})^2 / \kappa_i - \frac{1}{2} \sum (\text{mV}_{\text{obs}} - \text{mV}_{\text{true}})^2 / \lambda_i \quad (8.10)$$

where κ_i and λ_i give the variances of in pH and the measured potentials, resp. and the subscripts obs. and true designate experimentally observed and true but unknown data points, resp. If informations on variances are not available, the function to minimize is eq. 8.11 (Ripley & Thompson 1987):

$$L = -\frac{1}{2\lambda} \sum (\text{pH}_{\text{obs}} - \text{pH}_{\text{true}})^2 - \frac{1}{2\lambda} \sum (\text{mV}_{\text{obs}} - \text{mV}_{\text{true}})^2 \quad (8.11)$$

The least squares line therefore is given by the minimum of the perpendicular distances between maximum likelihood least square line and the data points of abscissa and ordinate. Following this procedure, the least squares line is independent whether pH or mV readings are taken as abscissa data. On the other hand, closed formulas for the confidence region, comparable to eq. 8.7, are not available for the likelihood method (Donaldson & Schnabel 1987). Approximate confidence regions in the parameter space (α, β) can be obtained from the diagonal elements of the variance-covariance matrix of (α, β) by eq. 8.12:

$$V = s^2 (J(\Theta)^T J(\Theta))^{-1} \quad (8.12)$$

where s^2 is the residual sum of squares and $J(\Theta)$ is the Jacobian matrix in the minimum of the parameter space $\Theta = (\alpha, \beta)$. Among several possible approximations to the variance-covariance matrix V , eq. 8.12 is report to be the most robust variant (Donaldson & Schnabel 1987). When calculating the Jacobian matrix V for the OLS regression line, numerically values identical with the standard deviations in (α, β) according to eqs. 8.4/5 are obtained. By evaluating eq. 8.12 the maximum likelihood least squares line will show whether a significant improvement in the accuracy of parameters (α, β) can be obtained.

Using the likelihood approach, where the residuals are given by the perpendicular distances between experimental data and least squares line, similar standard deviations are obtained compared to the OLS regression method, as shown in table 8.3. For the time being, it is concluded that for laboratory determinations the lack of simple and efficient means to calculate confidence ellipses and related statistical parameters outweighs the principal advantage of unbiasedness in the maximum likelihood approach.

8.3 Application Example

CO_2 dissolves in aqueous solutions under partial dissociation into HCO_3^- and CO_3^{2-} ions. The concentrations of these ions can be determined by potentiometric titration. From such an experiment, the data pairs given in Table IV in 0.1 M perchlorate medium at 25 °C and under an nitrogen/ CO_2 (1.0%) atmosphere have been obtained. Interpreting these data by eq. 8.13

$$\lg [\text{CO}_3^{2-}] = \lg K + \lg \text{pCO}_2 + 2 \text{pH} \quad (8.13)$$

without taking into account the uncertainty in pH, $\lg K = -17.62 \pm 0.07$ is obtained. By allowing the experimentally determined pH values to float within the specified uncertainties during 1000 resampling cycles however, a parameter $\lg K = -17.63 \pm 0.18$ is obtained. In these studies, pH values are randomly drawn from a normal variate with mean value at the given pH and deviation σ , included in table 8.4 and calculated by eq. 8.8. The slope β is fixed at the theoretical slope of 2. The uncertainty contributed by pH nearly triples the over-all uncertainty in the parameter $\lg K$. This simple example shows that the uncertainty in the determination of thermodynamic constants for pH dependent species must be considered as biased if the error contributions from the pH determination to the over-all uncertainty are neglected.

Table 8.4 : experimental carbonate concentrations as a function of pH ($\text{pCO}_2 = 1\%$)

$\lg [\text{CO}_3^{2-}]$	pH	uncertainty σ
-4.18	7.63	$\pm 0.02_7$
-4.00	7.71	$\pm 0.03_2$
-3.64	7.93	$\pm 0.03_3$
-3.33	8.10	$\pm 0.03_4$
-3.17	8.26	$\pm 0.02_9$
-2.97	8.36	$\pm 0.04_0$
-2.34	8.43	$\pm 0.03_9$
-2.27	8.60	$\pm 0.03_2$
-1.87	8.75	$\pm 0.03_3$

The discussion focused on a comparison of different suitable procedures to assign a realistic estimate to the uncertainty of pH, based on the MPC procedure. The theoretical relationship between observed pH and pH meter readings is a linear function and thus, the correct elliptical confidence region in the parameter space (α, β) can be calculated from linear regression. A comparison of Monte Carlo simulations from the confidence ellipse with the OLS predictor eq. 8.7 as shown that an estimate can be directly obtained from eq. 8.8. A maximum likelihood approach is found to be of little practical advantage despite its theoretical merit of unbiasedness.

Assessment of uncertainty in the determination of an individual pH value is an essential task in many fields of science. However, the procedures proposed by IUPAC for evaluation of pH do not allow for detailed assessment of this uncertainty, because calibration of the electrode system against only one and two, resp. standard pH solutions is recommended. The obser-

vation that glass electrodes tend to have effective slopes considerably lower than the theoretical Nernstian slope of $-59.16 \text{ mV pH}^{-1}$ at $25 \text{ }^\circ\text{C}$ is confirmed. This observation indicates that use of BSI calibration procedure, where pH are estimated after calibration against one buffer standard by means of the theoretical Nernstian slope, might introduce systematic errors in the evaluation of thermodynamic constants. The advantage of MPC to allow detailed assessment of respective uncertainties is demonstrated on basis of 50 randomly selected five-point calibrations by Monte Carlo simulation. Calibration of the electrode against six standard buffer solutions will improve the precision of the MPC procedure, since $F_{2,3,0.95} = 9.554$, while $F_{2,4,0.95} = 6.945$. The size of the confidence ellipse (cf. eq. 8.7) will be reduced further.

The discussion is directed to the determination of thermodynamic constants for aqueous solution species. However, due to the general importance of pH, related questions occur as well in other areas, where thermodynamic interpretation of the measured pH values is of central interest. As outlined by Bates (1981), "only in the study of chemical equilibrium is it necessary to inquire about the precise nature of the quantity (pH) measured". Hence, determination of thermodynamic parameters is one of the areas where the given discussion addresses a relevant subject. In other areas, e.g. process control in commerce and industry, where pH is well established as a useful parameter, reproducibility is emphasized over thermodynamic interpretation (Galster 1991, Bates 1981). To illustrate the influence of uncertainty in determination of pH on the over-all uncertainty of thermodynamic constants in pH dependent reactions, a simple application example is given.

8.4 Statistical Calibration - A Comment

Chemists in many cases are satisfied to determine parameters of a least-square straight line when calibrating equipment. Often, there is no awareness of different approaches to calibration; e.g. classical, inverse (Krutchkoff 1967), bivariate (Riu & Rius 1996), orthogonal (Danzer et al. 1995) or even robust regression (Danzer 1989). Hence, few consideration is often devoted to the assessment of probable uncertainties in the determined quantities. As a matter of fact, each experimental datum is affected by errors, both bias and stochastic errors. The ignorance of these unavoidable contributions may affect the results to a degree that makes the forwarded conclusions void. On the other hand, selection of a suitable model for straight-line calibration may become a delicate task, too. In the present discussion, the pH electrode is calibrated by classical least-square regression. A model $y_i = a + b x_i + \varepsilon_i$ is used, where ε_i is a stochastic homoscedastic error with mean zero and standard deviation σ . However, it may be argued that a model $y_i = a + b x_i + e_j + \varepsilon_i$ should be more adequate, where e_j is a -basically non-stochastic- liquid junction potential. There is no reason to reject this argument. But fig. 8.3 clearly points out the strong stochastic nature of measurement residuals in pH calibration. There is no way to argue about the deviations between the experimental distribution curve and the cumulative Normal distribution. In nature, both normal distributions and homoscedastic errors are very rare -especially if the data are collected during a nearly ten-year-period. Nevertheless, the calibration of a pH electrode remains a field worth for further activity.

9. Uranium(VI) Spectroscopic Speciation

Generally, fundamental science does not reflect directly on practical application of research results. However, an actinide chemist should be prepared to answer an inquiry. After all, actinide science is closely related to questions of central political interest. However, in the present case, the answer is 'learning'. Actinides with their comparatively intense UV-Vis spectra, their variety of redox states and their radioactivity make them valuable tools for investigating natural systems. E.g. isotope hydrogeology is an essential tool to understand global cycles, geologic transformation as well as fundamental processes like sorption. Uranium, e.g. via its $^{234/238}\text{U}$ disequilibria, has added a tremendous amount of knowledge to our understanding of natural systems.

Currently, the remediation of areas contaminated by mining -not only uranium mining- is a question of major importance in many countries of this world, e.g. Czech Republic, South Africa, Brazil or Canada. Therefore, the following pages are devoted to an assessment of prospects and limitations of uranium(VI) spectroscopic studies in natural aquatic systems.

Because of its nuclear applications, an enormous amount of scientific work was directed to uranium after discovery of nuclear fission in 1939. The results of spectroscopic studies on U(VI) done during the Manhattan Project have been summarized by Rabinovitch and Belford in 1964. As these authors stated: "Yet many basic experimental questions remain unsettled and a theory of the uranyl ion explaining its spectroscopic behaviour is only rudimentary". The lasting controversial discussion of the electronic structure of the UO_2^{2+} entity has been settled only recently (Denning 1992). Thus, a more reliable basis for interpretation of spectroscopic studies has been reached.

Owing to the low solubility and high sorption tendency of U(IV), uranium is dissolved in aqueous systems mainly in the hexavalent form (Williams 1994). Uranium(V) is stable only in a limited pH/ E_{H} range and has a high tendency for disproportionation (Selbin & Ortego 1969). It is not likely to play a role in natural systems.

Current interest in the physico-chemical properties of the uranyl(VI) entity UO_2^{2+} originates mainly from the fact that uranium is a major constituent of highly radioactive nuclear waste as well as the need to remediate areas contaminated by uranium mining after World War II. Therefore, spectroscopic properties of U(VI) are of considerable interest for speciation of uranium e.g. in natural systems contaminated by uranium mining. Speciation in the present context aims at the characterization of specific forms of a metal ion in aqueous solution. Specific form does not only refer to the oxidation state, but on revealing the specific environment of a metal ion, e.g. its specific structure in solution. A broader outline of different aspects of speciation is given elsewhere (Frimmel & Gremm 1994).

In the following, spectroscopic properties of hexavalent uranium will be discussed with respect to its potential application in site-specific characterization of U(VI) in areas contaminated by uranium mining. Some emphasis is put on the correlation between absorption and emission spectra of U(VI) solution species.

9.1 Spectroscopic Speciation by UV-Vis Spectroscopy

Uncertainties and mutually exclusive interpretations concerning the electronic structure and the multiplicity of the electronic ground state have hampered application of spectroscopic techniques to speciation of uranium(VI) in aqueous solutions. Noted exceptions are e.g. the studies of Bartusek and Sommer (1964) as well as Rush and Johnson (1963). Both studies were directed to the hydrolysis of the uranyl(VI) ion. Hydrolysis is a most fundamental reaction of a metal ion in aqueous solutions. For actinides like uranium(VI), hydrolysis and coordination by carbonate have been recognized as predominant geochemical reactions in natural aqueous systems (Langmuir 1978).

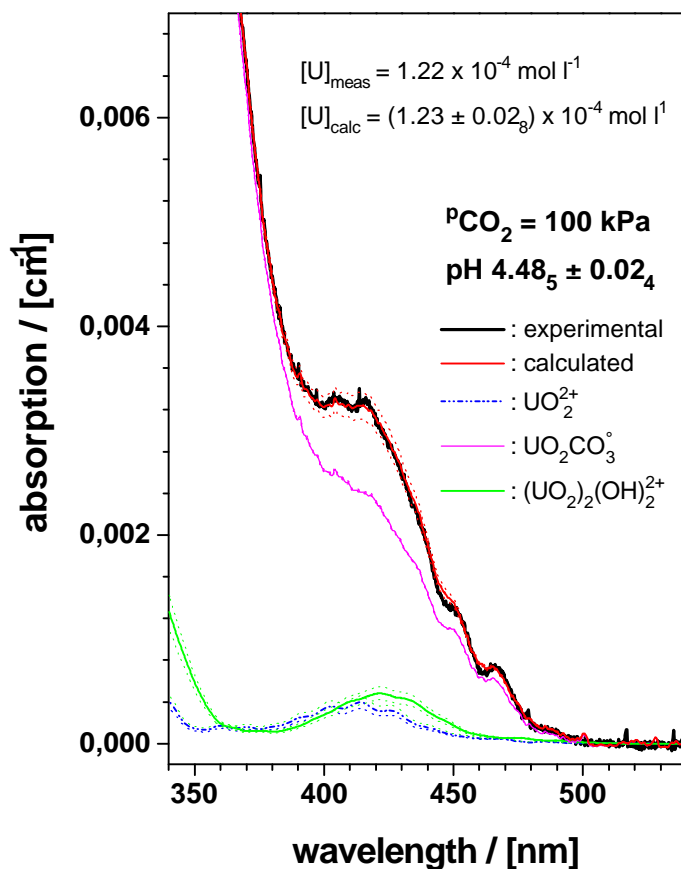


Fig. 9.1 : UV-Vis absorption spectrum of U(VI) at $\text{pH } 4.48_5 \pm 0.02_4$ under a CO_2 atmosphere in solid/aqueous phase equilibrium with $\text{UO}_2\text{CO}_3(\text{s})$ (Meinrath 1997b). The spectrum is interpreted by the single component spectra of UO_2^{2+} , $\text{UO}_2\text{CO}_3^\circ$ and $(\text{UO}_2)_2(\text{OH})_2^{2+}$.

In Fig. 9.1, an application example is given to illustrate the principle and potential of spectroscopic speciation for the characterization of the state of a uranyl(VI) species in aqueous solution. The spectrum is recorded from a solution in solid/aqueous phase equilibrium with $\text{UO}_2\text{CO}_3(\text{s})$ under a CO_2 atmosphere (Meinrath 1997b). By spectroscopic speciation, not only a total uranium concentration is obtained, but detailed information on the physicochemical state in solution.

UV-Vis spectroscopy with a few exceptions most probably might be not sensitive enough to detect U(VI) concentrations even in areas contaminated by uranium mining (Helling et al.

1997). The single component spectra in figs. 4.7 and 4.9 however will be helpful in verifying thermodynamic data bases used for geochemical modelling of uranium e.g. in the assessment of remediation strategies in former uranium mining areas. Furthermore, these spectra will be helpful in development of TRLFS towards quantitative analysis of hydrolyzed U(VI) solutions.

9.2 Fluorescence Spectroscopy of Uranium(VI)

Fluorescence of uranium(VI) in salts and solutions is studied over more than 150 years. As early as 1853, Stokes reported the "mirror-image" relationship between absorption spectrum and emission spectrum while studying uranyl nitrate crystals (Stokes 1852, 1853). By using pulsed laser excitation and time resolution of the emission process, there is a potential for speciation of U(VI) at the nanomol level (Kato et al. 1994). Advanced spectroscopic techniques like time-resolved laser-induced fluorescence spectroscopy are able to routinely collect emission spectra and determine lifetimes. The potential as well as its limiting factors for application of TRLFS will be focused on in the sequel.

9.2.1 Application of TRLFS to Spectroscopic Speciation

Despite these promising features, fluorescence spectroscopy has not been used for spectroscopic speciation of uranium(VI) solutions until recently. Application of fluorescence spectroscopy has been hampered by inconsistent interpretation of fluorescence lifetimes observed in solutions with increasing pH. While it has been well known that the $\text{UO}_2^{2+}(\text{aq})$ species has a fluorescence lifetime of about 1 μs in acid solution $<\text{pH } 2$, a second lifetime contribution had been reported to appear on lowering the pH value to about pH 3 (Matsushima 1972). This second lifetime of about 2.5 μs has been interpreted due to different fundamental processes, e.g. intersystem crossing (Formosinho et al. 1984) or exciplex formation of $\text{H}^*(\text{UO}_2)_2^{4+}$ (Marcantonatos 1980) (*): electronically excited).

An interpretation of the second lifetime due to formation of UO_2OH^+ species was suggested by Zheng et al. (1986), thus indicating the potential of applying time-resolved laser-induced fluorescence spectroscopy (TRLFS) to speciation of uranium(VI). By correlating UV-Vis spectroscopic evidence on formation of the $(\text{UO}_2)_2(\text{OH})_2^{2+}$ species with TRLFS, the speciation capabilities of TRLFS have been demonstrated and the occurrence of a second lifetime has been attributed to formation of the $(\text{UO}_2)_2(\text{OH})_2^{2+}$ species (Meinrath et al. 1993). Meanwhile, TRLFS is extended successfully to a variety of pH-dependent U(VI) systems (Kato et al. 1994, Bernhard et al. 1996, Couston et al. 1995, Brendler et al. 1996).

To illustrate the fundamental relationship between absorption and emission spectra, a schematic illustration of a molecular fluorescence process is given in fig. 9.2. Energy transfer between an electronic ground state $0v_n$ with vibrational quantum levels n and two different excited levels $1v_n$ and $2v_n$ is shown, each with n vibrational levels. Upon light absorption, an electron is excited from the ground state level to excited levels. This process is indicated by top arrows. Under moderate temperatures of 298 K, in thermal equilibrium usually only the vibrational ground levels ($n = 0$) only are occupied. As a rough rule, first excited vibrational levels at temperatures <300 K are occupied usually with a few percent only, while occupation of higher excited vibrational levels can be neglected.

Excitation from ground state to one of the excited states is governed by the Franck-Condon principle (Rabinovitch & Belford 1964) with the consequence that molecules in non-equilibrium vibrational levels ($n>0$) are formed in the excited electronic state (Sykora & Sima 1990). Hence, the excited molecule strongly vibrates. This vibrational energy however is quickly dissipated by collisions with neighboring molecules. Collision rates in aqueous solutions at room temperatures occur at about 10^{12} s^{-1} (Porter 1983). A thermally equilibrated excited state is formed with excited electrons occupying the vibrational ground state of the excited electronic states: $1v_0$ and $2v_0$, resp. The electronic relaxation of excited state $2v_0$ may occur by either direct relaxation to the electronic ground state or via the first excited state $1v$. Some transitions to and from the state $2v$ are considered by dashed lines in fig. 9.2. Experimental work has shown that uranyl(VI) that is excited to higher states than $1v$ relaxes to the first excited state on a time scale short compared to 10 ns (Sugitani et al. 1980). Occupation of the fluorescent first excited state $1v$ may be more efficient via higher excited states than via direct excitation (Sykora & Sima 1990). In case of the $\text{UO}_2^{2+}(\text{aq})$ ion, the direct excitation of the fluorescent state by absorption

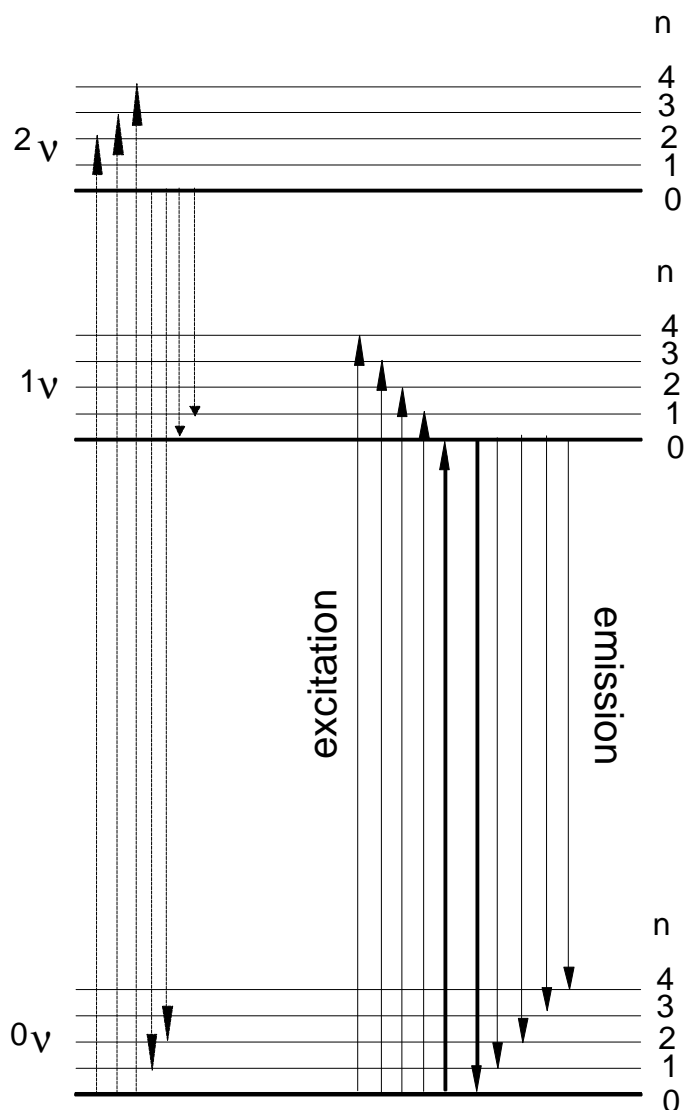


Fig. 9.2 : Jablonski diagram illustrating fundamental relationship between absorption and emission spectrum

of light in the range 500 nm to 370 nm, is a very weak process compared to the intense absorption in the UV range, as shown in fig. 3.2. Hence, excitation in the UV range is often preferred (Kato et al. 1994, Couston et al. 1995, Bernhard et al. 1996) in practical TRLFS studies.

Taking the case of the UO_2^{2+} group, state ${}^2\nu$ in the schematic representation of fig. 9.2 corresponds to an intense UV absorption, while state ${}^1\nu$ represents the symmetry forbidden low-lying absorption in the visible range. Due to symmetry effect, relaxation rate from ${}^1\nu$ to ${}^0\nu$ state is forbidden in the same way as is direct excitation. This relationship qualitatively explains the long lifetime of the emission process in uranyl(VI) compounds. Since the lifetime of the fluorescent state is in the μs range, a time scale long against collision frequency in solution, relaxation takes place from the vibrational ground state ($n = 0$) of the fluorescent state ${}^1\nu$, too.

Like the absorption process, the emission process is governed by the Franck-Condon principle (Porter 1983). Therefore, the ${}^0\nu_0 \leftarrow {}^1\nu_0$ relaxation is not the only transition observed in the emission spectrum, even not necessarily the predominant transition. The relaxation processes from ${}^1\nu_0$ to ${}^0\nu_n$ states are indicated by solid bottom arrows. As indicated by fig. 9.2, energy of maximum emission will usually be found at longer wavelength than the maximum of absorption. Furthermore, the emission spectrum will occur at the long-wavelength side of the absorption spectrum, provided the absorption and emission bands correspond to the same transition and the species does not change itself between excitation and emission, e.g. by ligand exchange. The only transition energy that is common to both absorption and emission spectrum corresponds to the transition between the vibrational ground states of the ground and first excited state. These transitions are given as bold lines. Thus, the spectral correlations given in figs. 6.2 - 6.4 validate the consistency of spectral data despite the fact that spectral informations have been collected during the past five years by different equipment in different laboratories and evaluated by in part highly sophisticated data treatment techniques.

Concerning application of TRLFS to speciation of uranium(VI) in environmental systems, these features are most favourable. In natural systems, the fluorescence of the UO_2^{2+} entity can be readily distinguished from organic fluorescence due to its longer lifetime. Naturally occurring organic materials have fluorescence lifetimes in the nanosecond range, while the UO_2^{2+} entity has fluorescence lifetimes in the microsecond range. Other inorganic fluorescent ions, e.g. Eu^{3+} or Tb^{3+} will occur in nature only under exceptional conditions at sufficient concentration levels.

9.2.2 Quenching

The advantageous features of U(VI) TRLFS speciation discussed above are opposed by interfering effects. The fluorescence emission process illustrated in fig. 9.2 has to compete with concurrent processes. These processes are e.g. radiationless decay or quench. It should be noted that uranium(VI) ion in its electronically excited state is expected to be a strong oxidizing agent. As outlined elsewhere in more detail (Balzani et al. 1978), the energy of the excited electron in the UO_2^{2+} entity corresponds to a redox potential of about 2.6 V.

Therefore it is not surprising that a series of quenching reactions with organic substances, e.g. alcohols (Hill et al. 1974) and aromatic hydrocarbons (Ahmed et al. 1975) has been reported. Formation of benzil from benzaldehyde (Matsushima et al. 1976) and biacetyl from acetaldehyde (Sakuraba & Matsushima 1972) are described in solutions containing $^*(\text{UO}_2^{2+})$. In all these cases, the energy transferred to the system by exciting the uranyl(VI) ions induces chemical reactions that otherwise would not take place. Similar potential quenchers as the organic substances mentioned above are expected to exist in environmental samples and thus may interfere in the applicability of TRLFS to environmental samples.

Inorganic ions like Fe^{3+} and Cl^- (Matsushima et al. 1974, Yokoyama et al. 1976) are able to either abstract the excited electron from the uranyl entity or transfer an electron to electronically excited $^*(\text{U(VI)})$ thus reducing the emission yield from the excited uranyl(VI) species. Quench by Br^- and I^- is found more efficient than quench by Cl^- (Yokoyama et al. 1976). In environmental systems however, chloride is more abundant than the heavier halogen ions. In case of Eu^{3+} , quench due to electron transfer from the excited uranyl(VI) to Eu^{3+} could be demonstrated by selectively exciting the uranyl entity, while observing the emission spectrum of the Eu^{3+} ion (Matsushima et al. 1974, Kropp 1967).

A further possible quenching mechanism is formation of carbonate radicals $\text{CO}_3^{\cdot-}$ (\cdot : unpaired electron) (Balzani et al. 1978). Evidence for formation of this radical species upon excitation of a solution containing $2 \cdot 10^{-3}$ M U(VI) and 0.01 M NaHCO_3 by flash light photolysis has been discussed. It has to be noted that fluorescence of higher carbonate species $\text{UO}_2(\text{CO}_3)_2^{2-}$ and $\text{UO}_2(\text{CO}_3)_3^{4-}$ could not be observed (Kato et al. 1994, Meinrath et al. 1993) due the strongly decreasing fluorescence yields at free carbonate concentrations above 10^{-7} M. Since such carbonate concentrations must be expected to occur widely in environmental systems, further limitations concerning the application of TRLFS to direct speciation of U(VI) in natural samples are not to be excluded. Here, further studies are necessary and will promise further interesting insight. More detailed reviews concerning the photochemistry of uranyl(VI) are available e.g. (Sykora & Sima 1990, Güsten 1983).

9.3 Speciation Needs in Natural Samples

To illustrate speciation needs in field samples, stability fields of relevant U(VI) hydrolysis and carbonate species are given in the U(VI)-pH diagram fig. 9.3. Conditions for which fig. 6 holds are 0.03% CO_2 partial pressure, an ionic strength of 0.1 M at 25 °C and neglectance of uranate solid phases. The stability fields indicate > 5% relative species amount. It is evident that oligomeric species, despite the great consideration devoted to them during the past half century, are stable only in a quite limited U(VI)-pH range close to the saturation limit of the solid phase.

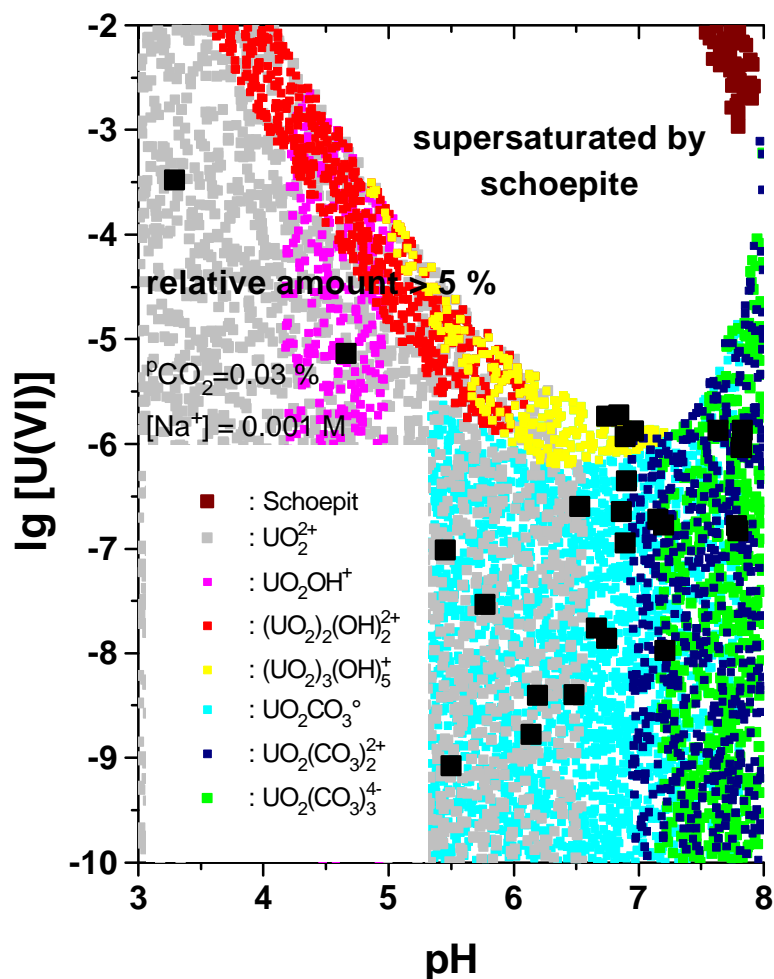


Fig. 9.3 : Stability fields of U(VI) species in aqueous solution with relative abundance > 5%. As can be seen, the stability field of intensively investigated oligomeric hydrolysis products is quite limited to a region close to the stability field of solid phase $\text{UO}_3 \cdot 2 \text{H}_2\text{O}$. Formation of solid uranate is suppressed by assuming a low Na^+ concentration. The diagram is calculated from the thermodynamic data discussed in this work.

The hydrated UO_2^{2+} species has the by far largest stability area. At $\text{pH} > 7$, the stability field of $\text{UO}_2(\text{CO}_3)_3^{4-}$ starts. Under conditions given in fig. 9.3, a pH value larger than 8 can not be attained due to restriction in ionic strength. It is however evident that the tricarbonato complex is the limiting U(VI) carbonato species for steric reasons (Meinrath 1996).

Stability fields of monomeric species UO_2OH^+ , UO_2CO_3^0 and $\text{UO}_2(\text{CO}_3)_2^{2-}$ are found at relative amounts >5 % within narrow pH limits. The stability fields are quite limited to about one pH unit only. Formation of carbonato species starts already at pH 5.3, strikingly illustrating the high affinity of U(VI) towards carbonate.

It should be noted that fig. 9.3 is based on the mean values of respective formation constants only. The intention of fig. 9.3 to provide a general overview on conditions and species in field samples contaminated by uranium(VI), comparable to the well-known Pourbaix diagrams (Brookins 1990). Included into fig. 9.3 are experimentally determined U(VI)-pH pairs (■) from field samples obtained from a uranium mill tailing (Butters 1994). It should be principally possible to speciate U(VI) directly in the field samples at $\text{pH} < 7$ where the U(VI) fluorescence is not affected by quenching from carbonate (Kato et al. 1994). However, the fluorescence intensities of U(VI) species dominating under these conditions are quite low and

the life times do not seem to be very characteristic. The life time of the UO_2OH^+ species e.g. is given with $\tau_{11} = 10 \mu\text{s}$ (Bernhard et al. 1996), $\tau_{11} = 35 \mu\text{s}$ (Eliet et al. 1995) and $\tau_{11} = 80 \mu\text{s}$ (Moulin et al. 1995). Fig. 9.3 might be helpful to prepare solutions wherein the UO_2OH^+ species can be detected unambiguously by suitable techniques like photoacoustic spectroscopy or TRLFS. At present, there is no method to speciate these field samples spectroscopically, because UV-Vis spectroscopy is not sensitive enough while the low fluorescence intensity of U(VI) species formed in the region of interest reduces the power of TRLFS. Thus, only indirect speciation e.g. correlation with stability field diagrams like fig. 9.3 can be provided to characterize U(VI) field samples from most uranium mining areas.

Generally, TRLFS may become a powerful tool for direct spectroscopic speciation of U(VI) in environmental samples. However, it is to be expected that TRLFS can not be applied as a general method suitable for all environmental systems. Nevertheless, the promising features of this technique will certainly attract continued interest, because the use of spectroscopy for speciation of uranium(VI) in environmental samples is just at its beginning.

10. References

- ÅBERG, M. (1969): "The Crystal Structure of $[(\text{UO}_2)_2(\text{OH})_2\text{Cl}_4(\text{H}_2\text{O})]^{2+}$ ", *Acta Chem. Scand.*, **23**, 791 - 810
- ÅBERG, M. (1970): "On the Structure of the Predominant Hydrolysis Products of Uranyl(VI) in Solution", *Acta Chem. Scand.*, **24**, 15
- ÅBERG, M., FERRI, D., GLASER, J. & GRENTHE, I. (1983): "Structure of the Hydrated Dioxouranium(VI) Ion in Aqueous Solution.-A X-ray Diffraction and ^1H NMR Study", *Inorg. Chem.*, **22**, 3986 - 3989
- AHMED, M., COX, A., KEMP, J.T., SULTANA, Q. (1975): *J. Chem. Soc. Perkin Trans.*, **2**, 1867
- ALCOCK, N.W. & ESPERÀS, S. (1977): "Crystal and Molecular Structure of Uranyl Perchlorate Heptahydrate", *J. Chem. Soc. Dalton Trans.*, 893 - 89
- ALLEN, D.M., BURROWS, H.D., COX, A., HILL, R.J., KEMP, T.J. & STONE, T.J. (1973): "Absorption Spectrum and Reaction Kinetics of the Photosensitive State of the Uranyl Ion", *J. Chem. Soc. Chem. Comm.*, 59
- ALLEN, P.G., BUCHER, J.J., CLARK, D.L., EDELSTEIN, N.M., EKBERG, S.A., GOHDES, J.W., HUDSON, E.A., KALTSOYANNIS, N., LUKENS, W.W., NEU, M.P., PALMER, P.D., REICH, T., SHUH, D.K., TAIT, C.D. & ZWICK, B.D. (1995): *Inorg. Chem.*, **34**, 4797
- AZENHA, M.E.D.G., BURROWS, H.D., FORMOSINHO, S.J., LEITÃO, M.L.P. & MIGUEL, M.D.G.M. (1988): "Coordination Behaviour of Dioxouranium(VI) Nitrate in Water-Aceton Mixtures", *J. Chem. Soc. Dalton Trans.*, 2893
- AZENHA, M.E.D.G., BURROWS, H.D., FORMOSINHO, S.J. & MIGUEL, M.D.G.M., (1989): "Photophysics of the Excited Uranyl Ion in Aqueous Solutions: Part 6 - Quenching Effects of Aliphatic Alcohols", **85**, 2625
- BALZANI, V., BOLETTA, F., GANDOLFI, M.T. & MAESTRI, M. (1978): "Bimolecular Electron Transfer of Excited States of Transition Metal Complexes", *Topics in Current Chemistry*, **75**, 1 - 64
- BARAN, V. (1965): "Uranyl(V)-hydroxokomplexe", *Z. Chem.*, **5**, 56
- BARAN, V. (1992): Uranium(VI)-Oxygen Chemistry; Czech Nuclear Research Institute, Rez, 135 p.
- BARAN, V. & TYMPL, M. (1962): "Hydrolyse des Uranyls. II. Magnetochemische Untersuchungen", *Coll. Czech. Chem. Comm.*, **27**, 1340 - 1344
- BARCLAY, G.A., SABINE, T.M. & TAYLOR, J.C. (1965): "The Crystal Structure of Rubidium Uranyl Nitrate: A Neutron Diffraction Study", *Acta Cryst.*, **19**, 205
- BARKER, T.J., DENNING, R.G. & THORNE, J.R.G. (1987): "Application of Two-Photon Spectroscopy to Inorganic Compounds. 1. Spectrum and Electronic Structure of $\text{Cs}_2\text{UO}_2\text{Cl}_4$ ", *Inorg. Chem.*, **26**, 1721
- BARTLETT, M.S. (1950): "Tests of Significance in Factor Analysis", *Brit. J. Psych. Stat. Sect.*, **3**, 77 - 85
- BATES, R.G. (1981): "The Modern Meaning of pH", *CRC Critical Reviews in Analytical Chemistry*, **10**, 247
- BATES, D.M. & WATTS, D.G., (1988): Nonlinear Regression Analysis and its Application; Wiley Series in Probability and Mathematical Statistics, (1988), New York/USA., 364 p.
- BAUCKE, F.G.K., NAUMANN, R. & ALEXANDER-WEBER, CH. (1993): "Multiple-Point Calibration with Linear Regression as a Proposed Standardization Procedure for High-Precision pH Measurement", *Anal. Chem.*, **65**, 3244 - 3251
- BAUCKE, F.G.K. (1994a): "The Modern Understanding of the Glass Electrode Response", *Fresenius J. Anal. Chem.*, **349**, 582 - 596
- BAUCKE, F.G.K. (1994b): "Thermodynamic Origin of the Sub-Nernstian Response of Glass Electrodes", *Anal. Chem.*, **66**, 4519 - 4524
- BEHAR, D., CZAPSKI, G. & DUCHOVNY, I. (1970): *J. Phys. Chem.*, **74**, 2206
- BELFORD, R.L. (1961): "Paramagnetism of Uranyl Ion", *J. Chem. Phys.*, **34**, 318
- BELFORD, R.L. & BELFORD, G. (1961): "Pi Bonding in Uranyl Ion", *J. Chem. Phys.*, **34**, 1330 - 1332
- BELL, J.T. & BIGGERS, R.E. (1965): "The Absorption Spectrum of the Uranyl Ion in Perchlorate Media. Part I. Mathematical Resolution of the Overlapping Band Structure and Studies of the Environmental Effects", *J. Mol. Spectr.*, **18**, 247
- BELL, J.T. & BIGGERS, R.E. (1967): "The Absorption Spectrum of the Uranyl Ion in Perchlorate Media. Part II. The Effect of Hydrolysis on the Resolved Spectral Bands", *J. Mol. Spectr.*, **22**, 262
- BELL, J.T. & BIGGERS, R.E. (1968): "The Absorption Spectrum of the Uranyl Ion in Perchlorate Media. Part III. Resolution of the Ultraviolet Band Structure; Some Conclusions Concerning the Excited Electronic State", *J. Molec. Spectr.*, **25**, 312
- BELOVA, V.I., SYRKIN, YA.K., MARKOV, V.P. & TSAPKINA, I.V. (1961): "Magnetic Susceptibility of Uranyl Compounds", **6**, 251 - 253
- BENSON, P., COX, A., KEMP, T.J. & SULTANA, Q. (1975): "Concentration and Temperature Quenching of the Excited State of the Uranyl Ion in Aqueous Solution by Laser Flash Photolysis", *Chem. Phys. Letters*, **35**, 195

- BERNHARD, G., GEIPEL, G., BRENDLER, V., NITSCHKE, H. (1996): „Speciation of Uranium in Seepage Waters of a Mine Tailing Pile Studied by Time-resolved Laser-induced Fluorescence Spectroscopy (TRLFS); *Radiochim. Acta*, **74**, 87 - 91
- BLOCH, S. (1980): „Some Factors Controlling the Concentration of Uranium in the World Sea Ocean“, *Geochim. Cosmochim. Acta*, **44**, 373 - 377
- BOMBIERI, G., FORSELLINI, E., DAY, J.P. & AZZEZ, W.I. (1978) "Crystal Structure of Dichlorodioxobis(triphenylphosphine oxide) Uranium(VI)"; *J. Chem. Soc. Dalton Trans.*; 677 - 680
- BORING, M., WOOD, J.H. & MOSKOWITZ, J.W. (1975): "Self Consistent Field Calculation of the Electronic Structure of the Uranyl Ion (UO_2^{2+})"; *J. Chem. Phys.*, **63**, 638
- BOX, G.E.P. & DRAPER, N.R. (1987): Empirical Model Building and Response Surfaces, Wiley and Sons, New York./USA
- BRENDLER, V., GEIPEL, G., BERNHARD, G., NITSCHKE, H. (1996): „Complexation in the System $\text{UO}_2^{2+}/\text{PO}_4^{3-}/\text{OH}(\text{aq})$: Potentiometric and Spectroscopic Investigations at Very Low Ionic Strength“, *Radiochim. Acta*, **74**, 75 - 80
- BRINT, P. & M^CCAFFERY, A.J. (1973): "The Electronic Spectra and Magnetic Circular Dichroism of the Uranyl Ion"; *Mol. Phys.* **25**, 311
- BROOKINS, D.G. (1984); Geochemical Aspects of Radioactive Waste Disposal; Springer-Verlag Heidelberg/Germany
- BROOKINS, D.G. (1990): Eh-pH-Diagrams for Geochemistry; Springer-Verlag Heidelberg/Germany
- BROWN, D.R., DENNING, R.G. & JONES, R.H. (1994): "Synthesis and Crystal Structure of an Analogue of the Uranyl(VI) Ion, Containing a Linear O=U=N Group"; *J. Chem. Soc. Chem. Comm.*, 2601 - 2602
- BRUMBY, S. (1989): „Exchange of Comments on the Simplex Algorithm Culminating in Quadratic Convergence and Error Estimation“, *Anal. Chem.*, **61**, 1783
- BÜPPELMANN, K. (1988): „Chemisches Verhalten von Plutonium in chloridhaltigen wäßrigen Lösungen“, Dissertation, TU München/Germany
- BURROWS, H.D. & KEMP, T.J. (1974): „The Photochemistry of the Uranyl Ion“, *Chem. Soc. Rev. (London)* **3**, 139
- BURROWS, H.D. (1990): "Electron Transfer from Halide Ions to UO_2^{2+} Excited State Ions in Aqueous Solution: Formation and Decay of Dihalide Radical Anions"; *Inorg. Chem.*, **29**, 1549
- BUTTERS, A. (1994): „Sorptions- und Austauschverhalten turoner und cenomaner Sandsteine in Bezug auf Uran“, Diplomarbeit, TU Bergakademie Freiberg, Institut für Geologie, Freiberg/Germany
- CARNALL, W.T. & RAJNAK, K. (1975): "Electronic Energy Level and Intensity Correlations in the Spectra of the Trivalent Actinide Aquo Ions. II. Cm^{3+} "; *J. Chem. Phys.*, **63**, 3510 - 3514
- CARNALL, W.T. (1979): "The Absorption and Fluorescence Spectra of Rare Earth Ions in Solution"; Handbook of the Physics and Chemistry of the Rare Earth (Gschneider, K.A., Eyring, L. eds.), North-Holland Publ. Comp., Amsterdam/The Netherlands
- CATTELL, R.B. (1966): „The SCREE Test for the Number of Factors“, *Multivar. Behav. Res.*, **1**, 245 - 276
- CATTELL, R.B. (1978): Scientific Use of Factor Analysis in Behavioural and Life Sciences, Plenum, New York/USA
- CIAVATTA, L., FERRI, D., GRENTHE, I. & SALVATORE, F. (1981): "The First Acidification Step of the Tris(carbonato) dioxouranate(VI) Ion, $\text{UO}_2(\text{CO}_3)_3^{4-}$ "; *Inorg. Chem.*, **20**, 463
- CLIFFORD, A.A. (1973): *Multivariate Error Analysis*; Applied Science, London/U.K.
- CONNICK, R.E. & HUGUS JR., Z.Z. (1952): "The Participation of f Orbitals in Bonding in Uranium and the Transuranium Elements"; *J. Am. Chem. Soc.*, **74**, 6012
- CORDFUNKE, E.H.P. (1969): The Chemistry of Uranium; Elsevier Publ. Comp., Amsterdam/The Netherlands 250 p.
- CORNEHL, H.H., HEINEMANN, CH., MARCALO, J., PIRES DE MATOS, A. & SCHWARZ, H. (1996): The 'Bare' Uranyl(2+) Ion, UO_2^{2+} , *Angew. Chemie. Int. Ed. Engl.*, **35**, 891 - 894
- COULSON, C.A. & LESTER, G.R. (1956): "Possible f-Orbital Hybridization in Uranyl and Related Complexes"; *J. Chem. Soc.*, 3650
- COUSTON, L., POUYAT, D., MOULIN, V., DECAMBOX, P. (1995): „Speciation of Uranyl Species in Nitric Acid Medium by Time-resolved Laser-induced Fluorescence“, *Appl. Spect.*, **49**, 349 - 353
- COVINGTON, A.K. (1981): „Recent Developments in pH Standardisation and Measurement for Dilute Aqueous Solutions“, *Anal. Chim. Acta*, **127**, 1-21
- COVINGTON, A.K., BATES, R.G. & DURST, R.A. (1983): "Definition of pH Scales, Standard Reference Values, Measurement of pH and Related Terminology"; *Pure Appl. Chem.*, **55**, 1467
- DANZER, K. (1989): „Robuste Statistik in der analytischen Chemie“, *Fresenius Z. Anal. Chem.*, **335**, 869 - 875

- DANZER, K., WAGNER, M., FISCHBACHER, C. (1995): „Calibration by Orthogonal and Common Least Squares - Theoretical and Practical Aspects“, **352**, 407 - 412
- DAVID, F. (1986): "Thermodynamic Properties of Lanthanide and Actinide Ions in Aqueous Solution"; J. Less-Comm. Met., **121**, 27 -42
- DAVISON, W., WOOF, C. (1985): „Performance Tests for the Measurement of pH with Glass Electrodes in Low Ionic Strength Solutions including Natural Waters“; Anal. Chem., **57**, 2567 - 2570
- DAY, J.P. & VENANZI, L.M. (1966): "Some Six-co-ordinate Complexes of Uranium(VI)"; J. Chem. Soc. A, 1363 - 1367
- DE JAGERE, S. & GÖRLLER-WALRAND, CH. (1969): "A Vibronic Analysis of the Absorption Spectrum of the Uranyl Ion"; Spectrochim. Acta, **A25**, 559
- DEKOCK, R.L., BAERENDS, E.J., BOERRIGTER, P.M. & SNIJDERS, J.G. (1984): "On the Nature of the First Excited State of the Uranyl Ion"; Chem. Phys. Lett., **105**, 308
- DENNING, R.G., SNELGROVE, T.R. & WOODWARK, D.R. (1976): "The Electronic Structure of the Uranyl Ion -Part I. The Electronic Spectrum of Cs₂UO₂Cl₄"; Mol. Phys., **32**, 419 - 442
- DENNING, R.G., FOSTER, D.N.P., SNELGROVE, T.R. & WOODWARK, D.R. (1979a): "The Electronic Structure of the Uranyl Ion. II. The Electronic Spectra of Cs₂UO₂(NO₃)₂ and NaUO₂(CHCOO)₃"; Mol. Phys., **37**, 1089 - 1107
- DENNING, R.G., SNELGROVE, T.R. & WOODWARK, D.R. (1979b): "The Electronic Structure of the Uranyl Ion. III. Theory"; Mol. Phys., **37**, 1109 - 1143
- DENNING, R.G. (1983): "Properties of the UO₂ⁿ⁺ (n = 1,2) Ions"; Gmelin Handbuch der Anorganischen Chemie, Uran (Supplement) A6, 31 - 79
- DENNING, R.G. (1992): "Electronic Structure and Bonding in Actinyl Ions"; Structure Bond., **79**, 215 - 276
- DESCHAUX, M., MARCANTONATOS, M.D. (1979): „Time-resolved Luminescence and Mean Life Times of UO₂²⁺ in Aqueous Solution“; Chem. Phys. Letters, **63**, 283
- DIEKE, G.H. & DUNCAN, A.B.F. (1949): Spectroscopic Properties of Uranium Compounds; National Nuclear Energy Series, Div. III, **2**, McGraw-Hill, New York
- DIXON, J.W. (1950): „The Analysis of Extreme Values“, Ann. Math.Stat., **21**, 488 - 506
- DONALDSON, J.R. & SCHNABEL, R.B. (1986): „Computational Experience with Confidence Regions and Confidence Intervals of Nonlinear Least Squares“, Technometrics, **29**, 67
- DUNSMORE, H.S., HIETANEN, S. & SILLÉN, L.G. (1963): „Studies on the Hydrolysis of Metal Ions. 46. Uranyl Ion, UO₂²⁺, in Chloride, Perchlorate, Nitrate and Sulfate Media. Survey and Introduction“; Acta Chem. Scand., **17**, 2644 - 2656
- EBEL, S., GLASER, E., MOHR, H. (1978): „Fehler und Fehlerfortpflanzung bei der Bestimmung von pH-Werten“, FreseniusJ. Anal. Chem., **293**, 33 - 35
- EFRON, B. (1981): „Nonparametric Estimates of Standard Error: The Jackknife, the Bootstrap and other Methods“, Biometrika, **68**, 589 - 599
- EFRON B. & GONG, G. (1983): „A Leisurely Look at the Bootstrap, the Jackknife and the Cross-Validation“; Am. Stat., **37**, 36 - 48
- EISENSTEIN, J.C. & PRYCE, M.H.L. (1955): "The Electronic Structure and Magnetic Properties of Uranyl-like Ions. 1. Uranyl and Neptunyl"; Proc. Royal. Soc. (London), **A229**, 20
- EKBERG, C., SKARNEMARK, G., EMRÈN, A.T., LUNDÈN, I. (1996): „Uncertainty and Sensitivity Analysis of Solubility Calculations at Elevated Temperatures“, Material Res. Soc. Symp. Proc., **412**, 889 - 896
- EKBERG, C., EMRÈN, A.T., SAMUELSON, A. (1997): „The Effect of Mineral Variability on the Solubility of Some Actinides: An Uncertainty Analysis“, Material Res. Soc. Symp. Proc., **465**, 735 - 742
- ELLIS, D.E., ROSÉN, A & WALCH, P.F. (1975): "Application of the Dirac-Slater Model to Molecules"; Int. J. Quant. Chem. Symp., **9**, 351
- EVANS JR., H.T. (1963): "Uranyl Ion Coordination"; Science, **141**, 154 - 158
- FORMOSINHO, S.J., MIGUEL, M.D.GRACA M. & BURROWS, H.D. (1984): "Photophysics of the Excited Uranyl Ion in Aqueous Solutions : Part 1.-Reversible Crossing"; J. Chem. Soc. Faraday Trans., **80**, 1717
- FORMOSINHO, S.J. & MIGUEL, M.D.GRACA M. (1984): "Photophysics of the Excited Uranyl Ion in Aqueous Solution : Part 3.-Effects on Temperature and Deuterated Water: Mechanisms of Solvent Exchange and Hydrogen Abstraction from Water"; J. Chem. Soc. Faraday Trans., **80**, 1745 - 1756
- FRATIELLO, A., LEE, R.E., NISHIDA, V.M. & SCHUSTER, R.E. (1969): J. Inorg. Nucl. Chem., **31**, 1012
- FRATIELLO, A., KUBO, V., LEE, R.L. & SCHUSTER, R.E. (1970); "Direct Proton Magnetic Resonance Cation Hydration Study of Uranyl Perchlorate, Nitrate, Chloride and Bromide in Water-Acetone Mixtures"; J. Phys. Chem., **74**, 3726
- FRIMMEL, F.H., GREMM, T. (1994): „The Importance of Element Speciation in Water Analysis - A Plea for Further Investigations“, Fresenius J. Anal. Chem., **350**, 7 - 13

- FUGER, J. & OETTING, F.L. (1976): The Chemical Thermodynamics of Actinide Elements and Compounds.- Part 2: The Actinide Aqueous Ions; IAEA (Wien)
- FUGER, J. (1992): "Thermodynamic Properties of Actinide Aqueous Species Relevant to Geochemical Problems"; *Radiochim. Acta*, **58/59**, 81
- GALSTER, H. (1990); pH Measurement; VCH Verlagsgesellschaft, Weinheim/Germany, 356 p.
- GLUECKAUF, E. & M^CKAY, H.A.C. (1950): "Possible f-Shell Covalency in the Actinide Elements"; *Nature*, **165**, 594 - 595
- GOLUB, G.H. & REINSCH, C. (1970) „Singular Value Decomposition and Least Squares Solutions“, *Numer. Math.*, **14**, 403 - 420
- GORDON, G. & TAUBE, H. (1961): "The Exchange Reaction between Uranyl and Water in Perchloric Acid Solution"; **19**, 189
- GÖRLLER-WALRAND, CH. & DE JAGERE, S. (1972a): "Correlation between the Vibronic Spectra of the Uranyl Ion and the Geometry of its Coordination"; *Spectrochim. Acta*, **A28**, 257 - 268
- GÖRLLER-WALRAND, CH. & DE JAGERE, S. (1972b) "Etude comparative des spectres d'absorption de com-plexes d'uranyle en solution et a l'état solide. Complexes de symétrie C_s, D_{2h}(6) et D_{3h}(6)"; *J. Chim. Phys.*, **4**, 726 - 736
- GÖRLLER-WALRAND, CH. & DE JAGERE, S.(1973): "Etude comparative des spectres d'absorption d'halogé-nures d'uranyle"; *J. Chim. Phys.*, **5**, 360 - 366
- GÖRLLER-WALRAND, CH. & VANQUICKENBORNE, L.G. (1971): "Identification of the Lower Transition in the Spectra of Uranyl Complexes"; *J. Chem. Phys.*, **54**, 4178 - 4186
- GÖRLLER-WALRAND, CH. & VANQUICKENBORNE, L.G.(1972): "On the Coupling Scheme in Uranyl Complexes"; *J. Chem. Phys.*, **57**, 1436
- GÖRLLER-WALRAND, CH. & COLEN, W., DAO N.Q. (1982): "Absorption and MCD Spectra of Cs₃UO₂F₅"; *J. Chem. Phys.*, **76**, 13 - 19
- GÖRLLER-WALRAND, CH. & COLEN, W. (1982); "On the Coordination Symmetry of the Hydrated Uranyl Ion"; **93**, 82 - 85
- GREATOREX, D., HILL, R.J., KEMP, T.J. & STONE, T.J. (1972): "Electronic Spin Resonance Studies of Photo-oxidation by Metal Ions in Rigid Media at Low Temperatures. Part 4. - Survey of Photo-oxidation by the Uranyl Ion"; *J. Chem. Soc. Dalton Trans.*, **68**, 2059 - 2076
- GUIFFAUT, E. (1994): Ph.D. Thesis, Université Paris-XI
- GÜSTEN, H. (1983): "Photochemistry of Uranium"; *Gmelin Handbuch der Anorganischen Chemie*, Band Uran A6, 80 - 117
- HAAS, Y. & STEIN, G. (1975): *Chem. Phys. Lett.*, **15**, 12
- HAHN, O. (1962): "Die 'falschen' Transurane; zur Geschichte eines wissenschaftlichen Irrtums"; *Naturwiss. Rund.*, **15**, 43
- HALL, D., RAE, A.D. & WATERS, T.N. (1967): *Acta Cryst.*, **22**, 258 - 268
- HARBINSON, T.R, DAVISON, W. (1987): „Performance of Flowing and Quiescent Free-Diffusion Junctions in Potentiometric Measurements at Low Ionic Strength“, **59**, 2450 - 2456
- HASWELL, S.J. (1992): „Statistical Evaluation of Data“ in: Practical Guide to Chemometrics (S.J. Haswell, ed.), Marcel Dekker Inc., New York, 5 - 37
- HELLING, C., NITZSCHE, O, HEBERT, D., MERKEL, B. (1997): to be presented at MIGRATION '97, Sendai/Japan, October 26-31, 1997
- HILL, R.J., KEMP, T.J., ALLEN, D.M. & COX, A. (1974): "Absorption Spectrum, Lifetime and Photoreactivity towards Alcohols of the Excited State of the Uranyl Ion (UO₂²⁺)"; *J. Chem. Soc. Faraday Trans.*, **70**, 847 - 857
- HOPKE, P.K. (1989): „Target Transformation Factor Analysis“, *Chemometrics Intell. Lab. Syst*, **6**, 7 - 19
- HUGUS J.R. & EL-AWADY, A.A. (1971): "The Determination of the Number of Species Present in a System : a New Matrix Rank Treatment of Spectrophotometric Data"; *J. Phys. Chem.*, **75**, 2954 - 2957
- HUNT, R.D., YUSTEIN, J.T. & ANDREWS, L. (1993): "Infrared Matrix Spectra of NUN Formed by the Insertion of Uranium Atoms into Molecular Nitrogen"; *J. Chem. Phys.*, **98**, 6070
- IAEA (Fuger, J., Khodakovsky, I.L., Sergeyeva, E.J., Medvedev, V.A., Navratil, J.D.) (1992): The Chemical Thermodynamics of Actinide Elements and Compounds. - Part 12. The Actinide Aqueous Inorganic Complexes; IAEA, Wien
- IKEDA, Y., SOYA, S., FUKUTOMI, H. & TOMIYASU, H. (1979): "Nuclear Magnetic Resonance Study of the Kinetics of the Water Exchange Process in the Equatorial Positions of Uranyl Complexes"; *J. Inorg. Nucl. Chem.*, **41**, 1333
- ISRAELI, Y.I. (1965): "Le mécanisme d'hydrolyse de l'ion uranyle - Le spectre ultraviolet et visible de l'ion uranyle"; *Bull. Soc. Chim. Fr.*, 196
- JESSEN, R.J. (1975): „Square and Cubic Lattice Sampling“, *Biometrics*, **31**, 449 - 471

- JEZOWSKA-TRZEBIATOWSKA, B. & BARTECKI, A. (1962): "Fine Structure of the Electronic Absorption Spectra of Uranyl Compounds"; *Spectrochim. Acta*, **18**, 799
- JOHANSSON, L. (1974): "The Role of the Perchlorate Ion as Ligand in Solution"; *Coord. Chem. Rev.*, **12**, 241 - 261
- JONES, L.H. (1958): "Systematics in the Vibrational Spectra of Uranyl Complexes"; *Spectrochim. Acta*, **10**, 395
- JØRGENSEN, CH.K. (1957): "Complexes of the 4d and 5d Groups IV Including some Comments on U(VI)"; *Acta Chem. Scand.*, **11**, 85
- JØRGENSEN, CH.K. (1963): "Spectroscopy of Transition Group Complexes"; *Adv. Chem. Phys.*, **5**, 33 -146
- JØRGENSEN, CH.K. & REISFELD, R. (1975); "The Quantum Numbers of the Fluorescent State of the Uranyl Ion"; *Chem. Phys. Lett.*, **35**, 441
- JØRGENSEN, CH.K. (1979): "Excited States of the Uranyl Ion"; *J. Luminescence*, **18/19**, 63 - 68
- JØRGENSEN, CH.K. & REISFELD, R. (1982): "Uranyl Photophysics"; *Structure Bond.*, **50**, 121
- JØRGENSEN, CH.K. (1982): "Can the Highest Occupied Molecular Orbital of the Uranyl Ion be Essentially 5f?"; *Chem. Phys. Lett.*, **89**, 455
- KANELLAKOPOULOS, B., DORNBERGER, E., MAIER, R., NUBER, B., STAMMLER, H.-G. & ZIEGLER, M.L. (1993): "Elektrisches Dipolmoment von 1 : 2-Addukten des Uranyl-nitrats mit Trialkylphosphaten. Die Kristallstruktur von $\text{UO}_2(\text{TEP})_2(\text{NO}_3)_2$ und Bis[(μ -diethylphosphato-O,O') nitrato(triethylphosphato) dioxuran(VI), $\{(\text{UO}_2)[(\text{EtO})_2\text{PO}_2](\text{EtO})_3\text{PO}\}(\text{NO}_3)_2$ "; *Z. Anorg. Allg. Chem.*, **619**, 593 - 600
- KARPINSKI, R. (1985): „Paranoia: A Floating-Point Benchmark“, *Byte*, **10**, 223-235
- KATO, Y., KIMURA, T., YOSHIDA, Z. & NITANI, N. (1995): „Solid-liquid Phase Equilibria of Np(V) and of U(VI) under Controlled CO_2 Partial Pressures“, *Radiochimica Acta*, **74**, 21 - 25
- KATO, Y., MEINRATH, G., KIMURA, T. & YOSHIDA, Z. (1994): "A Study of U(VI) Hydrolysis and Carbonate Complexation by Time-resolved Laser-induced Fluorescence Spectroscopy (TRLFS)"; *Radiochim. Acta*, **64**, 107 - 111
- KATZIN, L.J. (1950): "Possible f-Shell Covalency in the Actinide Elements"; *Nature*, **166**, 605
- KNUTH, D.E. (1981): The Art of Computer Programming, Vol. II: Seminumerical Algorithms, Addison-Wesley, Reading/USA
- KORIN, P.P. (1975): Statistical Concepts for the Social Sciences, Winthrop Publishers Inc., Cambridge/USA
- KRAUSKOPF, K.B. (1986): "Thorium and Rare Earth Elements as Analogs for Actinide Elements"; *Chem. Geol.*, **55**, 323 - 335
- KRAMER-SCHNABEL, U., BISCHOFF, H., XI, R.H. & MARX, G. (1992): "Solubility Products and Complex Formation Equilibria in the Systems Uranyl Hydroxide and Uranyl Carbonate at 25 °C and I = 0.1 M"; *Radiochim. Acta*, **56**, 183
- KROPP, J.L. (1967): „Energy Transfer in Solution between UO_2^{2+} and Eu^{3+} “; *J. Chem. Phys.*, **46**, 843
- KRUPA, J.C., SIMONI, E., SYSTMA, J. & EDELSTEIN, N. (1994): „Optical Spectroscopic Studies of Uranyl Chloride UO_2Cl_2 “; *J. Alloy Comp.*, **213/214**, 471
- KRUTCHKOFF, R.G. (1967): „Classical and Inverse Regression Methods of Calibration“, *Technometrics*, **9**, 425-439
- LANGMUIR, D.(1978); "Uranium Solution-Mineral Equilibria at Low Temperatures with Applications to Sedi-mentary Ore Deposits"; *Geochim. Cosmochim. Acta*, **42**, 547
- LARSSON, S. & PYYKKÖ, P. (1986): "Relativistically Parameterized Extended Hückel Calculations. IX. An Iterative Version with Applications to Some Xenon, Thorium and Uranium Compounds"; *Chem. Phys.*, **101**, 355
- LECIEJEWICZ, J., ALCOCK, N.W. & KEMP, T.J. (1995): „Carboxylato Complexes of the Uranyl Ion: Effects of Ligand Size and Coordination Geometry upon Molecular and Crystal Structure“, *Structure Bond.*, **82** 43 - 84
- LEVI, J., IZABEL, C. & KALUZNY, Y (1990).; "Safety Assessment of Radioactive Waste Repositories"; OECD (Paris), 81
- LOPATKINA, A.P. (1964): "Characteristics of Migration of Uranium in the Natural Waters of Humic Regions and their Use in the Determination of the Geological Background for Uranium"; *Geochem. Int.*, **4-6**, 788 - 795
- LORD, E. (1947): „The Use of Range in Place of Standard Deviation in the t-Test“; *Biometrika*, **34**, 41 - 67
- MALINOWSKI, E.R. (1977): „Determination of the Number of Factors and the Experimental Error in a Data Matrix“, *Anal. Chem.*, **49**, 612 - 617
- MALINOWSKI, E.R. (1982): „Theory of Error for Target Factor Analysis with Application to Mass Spectrometry and Nuclear Magnetic Resonance“; *Anal. Chim. Acta*, **134**, 129 - 137
- MALINOWSKI, E.R. (1987): „Theory of the Distributions of error Eigenvalues Resulting from Principal Component Analysis with Applications to Spectroscopic Data“; *J. Chemometrics*, **1**, 33 - 40
- MALINOWSKI, E.R. (1991): Factor Analysis in Chemistry, 2nd ed. Wiley Interscience Publishers, New York/USA, 351 p.

MANDEL, J. & LINNIG, F.J., (1957): „Study of Accuracy in Chemical Analysis Using Linear Calibration Curves“; *Anal. Chem.*, **29**, 743 - 749

MANGINI, A., SONNTAG, C., BERTSCH, G., MÜLLER, E. (1979): „Evidence for a Higher Natural Uranium Content in World Rivers“; *Nature*, **278**, 337

MARCANTONATOS, M.D. (1977): "Acidity Effects on the Luminescence of the Uranyl Ion in Aqueous Acidic Solution"; *Inorg. Chim. Acta*, **25**, L101

MARCANTONATOS, M.D. (1979): "Chemical Quenching by Water of Photoexcited Uranyl Ion in Aqueous Acidic Solution"; *J. Chem. Soc. Faraday Trans.*, **75**, 2273

MARCANTONATOS, M.D. (1980): "Photochemistry and Exciplex of the Uranyl Ion in Aqueous Solution"; *J. Chem. Soc. Faraday Trans.*, **76**, 1093

MARSAGLIA, G. & TSANG, W.W. (1984): „A Fast, Easily Implemented Method for Sampling from Decreasing or Symmetric Unimodal Density Functions“, *SIAM J.*, **5**, 349 - 359

MASSEY JR., F.J. (1951): „The Kolmogorov-Smirnov test for goodness of fit“, *J. Am. Stat. Soc.*, **46**, 68 - 78

MATSUSHIMA, R. (1972): "Mechanism of Quenching of the Uranyl Fluorescence by Organic Compounds"; *J. Am. Chem. Soc.*, **94**, 6010 - 6016

MATSUSHIMA, R., FUJIMORI, H. & SAKURABA, S. (1974): "Quenching of the Uranyl (UO₂²⁺) Emission by Inorganic Ions in Solution"; *J. Chem. Soc. Faraday Trans.*, **70**, 1702

MAYA, L. (1982): "Hydrolysis and Carbonate Complexation of Dioxouranium(VI) in the Neutral pH Range at 25 °C"; *Inorg. Chem.*, **21**, 2895

MAZZI, F. & RINALDI, F. (1960): "Structural Studies on Me_{0.4}Me⁺⁺_{2.0}UO₂(CO₃)₃·nH₂O Compounds. I. The Crystal Structure of NaK₃UO₂(CO₃)₃"; *Acta Cryst.*, **13**, 1139

MAZZI, F. & RINALDI, F. (1961): "La struttura cristallina del K₃Na(UO₂)(CO₃)₃"; *Period. Min. (Rome)*, **30**, 1

M^CGLYNN, S.P. & SMITH, J.K. (1961a): "The Electronic Structure, Spectra and Magnetic Properties of Actinyl Ions : Part I. The Uranyl Ion"; *J. Mol. Spectr.*, **6**, 164

McKay, M.D., Beckum, R.J., Conover, W.J. (1979): „A Comparison of Three Different Methods for Selecting Values of Input Variables in the Analysis of Output from Computer Code“; *Technometrics*, **21**, 239 - 245

MEINRATH, G. (1991): "Carbonatkomplexierung des dreiwertigen Americiums unter Grundwasserbedingungen"; Dissertation, TU München/Germany, 189 p.

MEINRATH, G. (1993): „Study of Hydrolysis and Carbonate Complexation of Actinide Ions“, JAERI-memo 05-029, Japan Atomic Energy Research Institute, Tokai-mura/Japan, 160 p.

MEINRATH, G. (1996): „Coordination of Uranyl(VI) Carbonate Species in Aqueous Solutions“, *J. Radioanal. Nucl. Chem.*, **211**, 349 - 362

MEINRATH, G. (1997a): „Chemometric and Statistical Analysis of Uranium(VI) Hydrolysis at Elevated U(VI) Concentrations“, *Radiochim. Acta*, **77**, 221-234

MEINRATH, G. (1997b): Speziation von Uran unter hydrogeologischen Aspekten; *Wiss. Mitt. Inst. Geol., Technische Universität Bergakademie Freiberg/Germany*, **4**, 150 p.

MEINRATH, G. (1997c): „Uranium(VI) Speciation by Spectroscopy“, *J. Radioanal. Nucl. Chem.*, **224**, 119

MEINRATH, G. (1998a): „Determination of Uncertainties in Measurement of pH“

MEINRATH, G. (1998c): „Chemometric Analysis : Uranium(VI) Hydrolysis by UV-Vis Spectroscopy“, *J. Alloy Comp.*

Meinrath, G. (1998d): „Direct Spectroscopic Speciation of Schoepite-Aqueous Phase Equilibria“, *J. Radioanal. Nucl. Chem.*, **232**, 000

MEINRATH, G., KATO, Y., KIMURA, T. & YOSHIDA, Z. (1996): "Solid-Aqueous Phase Equilibria of Uranium under Ambient Conditions"; *Radiochim. Acta*, **75**, 159 - 167

MEINRATH, G., KATO, Y. & YOSHIDA, Z. (1993): "Spectroscopic Study of the Uranyl Hydrolysis Species (UO₂)₂(OH)₂²⁺"; *J. Radioanal. Nucl. Chem.*, **174**, 299 - 314 (Errata : *J. Radioanal. Nucl. Chem.* **175** (1994) 253)

MEINRATH, G., Kato, Y., Kimura, T., Yoshida, Z.; (1998b): „Stokes Relationship in Absorption and Fluorescence Spectra of U(VI) Species“; *Radiochim. Acta*, in press

MEINRATH, G. & KIMURA, T.(1993a): "Behaviour of U(VI) Solids under Conditions of Natural Aquatic Systems"; *Inorg. Chim. Acta*, **204**, 79 - 85

MEINRATH, G. & KIMURA, T. (1993b): "Carbonate Complexation of the Uranyl(VI) Ion"; *J. Alloy Comp.*, **202**, 89 - 93

MEINRATH, G. & SCHWEINBERGER, M. (1996): „Hydrolysis of the Uranyl(VI) Ion - A Chemometric Approach“, *Radiochim. Acta*, **75**, 205 - 210

MEINRATH, G. & TAKEISHI, H. (1993): "Solid-liquid Equilibria of Nd³⁺ in Carbonate Solutions“; *J. Alloy Comp.*, **194**, 93 - 99

MENTZEN, B.F. (1977): "The Crystal Structure of Sodium Uranyl Triformate Monohydrate, NaUO₂(HCOO)₃ · H₂O"; *Acta Cryst.*, **33B**, 2546 - 2549

MENTZEN, B.F., PUAUX, J.P. & LOISELEUR, H. (1977): "The Crystal Structure of Uranyl Diformate Monohydrate, $\text{UO}_2(\text{HCOO})_2 \cdot \text{H}_2\text{O}$ "; *Acta Cryst.*, **B33**, 1848 - 1851

METCALF, R.C. (1987): „Accuracy of ROSS pH Combination Electrodes in Dilute Sulphuric Acid Standards“, *Analyst*, **112**, 1573 - 1577

MIKEEV, N.B. (1989): "Die Stellung der Lanthaniden und Actiniden im Periodensystem des Mendeleev"; *Naturw.*, **76**, 107 - 113

MIKEEV, N.B. & KAMENSKAYA, A.N. (1991): "Complex Formation of the Lanthanides and Actinides in Lower Oxidation States"; *Coord. Chem. Rev.*, **109**, 1 - 59

MIKHAILOV, YU.N. & KUZNETSOV, V.G. (1971): *Russ. J. Inorg. Chem.*, **16**, 1340 - 1342

MORIYASU, M., YOKOHAMA, Y. & IKEDA, S. (1977): "Anion Coordination to Uranyl Ion and the Luminescence Lifetime of the Uranyl Complex"; *J. Inorg. Nucl. Chem.*, **39**, 2199

MORSS, L.R. (1995); "Comparative Thermochemical and Oxidation-Reduction Properties of Lanthanides and Actinides"; Handbook of the Physics and Chemistry of Rare Earth (K.A. Gschneider Jr., L. Eyring, G.R. Choppin, G.H. Lander, eds.) Vol. 18, 239 -290

NASH, J.C. & WALKER-SMITH, M. (1987): Nonlinear Parameter Estimation, Marcel Dekker, Basel

NAUMANN, R., ALEXANDER-WEBER, CH. & BAUCKE, F.G.K. (1994): "The Standardization of pH Measurements"; *Fresenius J. Anal. Chem.*, **349**, 603 - 606

NEA (Grenthe, I., Fuger, J., Konings, R.J.M., Lemire, R.I., Muller, A.B., Nguyen-Trung, C., Wanner, H.) (1992): Chemical Thermodynamics of Uranium; OECD/NEA (Paris)

NELDER, J.A. & MEAD, R. (1965): "A Simplex Method for Function Minimization"; *Comput. J.*, **7**, 308 - 313

NETA, P., HUIE, R.E. & ROSS, A.B. (1988): "Rate Constants for Reactions of Inorganic Radicals in Aqueous Solution"; *J. Phys. Chem. Ref. Data*, **17**, 1027

NEWMAN, J.B. (1965): "Exchange and Relativistic Effects on Pi Bonding in the Uranyl Ion"; *J. Chem. Phys.*, **43**, 1691

NEWMAN, J.B. (1967): "Near-visible Spectra of the $\text{CsUO}_2(\text{NO}_3)_3$ Crystal"; *J. Chem. Phys.*, **47**, 85 - 94

O'CONNOR, S., SCANLAN, J.P. & HYNES, M.J. (1975): "Equilibria in Uranyl Carbonate Systems"; *J. Inorg. Nucl. Chem.*, **37**, 1013

OTTO, M. (1997): Chemometrie; VCH Verlagsgesellschaft Weinheim/Germany, 355 p.

PARK, Y.Y., SAKAI, Y., ABE, R., ISHII, T., HARADA, M., KOJIMA, T. & TOMIYASU, H. (1990): "Deactivation Mechanism of Excited Uranium(VI) Complexes in Aqueous Solutions"; *J. Chem. Soc. Faraday Trans.*, **86**, 55

PERKAMPUS, H.-H. (1995) Encyclopedia of Spectroscopy, VCH Verlagsgesellschaft, Weinheim/Germany, 669 p.

PETERS, G. & WILKINSON, J.H. (1970): „The Least Squares Problem and Pseudo-Inverses“; *Comput. J.*, **13**, 309 - 316

PORTER, G.B. (1983): "Introduction to Inorganic Photochemistry"; *J. Chem. Educ.*, **60**, 785 - 790

PRESS, W.H., FLANNERY, B.P., TEUKOLSKY, S.A., VETTERLING, W.T. (1989): Numerical Recipes, Cambridge University Press, Cambridge/USA, 759 p.

PYYKKÖ, P. & LOHR, L.L. (1981): "Relativistic Parameterized Extended Hückel Calculations. 3. Structure and Bonding for some Compounds of Uranium and other Heavy Elements"; **20**, 1950

RABINOVITCH, E. & BELFORD, R.L. (1964): Spectroscopy and Photochemistry of Uranyl Compounds; Pergamon Press Frankfurt/Germany, 368 p.

RABIDEAU, S.W. (1967): *J. Phys. Chem.*, **71**, 2747 - 2750

RIPLEY, B.D., THOMPSON, M. (1987): „Regression Techniques for the Detection of Analytical Bias“, *Analyst*, **112**, 377 - 382

RIU, J., RIUS, F.X. (1996): „Assessing the Accuracy of Analytical Methods Using Linear Regression with Errors in Both Axis“; *Anal. Chem.*, **68** (1996), 1851 - 1857

RORABACHER, D.B. (1991): "Statistical Tests for Rejection of Deviant Values: Critical Values of Dixon's 'Q' Parameter and Related Subrange Ratios at the 95% Confidence Level“, *Anal. Chem.*, **63**, 139 - 146

ROSCOE, B.A. & HOPKE, P.K. (1981); „Comparison of Weighted and Unweighted Target Transformation Factor Analysis“; *Comput. Chem.*, **5**, 1 - 7

ROZETT, R.W., MCLAUGHLIN PETERSEN, E. (1975): „Factor Analysis of the Mass Spectra of the Isomers of $\text{C}_{10}\text{H}_{14}$ “; *Anal. Chem.*, **47**, 2377 - 2384

ROY, S.N., BOSE, R.C. (1953): „Simultaneous Confidence Interval Estimation“; *Ann. Math. Stat.*, **24**, 513 - 536

RUBINSTEIN, R.Y. (1981): Simulation and Monte Carlo Method; Wiley & Sons, New York/USA, 280 p.

RUFF, O. & HEINZELMANN, A. (1909): *Ber.*, **42**, 495

RUSH, R.M. & JOHNSON, J.S. (1963): "Hydrolysis of Uranium(VI) : Absorption Spectra of Chloride and Perchlorate Solutions"; *J. Phys. Chem.*, **67**, 821

- RYDBERG, J. (1955): Ark. Kemi, **8**, 113
- RYZHKOV, M.V. & GUBANOV, V.A. (1990): „Uranyl Compounds and Complexes: Electronic Structure, Chemical Bonding and Spectral Properties“; J. Radioanal. Nucl. Chem., **143**, 85 - 92
- SANWAL, D.N. & PANT, D.D. (1969): "Electronic Transitions of Uranyl Ion"; Proc. Indian Acad. Sci., **69**, 324 - 337
- SCATCHARD, G. (1936) : „Concentrated Solutions of Strong Electrolytes“, Chem. Rev., **19**, 309
- SCHÖNHAGE, A. (1961): „Zur Konvergenz des Jacobi-Verfahrens“, Numer. Math. **3**, 374 - 380
- SCHRÖDER, F.A.(1975): "Contribution to the Chemistry of Mo and W : XIV. The Mo-O-Bond Length/Bond Order Relationship. A Systematical Treatment"; Acta Cryst., **B31**, 2294 - 2309
- SCHMITZ, G. (1994): „The Uncertainty of pH“; J. Chem. Educ., **71**, 117 - 118
- SCHWARTZ, L.M. (1980): „Multiparameter Models and Statistical Uncertainties“, Anal. Chim. Acta, **122**, 291 - 301
- SCHWARZ, L. (1985): „Fluoreszierende Lanthanid- und Actinid-Festphasen der Alkalimetall- und Erdalkalimetallverbindungen“; Habilitationsschrift (Dissertation B), Universität Greifswald/Germany
- SEABORG, G.T. (1967): "History of the Synthetic Actinide Elements"; Actinide Rev., **1**, 3 -38
- SHCHERBAKOV, V.A. & SHCHERBAKOVA, L.L. (1976): "Study of the Solvation and Complex Formation of the Actinides by the Methods of NMR Spectroscopy.-I. Determination of the Hydrate Number of Uranyl"; Soviet Radiochem., **18**, 188 - 190
- SILLÉN, L.G. (1954a): "On Equilibria in Systems with Polynuclear Complex Formation. I. Methods for Deducing the Composition of the Complexes from Experimental data. "Core + Links" Complexes"; Acta Chem. Scand., **8**, 299 - 317
- SILLÉN, L.G. (1954b): "On Equilibria in Systems with Polynuclear Complex Formation. II. Testing Simple Mechanisms which give "Core + Links" Complexes of Composition B(A,B)_n"; Acta Chem. Scand., **8**, 318 - 335
- SPENDLEY, W., HEXT, G.R. & HIMSWORTH, F.R. (1962): „Sequential Application of Simplex Designs in Optimisation and Evolutionary Operation“, Technometrics, **4**, 441
- STADLER, S. (1988): "Chemisches Verhalten von Americium in natürlichen aquatischen Systemen : Hydrolyse, Radiolyse- und Redox-Reaktionen"; Dissertation, TU München, 142 Seiten
- STAPANIAN, M.A., METCALF, R.C. (1990): „State-of-the-Art pH Electrode Quality Control for Measurements of Acidic, Low Ionic Strength Waters“, J. Chem. Educ., **67**, 623 - 626
- STINES, R. (1990): „An Introduction to Bootstrap Methods“ in: Modern Methods of Data Analysis (Fox, J., Scott Long, J., eds.), 325 - 373
- STOKES, G.G. (1852): Phil. Trans., **142**, 517
- STOKES, G.G. (1853): Phil. Trans., **143**, 385
- ‘STUDENT’ (W. Gosset) (1908): „The Probable Error of Mean“; Biometrika, **6**, 1 - 25
- SUGITANI, Y., NOMURA, H. & NAGASHIMA, K. (1990): „A photoacoustic and fluorescence spectroscopic study of uranyl compounds“, Bull. Chem. Soc. Japan, **53**, 2677 - 2678
- SUTTON, J. (1949): „The Hydrolysis of the Uranyl Ion. Part I“, J. Chem. Soc. Suppl., 275
- SÝKORA, J. & SIMA, J. (1990): "Photochemistry of Coordination Compounds"; Coord. Chem. Rev., **107**, 1 - 203
- TATSUMI, K. & HOFFMANN, R. (1980): "Bent Cis d⁰ MoO₂²⁺ vs. Linear Trans d⁰f⁰ UO₂²⁺ : A Significant Role for Nonvalence 6p Orbitals in Uranyl"; Inorg. Chem., **19**, 2656
- TOMIYASU, H. & FUKUTOMI, H. (1982): "Kinetics of the Oxidation-Reduction and Ligand Substitution Reactions in Uranium Complexes"; Bull. Res. Lab. Nucl. Reactors (Tokyo Inst. Techn.), **7**, 57
- VAINIOTALO, A. & MÄKITIE, O. (1981): „Hydrolysis of Dioxouranium(VI) in Sodium Perchlorate Media"; Finn. Chem. Lett., 102 - 105
- VDOVENKO, V.M., MASHIROV, L.G. & SUGLOBOV, D.N. (1964): "Infrared Spectra of Uranyl Perchlorate and its Crystal Hydrates : Coordination of the Perchlorate Ion"; Soviet Radiochem., **6**, 289 - 294
- VEAL, B.W., LAM, D.J., CARNALL, W.T. & HOEKSTRA, H.R. (1975): "X-ray Photoemission Spectroscopy Study of Hexavalent Uranium Compounds"; Phys. Rev. **B12**, 5651 - 5663
- VEEH, H.H., CALVERT, S.E., PRICE, N.B. (1974): Marine Chemistry, **2**, 189
- VOCHTEN, R., DE GRAVE, E. & LAUWERS, H. (1990): „Transformation of Pitchblende and U₃O₈ into Different Uranium Oxide Hydrates“, **41**, 247 - 255
- VOCHTEN, R. & VAN HAVERBEKE, L. (1991): „Transformation of Schoepite into the Uranyl Oxide Hydrates: Becquerelite, Billietite and Wölsendorfite“, Miner. Petrol. **43**, 65 - 72
- VOLOD’KO, L.V., KOMYAK, A.I. & SLEPTSOV, L.E. (1967): "Absorption Spectra and Possible Classification of the Electronic State of Uranyl Compounds"; Optics and Spectr., **23**, 397
- WADT, W.R. (1981): "Why UO₂²⁺ is Linear and Isoelectronic ThO₂ is Bent"; J. Am. Chem. Soc., **103**, 6053
- WAIT, E.; "A Cubic Form of Uranium Trioxide"; J. Inorg. Nucl. Chem., **1**, 309

- WALCH, P.F. & ELLIS, D.E. (1976): "Effects of Secondary Ligands on the Electronic Structure of Uranyl"; J. Chem. Phys., **65**, 2387
- WARDMAN, P. (1989): "Reduction Potentials of One-Electron Couples Involving Free Radicals in Aqueous Solution"; J. Phys. Chem. Ref. Data, **18**, 1637
- WELLER, M.T., DICKENS, P.G. & PENNY, D.J. (1988): "The Structure of δ - UO_3 "; Polyhedron, **7**, 243 - 244
- WILLIAMS, P.A. (1994): Oxide Zone Geochemistry; Ellis Horwood Series in Inorganic Chemistry, Chichester/U.K.
- WOLD, H. (1966): „Estimation of Principal Components and Related Models by Iterative Least Squares“ in: Multivariate Analysis (Krishnaiah, P., ed.), 391 - 420
- WOOD, J.H., BORING, M. & WOODRUFF, S.B. (1981): "Relativistic Structure of UO_2^{2+} , UO_2^+ and UO_2 "; J. Chem. Phys., **74**, 5225
- WORKING, H., HOTELLING, H. (1929): „Application of the Theory of Error to the Interpretation of Trends“, Am. Stat. Assoc., 73 - 89
- YANG, C.Y., JOHNSON, K.H. & HORSLEY, J.A. (1978): "Relativistic X_α -Scattered Wave Calculation for the Uranyl Ion"; J. Chem. Phys., **68**, 1001
- YOKOYAMA, YU., MORIYASU, M. & IKEDA, S. (1975): "Electron Transfer Mechanism in Quenching of Uranyl Luminescence by Halide Ions"; J. Inorg. Nucl. Chem., **38**, 1329
- ZACHARIASEN, W.H.(1948): „Crystal Chemical Studies of the 5 f Series of Elements"; Acta Cryst., **1**, 265
- ZHENG, QI-KE, WANG, ZHI-LIN, PAN, XUN-XI, & TAN, FU-XING (1986): Acta Chim. Sin., **44**, 900 - 905